Perspective

Development of Azaindole-Based Frameworks as Potential Antiviral Agents and Their Future Perspectives

Urvashi, J. B. Senthil Kumar, Parthasarathi Das, and Vibha Tandon*

Cite This: https://doi.org/10.1021/acs.jmedchem.2c00444

Read Online

ACCESS | Metrics & More | Article Recommendations

ABSTRACT: The azaindole (AI) framework continues to play a significant role in the design of new antiviral agents. Modulating the position and isosteric replacement of the nitrogen atom of AI analogs notably influences the intrinsic physicochemical properties of lead compounds. The intra- and intermolecular interactions of AI derivatives with host receptors or viral proteins can also be fine tuned by carefully placing the nitrogen atom in the heterocyclic core. This wide-ranging perspective article focuses on AIs that have considerable utility in drug discovery programs against RNA viruses. The inhibition of influenza A, human immunodeficiency, respiratory syncytial, neurotropic alpha, dengue, ebola, and hepatitis C viruses by AI analogs is extensively reviewed to assess their plausible future potential in antiviral drug discovery. The binding interaction of AIs with the target protein is examined to derive a structural basis for designing new antiviral agents.
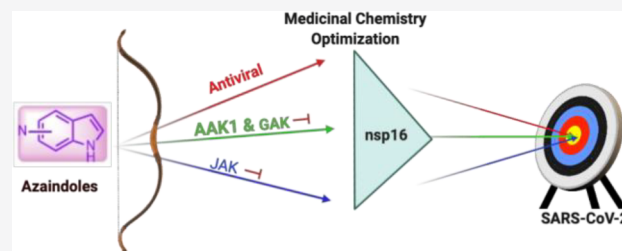
INTRODUCTION

The prevalence of fused *N*-heterocyclic building blocks in pharmaceuticals, functional materials, and natural products suggests their versatility for industrial and innovative applications with promising intellectual property scope.[1−8] In this context, azaindole (AI) analogs have been applied as diverse therapeutics due to their antiviral, antibacterial, anticancer, and antiasthma activity and have also been applied against central nervous system (CNS) disorders.[9−14] Their widespread therapeutic application is partially due to the unique physicochemical properties of the AI ring. Recently, it was observed that the introduction of a nitrogen atom to replace a −CH group in aromatic and heteroaromatic rings can, under some circumstances, lead to improved physicochemical and pharmacological properties.[9] AIs function as H-bond acceptors and donors through their pyridine moiety and pyrrole N−H, respectively, which make them attractive building blocks.[15] The different derivatives of azaindoles with diverse substituents at the C2, C3, C4, C5, and C6 positions can be synthesized easily in the laboratory.[13] Vemurafenib (**1g**), venetoclax (**1h**), peficitinib (**1i**), and decernotinib (**1j**), which are Food and Drug Administration (FDA)-approved drugs (Figure 1A), are fair representations of the potential for AIs to be efficacious drugs.

Currently, emerging RNA viruses, such as ebola, influenza, and severe acute respiratory syndrome (SARS) viruses, continue to pose a significant threat to global public health, causing substantial morbidity and mortality, leading to large, unpredictable health care burdens worldwide.[16] AIs are prominent heterocyclic motifs in inhibitors of structural and nonstructural proteins from a number of RNA viruses. Intrigued by the development of AI-based frameworks as potential antiviral agents and their future perspective, here we present a critical review spanning the first decade of the 21st century. This review encompasses the physicochemical properties and pharmacological activities of AI analogs against the target proteins of HIV-1, respiratory syncytial virus, dengue virus, ebola virus, hepatitis C virus, neurotrophic alphavirus, and influenza virus to provide an understanding of their application and potential in antiviral drug discovery.

PHYSICOCHEMICAL PROPERTIES THAT ENABLE AIS TO SERVE AS A POTENTIAL TOOL FOR BIOLOGICAL APPLICATIONS

Early investigations of the intrinsic physicochemical properties and in vivo and in vitro pharmacology of unsubstituted AIs have demonstrated their drug-like properties (Figure 1B).[1,2,17,18] The four positional isomers of AI analogs, i.e., 4-, 5-, 6-, and 7-AIs, exhibit significantly different pK_a values and lipid−water distribution ratios (*D* value) (Figure 1A).[19,20] The heterobicyclic ring system of AIs consists of a condensed, π-deficient pyridine ring and a π-excessive pyrrole ring.[12,13,21]
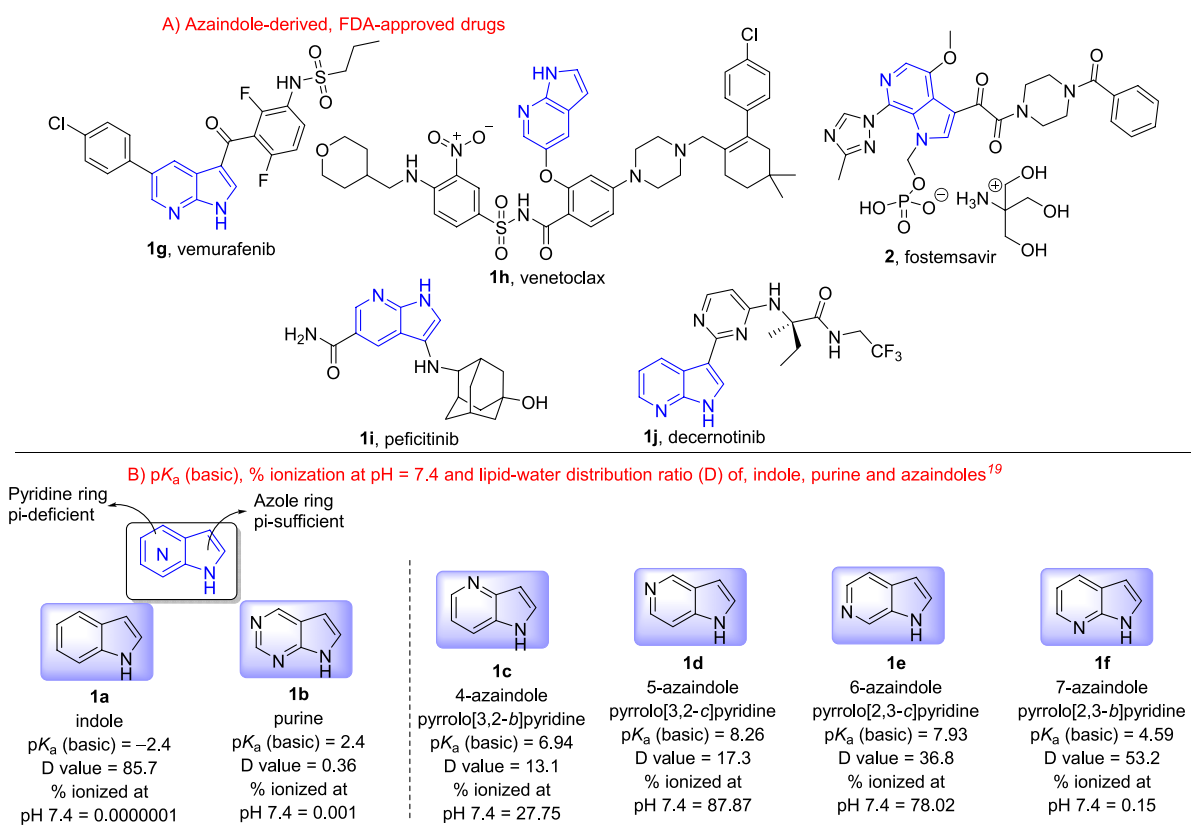
Figure 1. (A) AI-derived, FDA-approved drugs. (B) Comparison of the physicochemical parameters pK_a (basic), ionization, and lipid−water distribution ratios (D) of indoles, purines, and AIs.

Incorporating a nitrogen atom into indole to form an AI (**1c−f**, Figure 1A) confers basic properties to the molecule but reduces the lipid−water distribution ratio compared with that of indole (**1a** and **1c−f**, Figure 1B).[19] All 4-, 5-, 6-, and 7-AIs can form cations to different extents at pH 7.4 (**1c−f**, Figure 1B). More significantly, 5- and 6-AIs exist in their cationic form to an extent of 88% and 78%, respectively, at body pH (**1d** and **1e**, Figure 1B). However, 7-AI exists mostly as a free base at body pH since it exhibits a low degree of ionization (0.15%). The combination of the D value, the pK_a, and the degree of ionization critically determines the uptake of AIs across biological membranes. The reduced D values of 4-, 5-, 6-, and 7-AIs and 3-, 5-, and 7-triAIs (purine) compared with that of indole depends on both the number and the positions of the nitrogen atoms in the aromatic core (Figure 1A).[19] For example, the two nitrogen atoms in 7-AI are in close proximity, leading to a nearly 2-fold reduction in the D value compared with that of indole. However, when the two nitrogen atoms are further apart, the D value drops by nearly one-sixth. The combined effect of the numbers and positions of the nitrogen atoms is reflected in the D value of purine, which is 250-fold lower than that of indole. The chemical stability of AIs is higher than that of indoles under acidic conditions due to protonation of the pyridine nitrogen, which also renders them capable of forming salts. The 4-, 5-, 6-, and 7-AIs can be regarded as excellent bioisosteres of indole or purines that differ only by exchange of a sp^2 CH fragment(s) by a nitrogen atom(s) and vice versa.[12,13,19]

The fluorescence properties and proton-transfer tautomerism of AIs have been skillfully applied to form optical probes to investigate protein−protein and protein−nucleic acid inter-

actions.[22−29] The use of AIs as optical probes for macromolecular interaction studies provides distinctive advantages over the traditionally used indole analogs. For example, the fluorescence decay of 7-azatryptophan (a 7-AI analog) over most of the pH range is a single exponential when emission is collected over the entire band; however, for tryptophan (an indole analog), a nonexponential fluorescence decay was observed, which made the protein fluorescence more difficult to interpret.[30]

Thus, 7-azatryptophan was incorporated into synthetic peptides, bacterial proteins, and DNA oligonucleotides as an alternative to tryptophan to study the macromolecular structure and dynamics.[31,32] In these studies, 7-AI underwent solvent-assisted excited-state proton transfer (ESPT) catalyzed by alcohols, resulting in an N-7-H tautomer form (Figure 2) that exhibited green emission ($\sim$510 nm).[33−36] However, when water was used as the solvent, the N-7-H tautomer-mediated green color emission was not observed due to the slower proton-transfer rate constant ($\sim$10^{9}s^{-1}) as well as dominant radiationless deactivation pathways. One approach to overcome this difficulty was to increase the acidity of the N-1-H form by attaching an electron-withdrawing group such as cyano at C-3, which facilitated the overall ESPT rate in water, thus promoting intensive N-7-H proton-transfer tautomer emission of green light (Figure 2B).[33] Alternatively, the pyrrole element was replaced by a pyrazole moiety to form 2,7-diazaindole in which N-2 acted as an efficient electron-withdrawing group to increase the acidity of the N-1-H form (Figure 2C). Thus, 7-AIs and 2,7-diazaindole analogs serve as unprecedented biosensing tools for site-specific water environments in proteins without disrupting their native structure.[33]
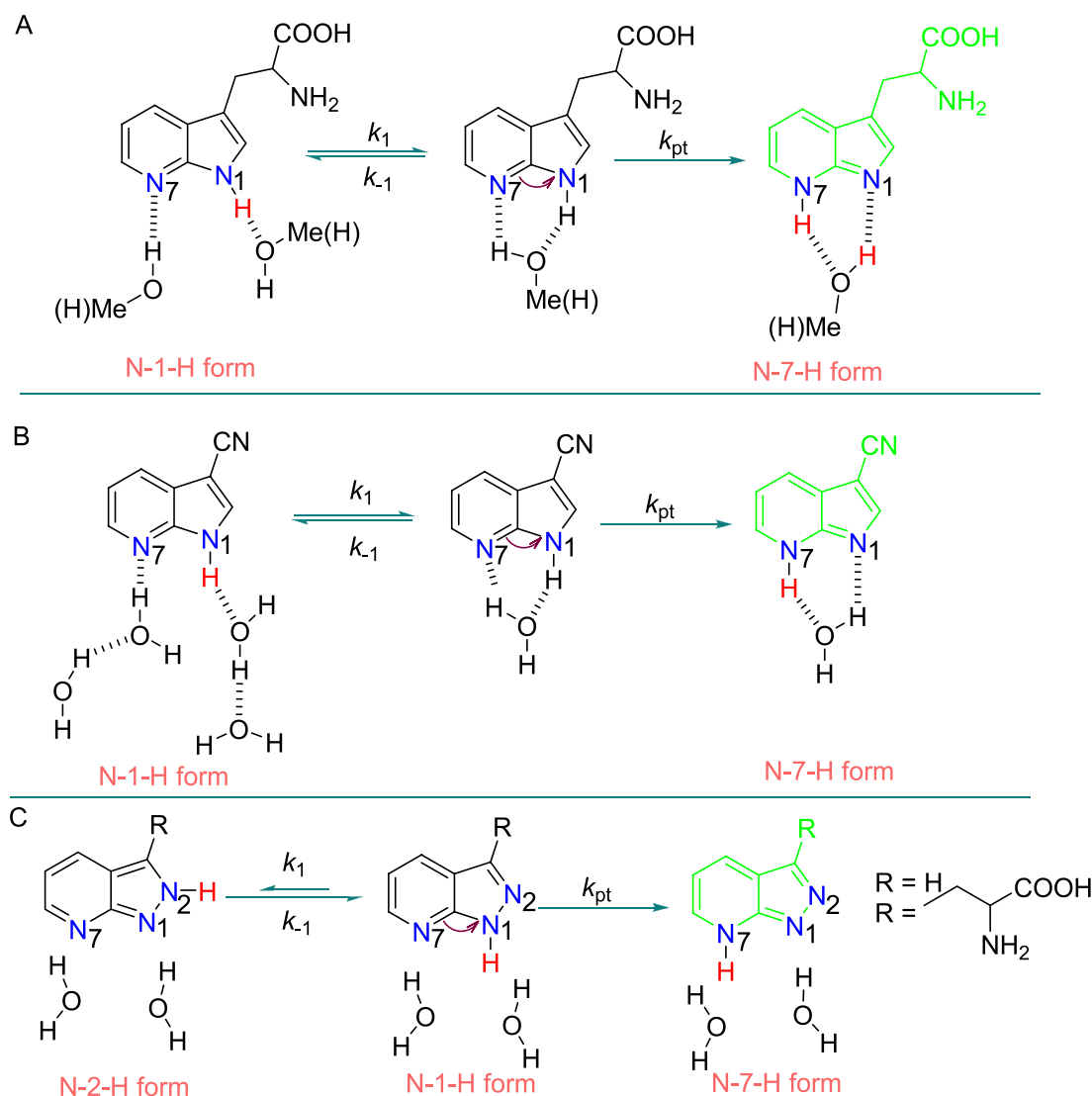
Figure 2. (A) Protic solvent-catalyzed ESPT mechanism for 7-AI and its derivatives. This mechanism incorporates a fast excited-state equilibrium between polysolvated and 1:1 cyclic hydrogen-bonded N-1-H/H$_2$O (or methanol) followed by proton tunneling k_{pt}, which has been unambiguously proven by the kinetic deuterium isotopic effect under the assumption of $k_{-1} > k_1$ and k_{pt}. Overall ESPT rate constant, k_{rxn}, can be expressed as $k_{rxn} = (k_1/k_{-1})k_{pt}$. (B) Proposed excited-state double-proton-transfer mechanism and hydrogen-bonded structure of 3-cyano-7-azaindole in water. (C) Proposed schematic diagram of a proton-transfer cycle for 2,7-diazaindole and 2,7-diazatryptophan in water.

We believe that the intrinsic fluorescence properties of AIs can also be strategically exploited for the detection and fluorescence imaging of viral macromolecules and thus possess diagnostic value.

■ HUMAN IMMUNODEFICIENCY VIRUS-1 (HIV-1) AND AZAINDOLE-BASED INHIBITORS

HIV belongs to the family *Retroviridae*, subfamily *Orthoretrovirinae*, and genus *Lentivirus*. HIV is classified into HIV-1 and HIV-2 based on genetic characteristics and differences in viral antigens. The genome of HIV-1 consists of two identical, single-stranded RNA molecules enclosed within the virus particle core. HIV-1 contains nine genes, namely, *gag, pol, env, tat, rev, nef, vpr, vif,* and *vpu/vpx*, that encode 16 viral proteins that play fundamental roles in the HIV-1 lifecycle.[37−39] The first three genes, *gag, pol,* and *env*, encode structural proteins (matrix, capsid, nucleocapsid, and p6), viral enzymes (protease, reverse transcriptase, and integrase), and env proteins (gp120 and gp41).[37] The rest of the genes encode

regulatory proteins (*tat* and *rev*) and accessory proteins (*nef, vpr, vif, vpu/vpx*). *vpu* is found exclusively in HIV-1, whereas HIV-2 carries *vpx*.[40] The efficient replication mechanism at different stages of the HIV-1 life cycle is achieved by the physical interaction of pairs of viral proteins.[41] For instance, the HIV-1 envelope glycoprotein gp120 physically interacts with gp41 during viral entry. In addition to HIV pairwise protein interactions, HIV−host protein interactions are known to play essential roles for HIV to take over human cellular systems.

The HIV-1 life cycle consists of approximately nine stages (Figure 3). Briefly, binding of the virus to a cluster of differentiation (CD4) glycoproteins on the host cell surface induces conformational changes in the env trimer that allow the interaction of gp120 with either the CCR5 or the CXCR4 coreceptor, which triggers the next step in the viral fusion process, the rearrangement of gp41. After fusion, the viral RNA is transcribed into linear, double-stranded DNA by HIV-1 reverse transcriptase. The double-stranded DNA is then
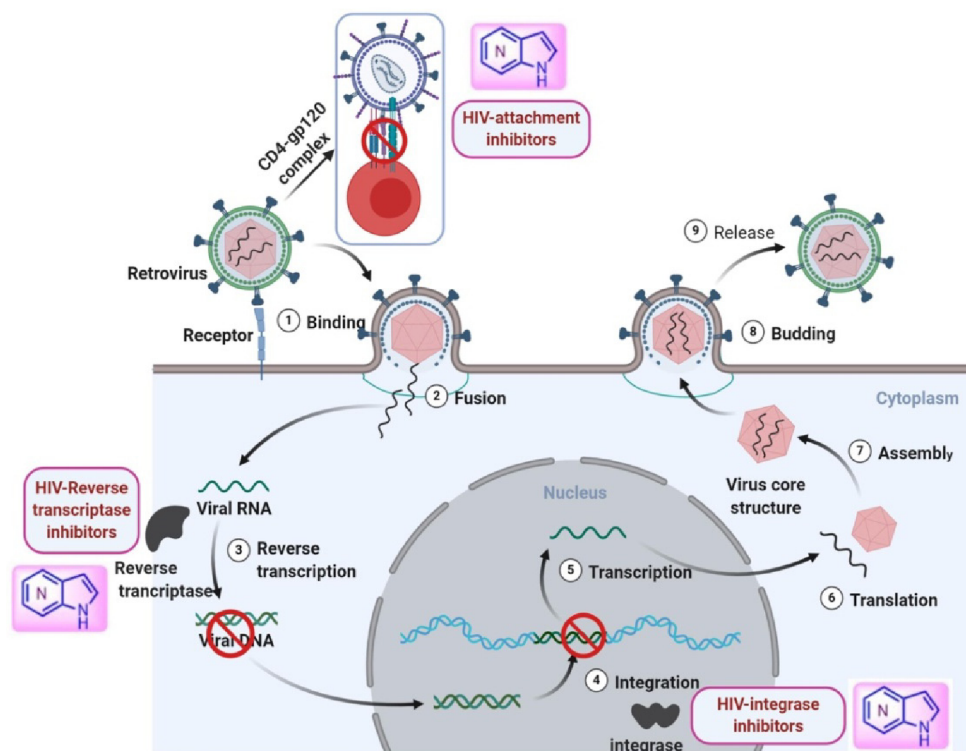
Figure 3. Different targets in the HIV-1 cycle and AI-based inhibitors in this cycle.
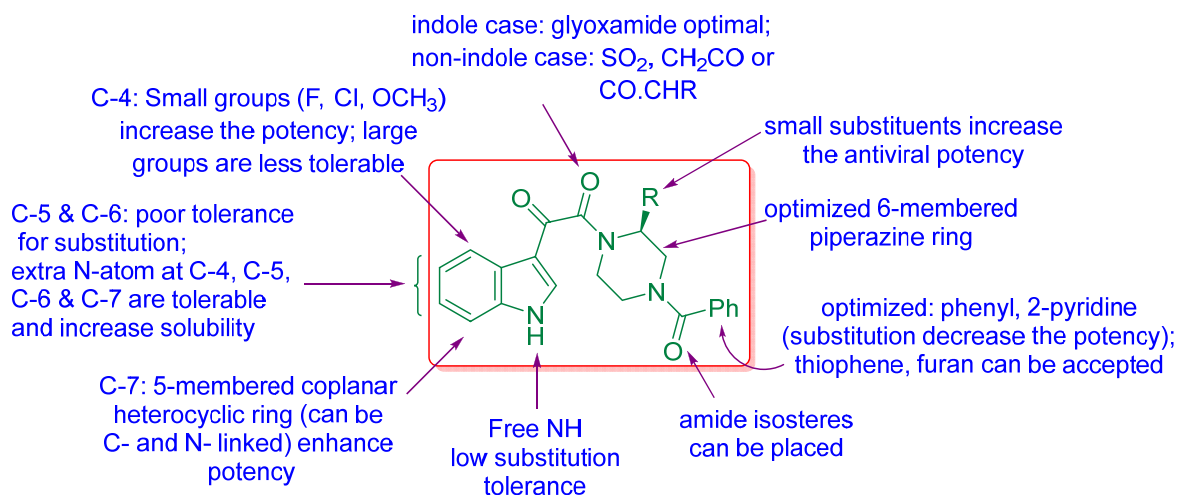

Figure 4. Summary of SAR studies conducted with indole-3-glyoxamide-based inhibitors of HIV-1 attachment.

transported across the nuclear membrane and inserted into the cellular DNA by the enzyme integrase. The integrated HIV-1 provirus serves as a template for the transcription of both viral messenger and genomic RNA by cellular Pol II polymerase. The fully spliced viral RNA, which encodes essential structural and nonstructural proteins, is translated, and the assembly of viral RNA and proteins on the cell surface forms new virions through budding, which are released to infect another host cell (Figure 3). Since the introduction of the first FDA-approved drug zidovudine to treat HIV-1 in 1987, significant progress has been achieved in HIV-1 drug discovery. Currently, 5 nucleoside reverse transcriptase inhibitors (NRTIs), 5 non-nucleoside reverse transcriptase inhibitors (NNRTIs), 6 protease inhibitors (PIs), 1 fusion inhibitor, 1 CCR5 antagonist, 4 integrase inhibitors, 1 attachment inhibitor, 1

pharmacokinetic enhancer, and 24 fixed-dose combinations of one or more drug classes have been approved by the FDA.

The latest addition to the above list, the attachment inhibitor fostemsavir (**2**), a 6-AI-based prodrug, was approved by the FDA on July 2, 2020 as a therapeutic agent for highly treatment-experienced subjects.[42] Despite the availability of 24 individual drugs (including **2**) and 24 fixed-dose combinations, the pursuit of a more effective, mechanistically distinct and noncross-resistant class of drugs to overcome drug toxicity continues in the absence of an effective vaccine, the risk of viral resistance, and the emergence of comorbidities associated with long-term combined antiretroviral therapy (cART).

AI analogs have played a prominent role in the development of HIV-1-attachment inhibitors (Figure 4). The insightful installation of a basic nitrogen atom to replace a CH moiety of

indole prototypes to form an AI core provided substantial improvements in the molecular, physicochemical, and pharmaceutical properties that translated into better pharmacological and developability profiles. This part of the perspective explores the salient element of the development of AI-based HIV-1-attachment and integrase inhibitors.

HIV-1-Attachment Inhibitors. HIV-1 particles infiltrate host cells (T-cells, monocytes, macrophages, and dendritic cells) which express the CD4 glycoprotein receptor to initiate infection. The glycosylated gp120 surface protein of HIV-1 particles physically interacts with gp41 via noncovalent interactions to form the trimeric env spikes. The gp120 protein contains five conserved domains (C1−C5) and five variable domains (V1−V5), which form three key structural regions: the inner domain, the outer domain, and the bridging sheet of the HIV-1 envelope.[43] The gp41 protein contains an N-terminal fusion peptide (FP), two heptad-repeat domains (HR1 and HR2), and a transmembrane anchor (TM).[44] Binding of the HIV-1 envelope protein gp120 to CD4 cells expressed on T-cells triggers an outward domain shift to relieve some of the noncovalent interactions between gp120 and gp41, opening the coreceptor (CCR5 or CXCR4) binding site.[45,46] Following engagement of the coreceptor, gp120 undergoes further conformational changes that trigger a conformational rearrangement of gp41 to expose the fusion peptide which inserts into the host membrane, leading to fusion of the host cell membrane with the virus and allowing the capsid to enter the cytosol. Each of these discrete steps in the HIV-1-entry process has been verified to be a promising target for anti-HIV-1 drug development. The classification of HIV-1-entry inhibitors depends on their distinctive mechanism of action in the sequential viral entry processes, such as virus attachment (CD4-gp120 interaction), coreceptor binding (CCR5 and CXCR4 inhibitors), and membrane fusion.[47]

Indole glyoxamide 3 (Figure 4), which is an early identified HIV-1 attachment inhibitor (EC$_{50}$ = 153 nM in a pseudotype assay), served as a prototype for many 6-AI-based inhibitors, including the recently FDA-approved prodrug 2 (Figure 1B).[48−50] The low in vitro cytotoxicity against a panel of human cell lines, specificity for HIV-1, and synthetic accessibility to allow the introduction of diverse chemical substituents on 3 led to a series of SAR investigations (Figure 4), which collectively contributed to development of the prodrug, fostemsavir (2, Figure 1B).

The introduction of either F or OCH$_3$ at the C-4 or C-7 position of the indole ring resulted in an increase in antiviral potency (Table 1).[48] The 4-fluoro derivative 4 was observed to be 50-fold more potent than the congener 3 in the pseudotype antiviral assay. The introduction of other substituents, such as Cl, Br, OC$_2$H$_5$, and CN, at C-4 or C-7 also enhanced antiviral potency as compared with 3. The observed increase in the antiviral potency of the disubstituted products 5 and 6 (Table 1) demonstrates the synergistic effect of C-4 and C-7 substitutions. Substitution on C-5 or C-6 and alkylation of the indole nitrogen, however, did not yield an impressive outcome. Furthermore, pharmacokinetic profiling indicated that 3 exhibited modest oral bioavailability (F_{po} = 29% at a dose of 25 mg per kilogram (mpk)) and high clearance (57 mL/min/kg) in rats. Similarly, 4 (EC$_{50}$ = 2.6 nM in the pseudotype assay) displayed modest bioavailability (17% at a dose of 25 mpk) and clearance (48 mL/min/kg). In contrast, the 4,7-dimethoxy derivative 6 afforded superior oral availability (107%) and low clearance (5.2 mL/min/kg).

Table 1. HIV-1 Pseudotype Virus Inhibitory Activity, Oral Bioavailability, and Clearance In Vivo of Substituted Indole Glyoxamide Analogs
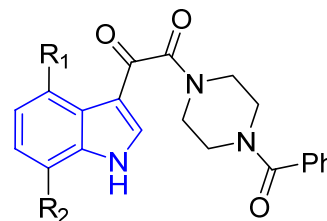
| | substituted indoles | | | | |
compound no.	R$_1$	R$_2$	EC$_{50}$ (nM)	F_{po} (%) in rats[a]	CL (mL/min/kg) after IV injection in rats
3	H	H	153	29[b]	57[c]
4	F	H	2.6	17[b]	48[c]
5	F	F	0.35	11[c]	46.9[d]
6	OCH$_3$	OCH$_3$	0.23	107[c]	5.2[d]

[a]Dosed as solutions in PEG 400/EtOH (90:10). [b]At 25 mpk. [c]At 5 mpk. [d]At 1 mpk.

Moreover, the potency of the 4,7-dimethoxy derivative was also 5-fold improved over that of the monofluoro analog 4 (Table 1).

Initially, a higher emphasis was placed on optimizing the 4-fluoro derivative 4 based on its promising antiviral profile toward a panel of HIV-1 viruses (Table 2) and its superior oral

Table 2. HIV-1-Inhibitory Activity of Compounds 4 and 7 against a Panel of Macrophage and T Cell-Tropic HIV-1 Viruses[a]

	4	7
virus	EC$_{50}$ (nM)	EC$_{50}$ (nM)
LAI (T)	2.93	2.68
SF-2 (T)	62.4	26.5
NL4−3 (T)	30.8	2.94
Bal (M)	18.1	15.5
SF-162 (M)	ND	3.46
JRFL (M)	2.39	1.47
TLAV (dual)	13.6	0.85

[a]ND: Not determined. T: T-tropic virus that utilizes the CXCR4 coreceptor. M: macrophage-tropic virus that utilizes both the CXCR4 and the CCR5 coreceptors for entry.

bioavailability (∼100%) in dogs and monkeys dosed at 10 mpk as a solution in PEG 400/ethanol (90:10 v/v). Compound 4 demonstrated good pharmacokinetic properties in the rat and dog following oral dosing as solutions in PEG 400/ethanol. However, the bioavailability of 4 was substantially poorer than that of the solution form when administered as a suspension. Further efforts were made to improve the physicochemical properties of 4 by installing a nitrogen atom and an electron-donating methoxy substituent at the C-7 and C-4 positions, respectively, to create the 7-AI analog 7, which showed a 34-fold improvement in solubility over 4 (Figure 6).[51] The X-ray cocrystal structure data for 7 indicated a mix of H-bonding and hydrophobic interactions with gp120, with the benzoyl group forming parallel and offset π-stacking interactions with Phe382 and Trp427 of gp120, respectively.[52] Two hydrogen bonds, one between the backbone N−H group of Trp427 and the
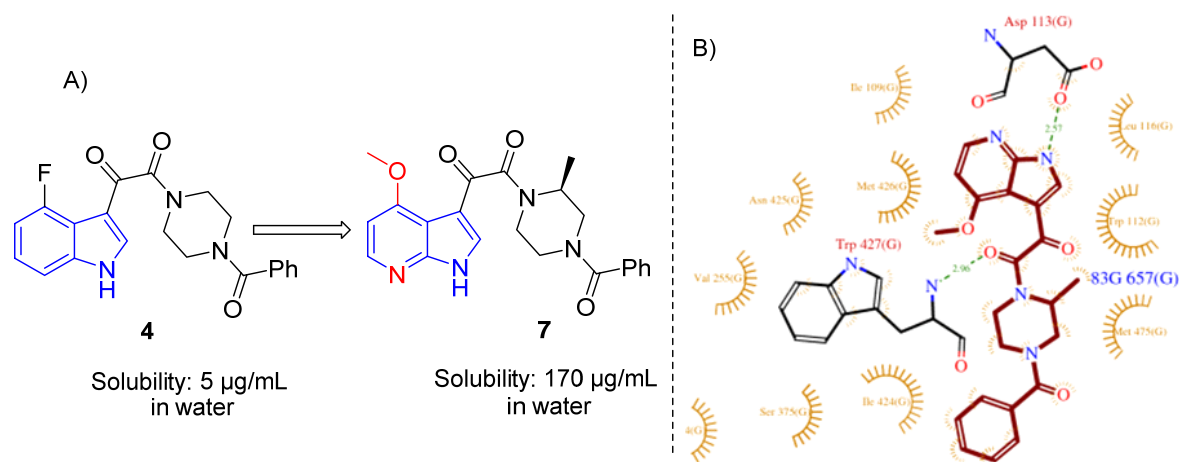
Figure 5. (A) Improvement in the solubility of **4** upon introduction of a nitrogen atom to replace C-7 and polar methoxy substituents on the indole ring. (B) Two-dimensional interaction diagram of **7** with HIV-1 gp120 (PDB 5U7M).

oxoacetamide carbonyl group of **7** and another bond between the carboxylate group of Asp113 and the azaindolic N−H group of **7**, were observed in the cocrystal (Figure 5B).

The antiviral potency of **7** against a panel of macrophage-tropic and T-cell-tropic HIV-1, which utilize the CCR5 (M-tropic) or CXR4 (T-tropic) coreceptors to enter host cells, respectively, is shown in Table 2, which revealed the combined effect of introducing nitrogen and a methoxy substituent on the indole ring in improving both the solubility and the antiviral properties.

The pharmacokinetic data also favored the advancement of **7** into clinical trials. However, a phase 1 dose-escalation study in normal healthy subjects revealed that the observed plasma concentration was lower than the targeted efficacious level in HIV-1-infected individuals; therefore, further studies were halted. In parallel, the 4-AI isomers **8** and **9** were also studied and found to have improved potency and PK profiles over those of **7** (Figure 6).[53] Nevertheless, more promising compounds in the related 6-AI core series were subsequently identified (vide infra).

The subsequent focus was directed toward the 4,6-dimethoxy analog **6**, which possessed good antiviral potency (EC$_{50}$ = 0.23 nM). However, oxidative metabolism of **6** in microsomal preparations from human liver resulted in demethylation at the C-4 and C-7 positions, arousing concern
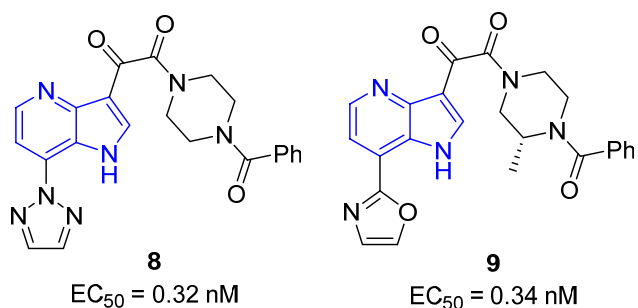

Figure 6. Active 4-AI analogs **8** and **9** with their potency and cytotoxicity. Here, a mnemonic in which substitution around the attached heteroaromatic ring at C-7 that allows coplanarity with the 4-azaindole was proven to be a useful guide as a predictor of optimal potency within a series.

for the potential formation of indoloquinolone **11** in *in vivo*. In order to prevent the formation of a reactive quinone, the analogue **10** was designed by introducing a nitrogen atom at the C-6 position of the indole core of **6** (Figure 7).

The oral bioavailability of **10** in rats, dogs, and monkeys after administration as a solution in 90% PEG 400, 10% EtOH was 90%, 57%, and 60%, respectively, whereas **7** exhibited 19%, 77%, and 24% oral bioavailability, respectively, in the same species. Compound **10** demonstrated a clean preclinical safety profile and advanced into phase 1 clinical study. However, in clinical trials, the area under curve (AUC) and C_{max} did not increase proportionally with the administration of increasing dose of compound **10** from 200 to 800 mg. The plasma exposure of **10** showed a 3-fold increase in a solution formulation at a dose of 200 mg, but a 3−5-fold increase was observed when it was administered along with a high-fat meal over the 400−1200 mg dose range. The excessive pill burden and the requirement for dosing with a high-fat meal to achieve targeted plasma exposure posed a challenge that hindered the further development of **10**.

A phosphonooxymethyl prodrug approach was designed to improve the solubility of **10** in the gastrointestinal tract (GIT) and to take advantage of the enzyme alkaline phosphatase, which is expressed on the intestinal brush border membrane, to release **10** from the phosphonooxymethyl prodrug **12** by a presystemic cleavage mechanism (Figure 8).[54] Thus, presystemic dephosphorylation of the phosphonooxymethyl prodrug **12**, formulated as its (S)-(+)-lysine salt, in the GIT releases the short-lived N-hydroxymethyl derivative **12a**, which rapidly liberates one molecule of formaldehyde to produce the parent drug **10**. However, a potential concern was the need to avoid precipitation of the parent drug upon dephosphorylation and prior to absorption; thus, balancing the kinetics of phosphate cleavage and the rate of absorption was essential for success. The successful delivery of parent drug **10** is a function of its biopharmaceutical classification system (BCS) class 2 designation based on its experimentally measured low solubility and high intrinsic membrane permeability. The lysine salt of phosphonooxymethyl prodrug **12** demonstrated an improved solubility of >12 mg/mL at pH 5.4 as compared to parent compound **10** which has a solubility of 0.04 mg/mL at pH 4−8. The rapid conversion of **12** into the parent molecule **10** was observed after iv administration to rats, dogs and monkeys.
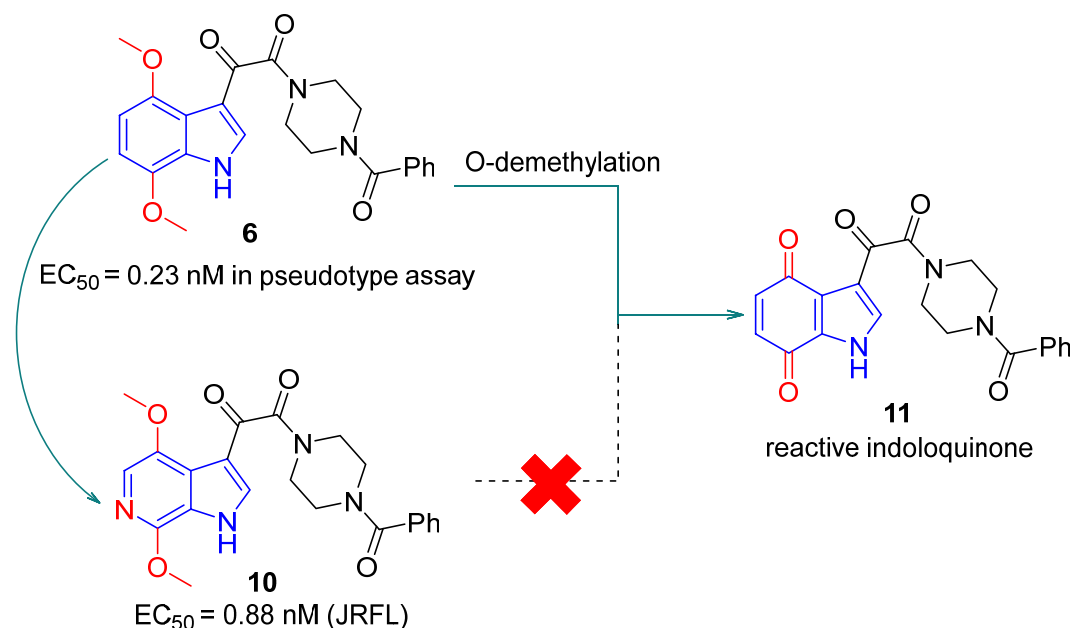
Figure 7. Installing a nitrogen at C-6 of **6** to form the 6-AI analog **10** to prevent formation of a reactive indoloquinone **11**.
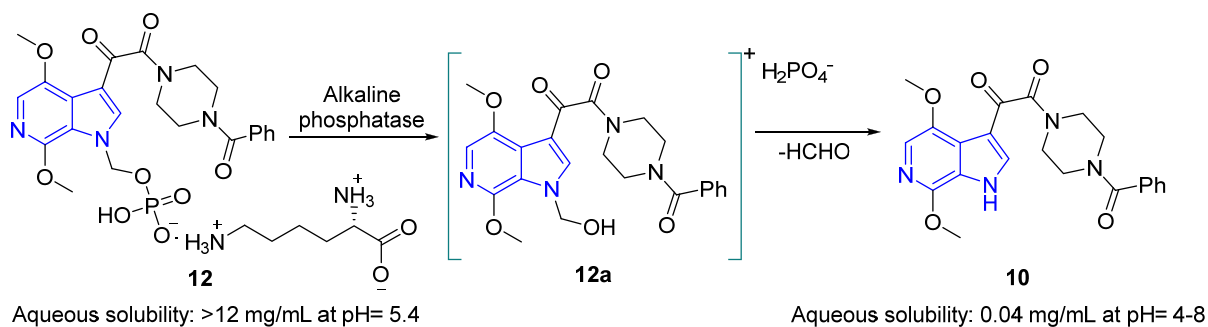

Figure 8. Structure of the (S)-(+)-lysine salt of the phosphonooxymethyl prodrug **12**, short-lived hydroxy methyl intermediate **12a**, and parent drug **10**.

The absolute bioavailability of the parent drug **10** after oral administration of **12** was 62%, 93%, and 67% in rats, dogs and monkeys, respectively. Plasma exposure of **12** increased in a linear manner following administration of 16, 72, and 267 mpk of the prodrug to rats. The AUC and C_{max} of **10** were increased up to 3-fold when administered in the prodrug form compared with the administration of the parent drug as a suspension. Similarly, prodrug **12** showed a dose-proportional increase in plasma concentrations at doses ranging from 25 to 800 mg in human clinical studies. Prodrug **12** showed improved clinical potential of **10**, further development was abandoned in favor of fostemsavir (**2**).

Continued SAR studies explored the introduction of carboxamide,[55] sulfonamide, and heteroaryl[56] substituents at the C-7 position of the indole core which led to the identification of compounds with enhanced antiviral potency. Carboxamide **13** showed high human liver microsome stability (HLM) and modest Caco-2 permeability, whereas oxadiazole **14** showed a balanced profile in terms of HLM stability and Caco-2 permeability. However, these substituted indoles were unable to deliver the targeted combination of physicochemical properties and drug-like profiles needed in a clinical candidate (**13** and **14**, Figure 9B). These findings resulted in the pursuit

of the 6-AI core in an effort to overcome the pharmaceutical issues confronted by **10**.[57]

In this context, C-7-linked amides and both substituted and unsubstituted heterocycles were installed on the 4-fluoro-6-AI template (Figure 10). The C-linked methylamide **17** (EC_{50} = 0.09 nM) was suggested to form internal H bonds with the indole NH (amide C=O) and pyridine nitrogen (amide NH) of the 6-AI core, thereby stabilizing a planar conformation. The presence of internal H bonding was corroborated by the X-ray structure of pyrazole **18** (EC_{50} = 0.07 nM), which revealed H bonding between N-1 of the pyrazole ring and NH of the azaindole to confer coplanarity to this part of the molecule (Figure 10). In the case of oxazole **19** (EC_{50} = 0.15 nM), despite poor internal H bonding, coplanarity was preserved by means of a positive electrostatic interaction between the O atom of oxazole and the indole NH.[57] However, the oxazole **20** (EC_{50} = 3.56 nM) and the imidazole **21** (EC_{50} = 1.3 nM) encountered unfavorable intramolecular interactions (Figure 10) due to electron pair repulsion. Thus, the observed loss of the antiviral potencies of **20** and **21** confirmed a correlation between coplanarity at this region of the molecule and antiviral potency.

Two structural analogs of 6-azaindoles (**22-23**) having 1,2,4-triazole and its 1,2,3-triazole isomer installed at the C-7
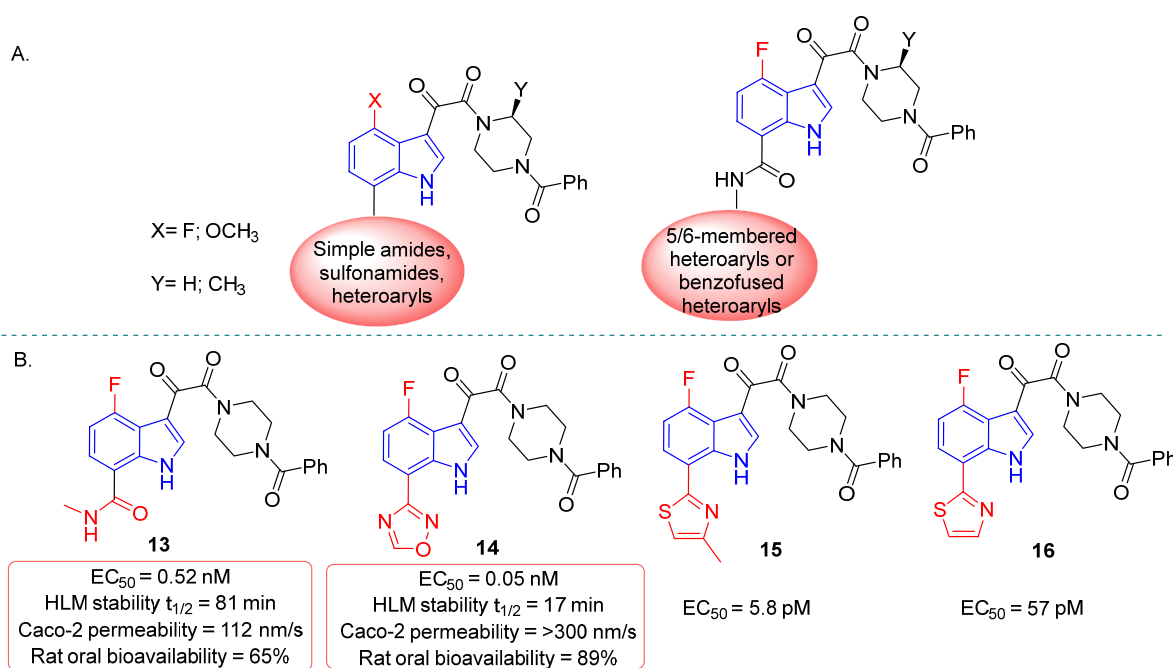
Figure 9. (A) General structure of 4-fluoro/methoxy indole glyoxamides. (B) C-7-Substituted 4-fluoroindole glyoxamides with the antiviral potency, microsomal stability, membrane permeability, and oral bioavailability of **13** and **14** presented, and structures of potent HIV-1 inhibitors **15** (methylated thiazole) and **16** (thiazole).

position offered promising antiviral and pharmacokinetic profiles (Table 3).

Compounds **22** (EC_{50} = 0.07 nM) and **23** (EC_{50} = 0.05 nM) showed 10-fold greater inhibitory activity against HIV-1 infection in the pseudotype assay compared with that of **10** (EC_{50} = 0.88 nM). The inhibitory activity of **23** was also preserved toward a much broader range of subtype B laboratory strains. Compared with that of **10**, the pharmacokinetic profiles of **22** and **23** were improved with 10-fold lower iv clearance, while the plasma exposure after oral dosing was improved by approximately 13-fold for **22** and **23** (Table 3). Safety pharmacology data for **23** indicated no significant cardiac liability in a hERG channel patch clamp assay and no mutagenicity in an Ames reverse mutation assay. On the basis of these data, the 1,2,3-triazole **23** was advanced into a phase I clinical trial with human subjects in which **23** was formulated as a spray-dried dispersion and dosed at 100, 200, 400, 800, and 1200 mg to normal healthy volunteers. However, the exposure profile was not satisfactory for conducting an efficacy study in HIV-1-infected patients. The aqueous crystalline solubility of **23** was found to be low (7 μg/mL), which was believed to be responsible for its poor bioavailability at high doses.

A phosphonooxymethyl prodrug formulation, **24**, similar to that of **10**, was also prepared (Figure 11) in an effort to enhance the plasma exposure profile of **23** following oral administration; however, at targeted exposure margins in preclinical toxicology studies, the low aqueous solubility of the parent resulted in crystallization in tissues.

The idea to attach C-7, N-linked azoles as a design concept was also explored in the 4-methoxy-substituted 6-AI series (Figure 13) in an effort to overcome the solubility limitations of the 4-fluoro-6-AI series, but the improvement in solubility was modest. The unsubstituted 1,2,4-triazole **25** was characterized by superior antiviral and pharmacokinetic

profiles in preclinical species. However, the safety pharmacology data were not encouraging, as **25** inhibited CYP3A4 and the hERG ion channel, arousing concern for potential drug–drug interactions and cardiac liabilities. However, these liabilities were solved with substitution on the 1,2,4-triazole ring of **25** which provided the 3-methyl-substituted analog **26** (also known as temsavir), which retained the improved pharmacokinetic properties in rats observed with the unsubstituted congener **25**.

Prominently, the pharmacokinetic profile of **26** was notably improved over **10** in terms of its low clearance, ~2-fold increased half-life, and 8-fold higher plasma exposure after oral dosing.[48,58] In addition, **26** demonstrated acceptable oral bioavailability (52%) when dosed as a suspension in dogs and monkeys. However, **26** showed low crystalline aqueous solubility (0.022 mg/mL) but high membrane permeability. These characteristics of **26** placed this molecule as a BCS class 2. The tris(hydroxymethyl)aminomethane salt of the phosphonooxymethyl derivative of **26**, known as fostemsavir **2** (Figure 12), was prepared as a prodrug. It exhibited >11 mg/mL aqueous solubility and 80−122% oral bioavailability for the parent drug **26** in rats, dogs, and monkeys.[48,58] At lower doses (≤25 mg), the AUCs of both **26** and **2** displayed similar trends in rats and dogs; however, at 200 mg/kg, administration of the prodrug **2** demonstrated superior plasma exposure of the parent drug compared with that of **26**.

Comprehensive biochemical profiling demonstrated that attachment inhibitors based on 6-AIs bind to HIV-1 gp120 and interfere with its attachment to the CD4 receptor.[50,58] Another mechanism has been proposed in which 6-AIs hinder the exposure of gp41 following CD4 and coreceptor-induced conformational changes by forming a ternary complex with gp41 and gp120. The binding mode of **26** to gp120 from X-ray cocrystal studies indicated that the benzoyl group of **26** engages in parallel π-stacking interactions with Trp427 in the
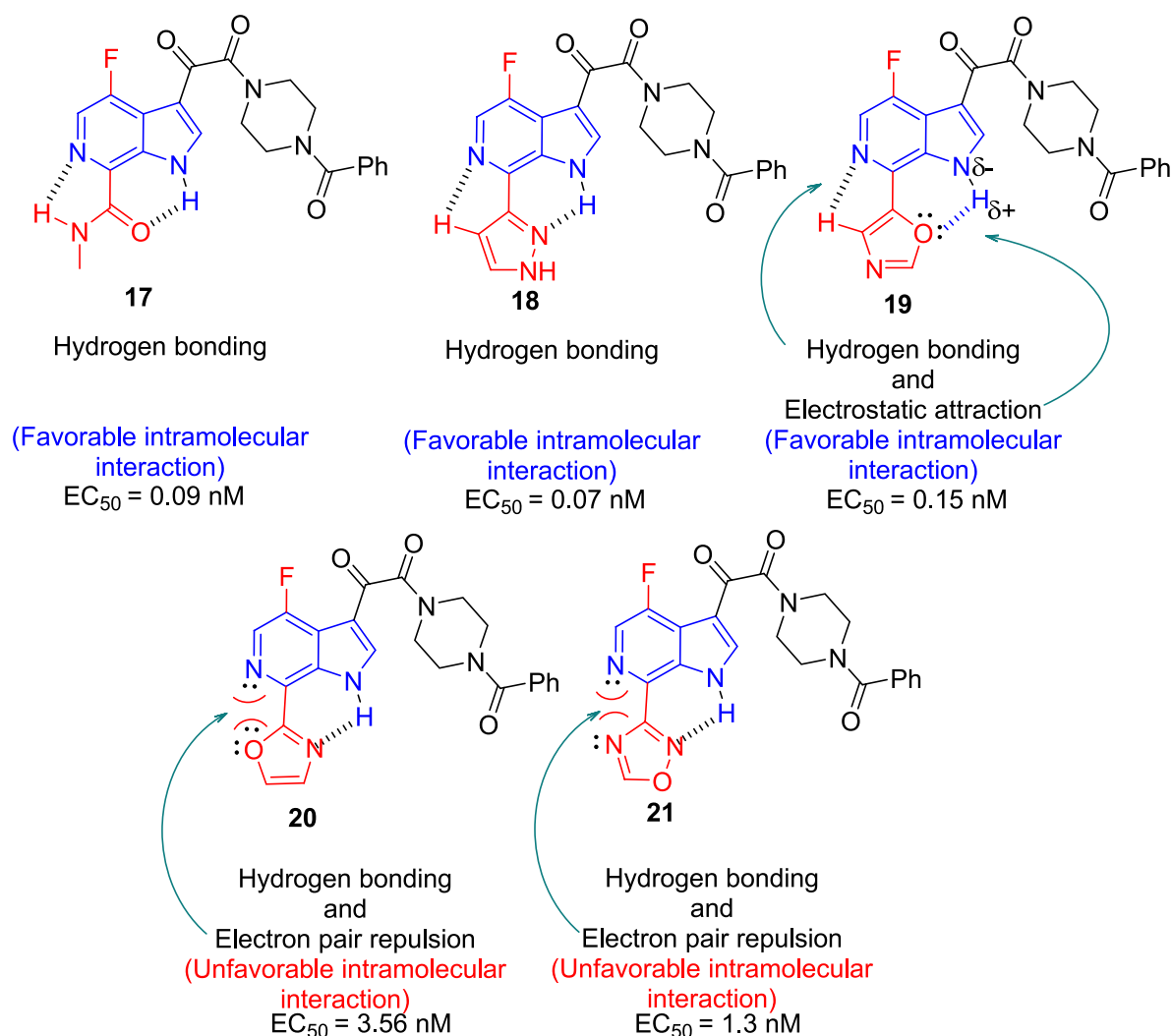
Figure 10. Suggested favorable and unfavorable intramolecular interactions exemplified by C-7-substituted, 4-fluoro-6-AI analogs.

Table 3. Comparison of Antiviral and Rat Pharmacokinetic Profiles of 10, 22, and 23[a]

Compound No.	R	JRFL virus EC_{50} (nM)	AUC, 24 h (μM.h)[b]	C_{max} (nM)[b]	CL, iv (mL min^{-1} kg^{-1})	F (%)	HuPB[c] (%)
10	-	0.88	6.3 ± 2.7	1889 ± 647	13 ± 4.0	90	-
22		0.07	83.7 ± 9.8	8764 ± 810	0.7 ± 0.12	95	97
23		0.05	86 ± 33	9484 ± 279	1.6 ± 0.2	64	95

[a]Dosed as solutions in PEG 400/EtOH (90:10 v/v). [b]Oral C_{max} and AUC adjusted to 5 mg/kg. [c]Human plasma binding.

inner and outer interface domains of the $\beta 20-\beta 21$ loop of gp120 (Figure 13). Two H bonds, first between the backbone NH moiety of Trp427 and the oxoacetamide C=O of **26** and

second between the azaindolic N—H group and the side chain carboxylate group of Asp113, have been observed. In addition to the above, compound **26** binds with gp120 through
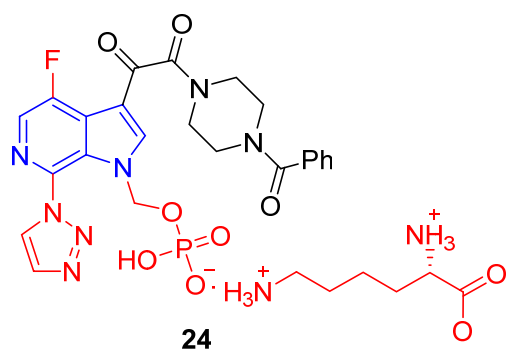
Figure 11. Structure of the (S)-(+)-lysine salt of phosphonooxymethyl prodrug **24**.

hydrophobic interactions with Trp112, Asp113, Leu116, Thr202, Val255, Phe382, Ile424, Met426, Trp427, Gln432, Met434, and Met 475. The analysis of the cocrystal structure of **26** with HIV-1 env revealed that **26** does not allow CD4 to bind to gp120, which is necessary for conversion of the prefusion conformation of the env trimer to the postfusion conformation. At low concentration, **26** stabilizes a prefusion conformation of the env trimer and interferes with the env conformational changes induced by the CD4, whereas at higher concentration **26** binds at the allosteric site in such a manner that it does not allow CD4 attachment on gp120.

Figure 14A provides the summary of the structure-guided optimization pathway along with a brief synopsis on the

important outcome of each pathway presented. Figure 14B presents important essential structural features for AI-based attachment inhibitors.

The application of a bioconjugation strategy to generate chemically programmed antibodies by covalently attaching the entry inhibitors 7 and **10** to monoclonal antibody (mAb) 38C2 via an N-acyl-β-lactam-derived linker has been described.[59] This study was focused on identifying an AI–antibody conjugate that would recognize gp120 by targeting the conserved attachment inhibitor binding site. It was hypothesized that the covalent conjugation of a mAb 38C2 (aldolase antibody) with gp120 inhibitors will improve the pharmacokinetics profile of the inhibitors. Accordingly, N-acyl-β-lactam derivatives **31** and **32** were synthesized using inhibitors 7 and **10** and then covalently linked to mAb 38C2 to afford chemically programmed antibodies **33** and **34** (Figure 15). Subsequently, the conjugated bivalent antibodies **33** and **34** and their corresponding N-acyl-β-lactam derivatives **31** and **32** were advanced into virus neutralization assays using U87.CD4.CCR5 cells transfected with HIV-1 infectious virus (JRFL) to monitor their antiviral efficacy. Compounds **31** and **32** demonstrated IC$_{50}$ values of >200 and 67.50 nM, respectively. The conjugated antibodies **33** and **34** exhibited IC$_{50}$ values of >1000 and 128.6 nM, respectively.

The weak neutralization activities of **31** and **33** were consistent with low gp120 binding due to the C-4 substitution, which disrupted JRFL−gp120 binding, as reported earlier. The significant IC$_{50}$ values of **32** and **34** indicates that the linker attachment at the C-7 position preserved the binding affinity.
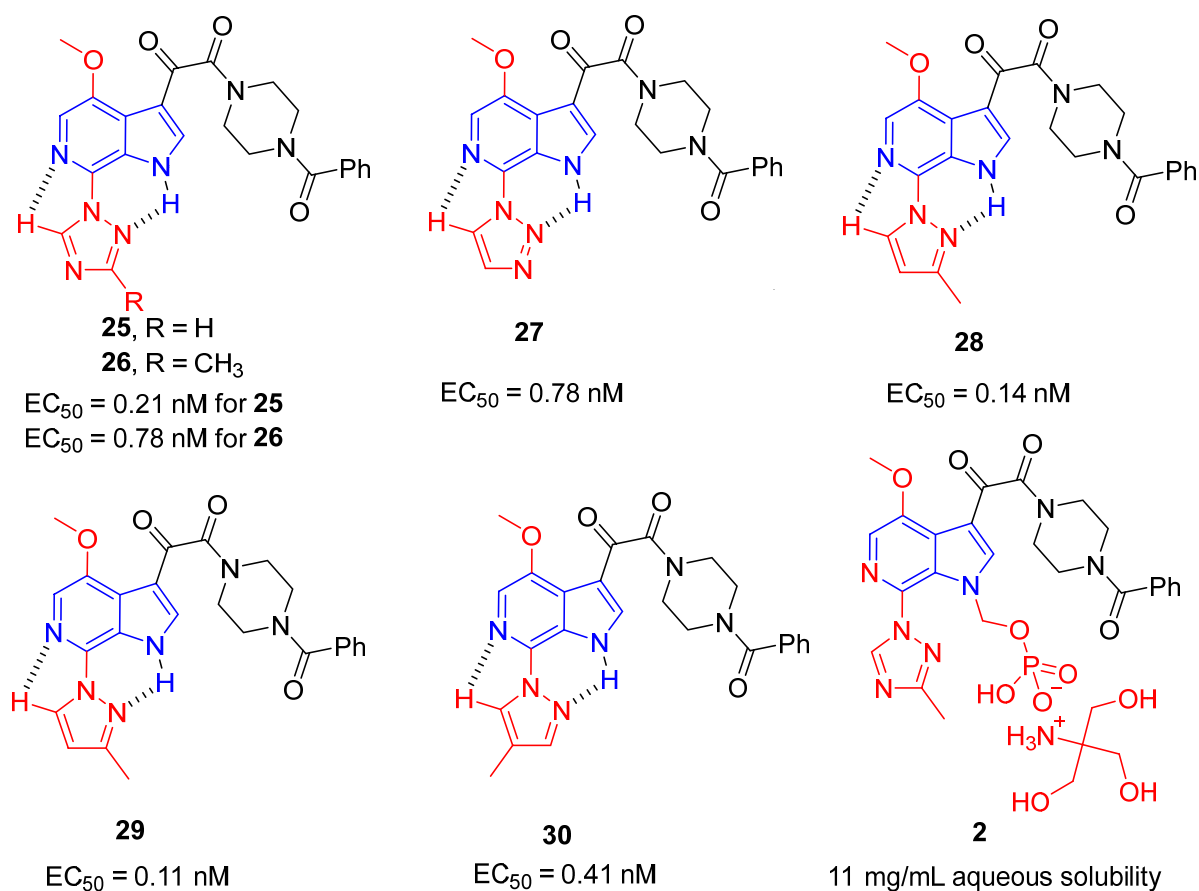

Figure 12. Structure, intramolecular H bonding between N-linked C-7 azoles and the 6-AI ring (**25**−**30**), and structure of fostemsavir (**2**).
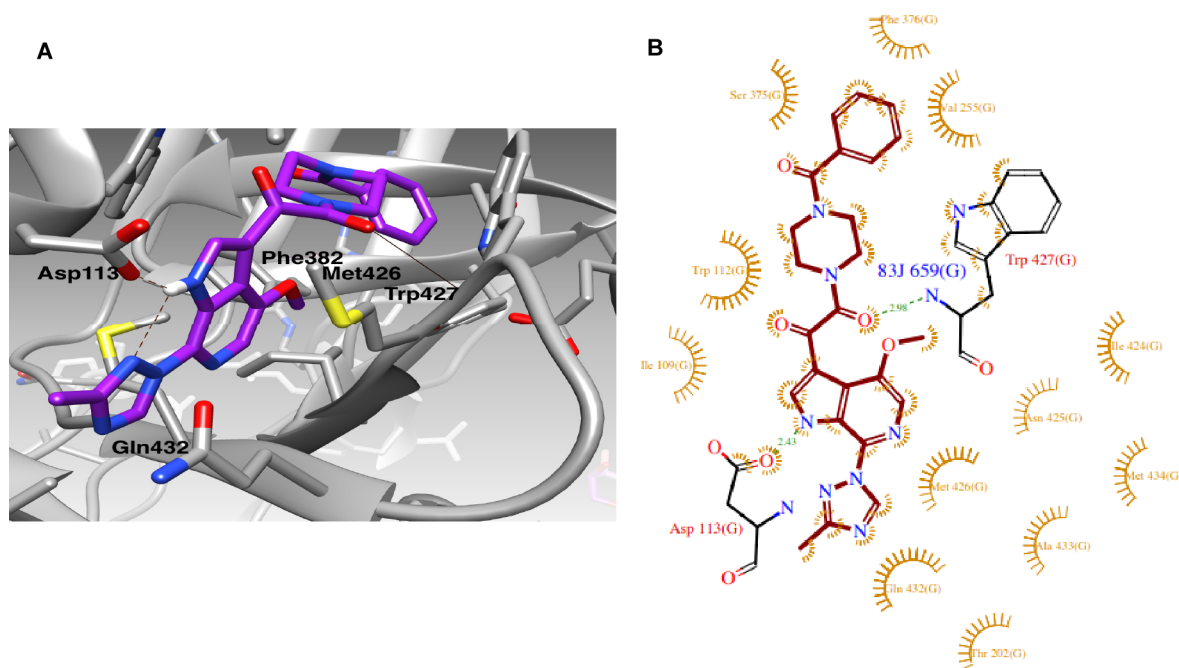
Figure 13. (A) Temsavir (**26**) binds between the inner and the outer domains of gp120 and under the $\beta20-\beta21$ loop (PDB 5U7O). AI moiety interacts with gp120 via hydrophobic interactions and forms H bonds with Asp113 from the $\alpha1$-helix of the gp120 inner domain and Trp427 of the outer domain. Benzamide moiety occupies the site of gp120 that is occupied by Trp427 in the open state such that Trp427 and the $\beta20-\beta21$ loop are pushed toward the CD4-binding loop, thereby blocking CD4. (B) Two-dimensional diagram of temsavir interactions with the gp120 protein. (C) Structure of temsavir (**26**).

This SAR study discovered C-7 as a viable site of conjugation on the attachment inhibitors for increased antiviral activity.

The mAb-conjugated derivative **34** showed higher IC$_{50}$ values when compared to the nonconjugated derivative **32**, suggesting that the bivalent conjugate between the small molecule and the antibody does not interact effectively with HIV-1 gp120. Hence, a similar strategy may facilitate their application in designing novel chemically programmed antibodies, chemically programmed vaccines , and topical microbicides.[59]

A field-based three-dimensional (3D) virtual-screening program using Blaze (Cresset, Litlington, UK) software was carried out by Tuyishime et al. in the search for new leads to design a novel HIV-1-entry inhibitor.[60] Initially, a bioactive 3D conformation template for screening and bioisosteric replacement was created by applying field and shape information from compounds **26**, **7**, and **10** (Figure 16). This template consists of a field point pattern showing a condensed representation of the compound's shape, electrostatics, and hydrophobicity. When two structures have similar field point patterns, they are predicted to have similar receptor receptivity patterns. The top 1000 compounds out of 6 million commercially available compounds were found to have field point similarity to the template molecule **26** (Figure 16). Fifty of them were purchased and evaluated for their activity against the HIV-1$_{YU-2}$env pseudotype and amphotropic murine leukemia virus (AMLV) env pseudotyped HIV-1 virus. However, this study resulted in very few potent structures, with **35** demonstrating an IC$_{50}$ value of 13.1 μM (Figure 16). Compound **35** lacks an azaindolic NH moiety, which is a critical element of the HIV-1 attachment inhibitor pharmacophore, and while showing a degree of chemical diversity, it shares the piperazine benzamide moiety found in the BMS compounds.

Furthermore, an in silico scaffold-hopping experiment and subsequent in vitro studies revealed that replacement of the piperazine ring of **35** with a octahydropyrrolo[3,4-c]pyrrole heterocycle (**36**) preserved the in vitro antiviral properties. By appending the headgroup of **36** to **8**, a new molecule **37** was designed and synthesized to study the potential attributes of octahydropyrrolo[3,4-c]pyrrole substitution (Figure 16). In subsequent studies, a 1,2,4-triazole ring was incorporated at the C-7 position of the AI, yielding **38**, which exhibited an IC$_{50}$ value of 0.0008 μM in a HIV-1$_{JR-CSF}$ assay. In a parallel study, the cyclohexene variant **39** of **38** was also designed, which exhibited high antiviral potency, i.e., IC$_{50}$ values of 2.0 and 0.6 nM against HIV-1$_{JR-CSF}$ (pseudotyped HIV-1 virus) and HIV-1$_{HxBc2}$ (wild-type mutant), respectively.

Recently, a group of researchers tried lattice-based engineering in an effort to identify better conditions for obtaining cocrystal data with HIV-1 entry inhibitors. In this study, small-molecule-based entry inhibitors, including temsavir (**26**), were examined against the improved lattice (Figure 17).[61] From the compounds screened, **40** showed ~100-fold higher potency than **26** against laboratory-adapted HIV-1 strain NL4-3 (EC$_{50}$ values = 0.019 vs 2.2 nM) and ~20-fold higher potency (IC$_{50}$ ≈ 0.002 μM) than that of **26** (IC$_{50}$ ≈ 0.04 μM) against a panel of 30 strains of HIV-1. Interestingly, more than one-half of the virus strains were neutralized with IC$_{50}$ values in the subnanomolar range. Further, **40** showed 10.6-fold higher potency (IC$_{50}$= 0.0015 μM) than **26** (IC$_{50}$ = 0.0159 μM) against 208 strains of HIV-1. Moreover, in isothermal calorimetry studies, **40** showed 8.6-fold higher affinity toward the HIV-1 env trimer than **26**. It was observed that the piperidine ring in **40** adopted a twisted-boat conformation and had higher energy as compared to other derivatives of this class of compounds having a piperidine ring in the chair conformation.
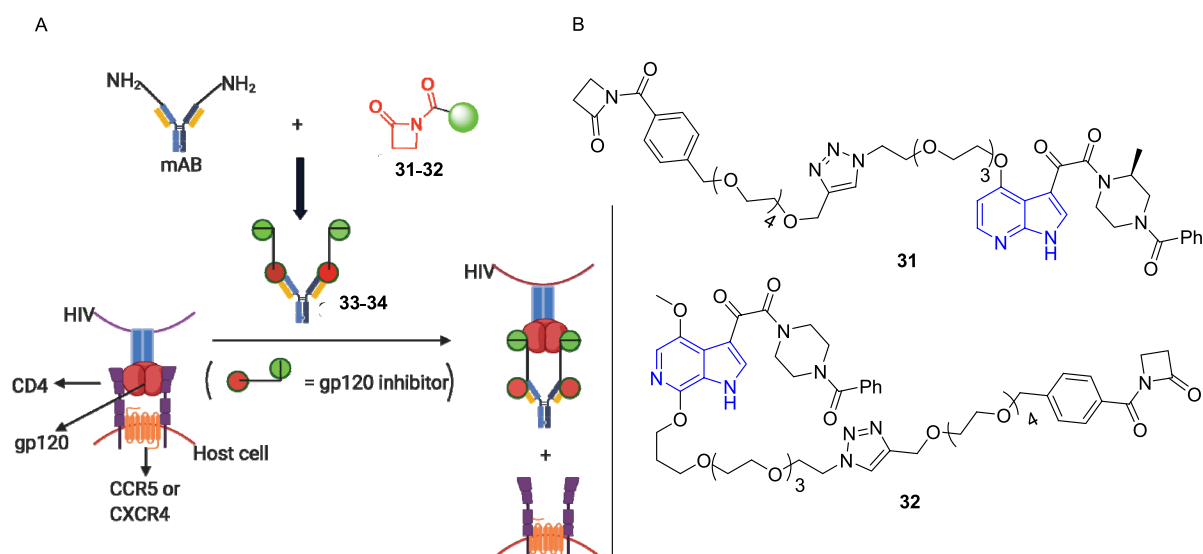
A)

3 ⟶ 4, 6 (F, Cl, Br, CN, OMe substitution either at C-4 or both on C-4 & C-7; boost antiviral potency)

6 ⟶ 10 (N-insertion at C-6; prevent reactive indoloquinone metabolite formation)

10 ⟶ 12 (phosphonooxymethyl prodrug; enhances aqueous solubility than the parent drug 10)

4 ⟶ 7 (enhanced aqueous solubility)

4 ⟶ 14 (enhanced aq. solubility, potency, HLM stability and membrane permeability)

14 ⟶ 23 (triazole helps in forming nonbonded interaction, C-6 nitrogen improved PK profile)

23 ⟶ 24 (phosphonooxymethyl prodrug; improves pharmaceutical properties)

7 ⟶ 25 (coplanar 1,2,4 triazole addition at C-7; improved PK profile than 23 and 10)

25 ⟶ 26 (methyl substitution at C-3 of 1,2,4 triazole; prevent cardiac and drug interaction liabilities of 25)

26 ⟶ 2 (phosphonooxymethyl prodrug fostemsavir 2 got FDA approval)

B)

Figure 14. (A) Summary of the structure−activity-guided optimization of HIV-1 entry inhibitors leading to the discovery of fostemsavir. (B) Required structural features of AI-based HIV-1 attachment inhibitors.

Figure 15. (A) Inhibition of the HIV-1 gp120 protein through the monoclonal antibody (mAb)-conjugated inhibitors **33** and **34** synthesized from *N*-acyl-*β*-lactams **31** and **32**, respectively; mAb covalently linked to **33** and **34** promoted binding of these molecules to gp120 and inhibited CD4-mediated entry of HIV-1 into cells. (B) Structures of *N*-acyl-*β*-lactam derivatives **31** and **32** derived from **7** and **10**.
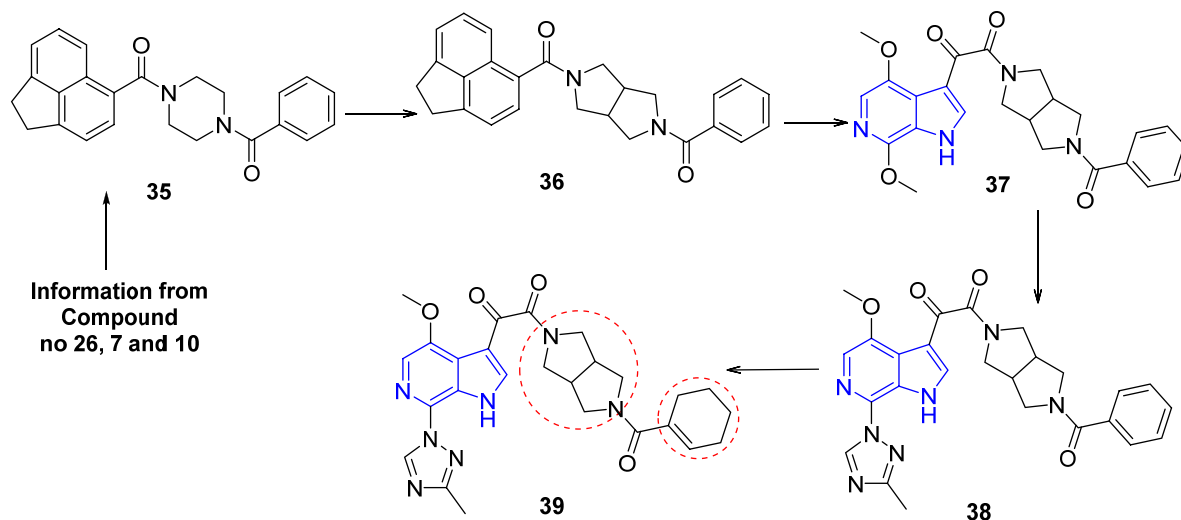

Figure 16. Structure of the top-scored entry inhibitors using the Blaze (Cresset, Litlington, UK) field-based virtual screen experiments. Point-wise procedure was as follows: (1) a relevant bioactive conformation was prepared based on an active molecule, (2) field points were generated to its specified conformation to obtain the Blaze pharmacophore seed, (3) alignment of every structure to this seed was searched in the Blaze database based on their field point patterns, and (4) top-scoring molecules are listed as 3D alignments to the search query, along with their score (molecular similarity based on 50% shape, 50% fields).

Investigation of the cocrystal structures of **40** with the BG505 SOSIP.664 env trimer revealed hydrophilic interactions between the tail of **40** and the BG505 trimer protein. The direct interaction of the *N*-acylethanolamine tail with the side chains of residues Lys117, Arg429, and Gln432 of the HIV-1 env trimer through its terminal hydroxyl group accounted for the improved potency of **40**. In addition, an H-bond was formed between Asp113 of env and the amidic nitrogen on the tail of **40**. Furthermore, these functional groups present on the tail can adopt different conformations that are, in turn, useful to accommodate the different conformations of the *β*20−*β*21 structural element in different viral clades. Compound **40** was found to be potentially versatile for interacting with HIV-1 env as its tail contains two functional groups that can be either hydrogen-bond donors or acceptors. Thus, investigation of the

functional groups on the tail side of other AI analogs may lead to a better understanding of protein-binding interactions.

3.2. HIV-1 Integrase Inhibitors. Integrase strand transfer inhibitors (INSTIs) are a class of antiretroviral agents used to treat HIV-1 infection. Four drugs raltegravir (**41a**), elvitegravir (**41b**), dolutegravir (**41c**), and bictegravir (**41d**) are used for the treatment of patients preferably in combination with two nucleosides reverse transcriptase inhibitors. HIV-1 integrase (IN) is responsible for catalyzing viral cDNA integration into the host cell genome.[62,63] Since human cells lack a homologue, HIV-1 IN has been considered an attractive therapeutic target for HIV-1 treatment. However, the appearance of mutations in integrase causes resistance to several IN inhibitors, and the development of better tolerable and more effective drug
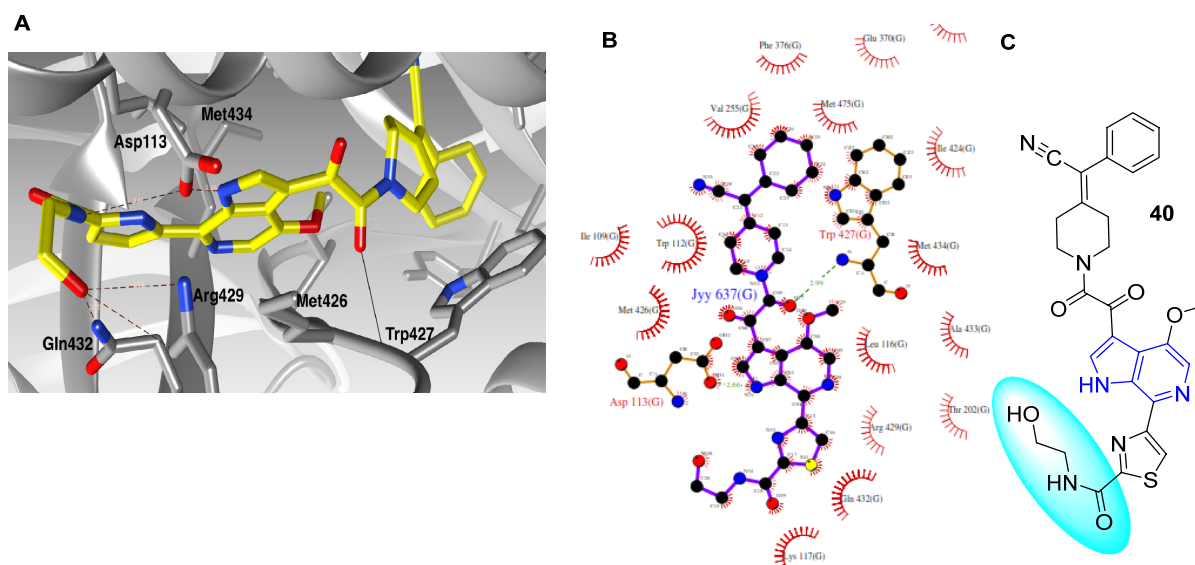
Figure 17. (A) Interaction of **40** with the BG505 SOSIP.664 env trimer (PDB 6MU7), resulting in improved lattice and molecular features associated with enhanced neutralization potency; **40** is shown as yellow sticks. (B) Two-dimensional diagram demonstrating the interaction between the inhibitor (**40**) and BG505 SOSIP.664 env trimers. (C) Structure of **40**.
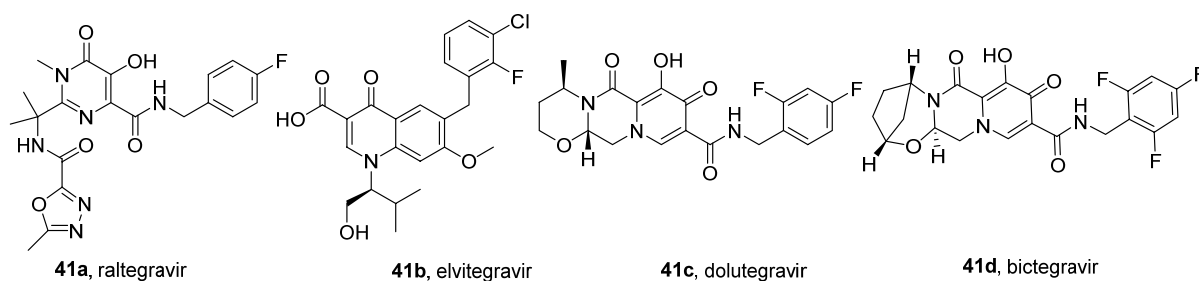

Figure 18. FDA-approved HIV-1 integrase inhibitors **41a–d**.

regimens aiming to improve long-term HIV-1 therapy remains an unmet need.[64,65]

The discovery of improved integrase inhibitors has mainly focused on preventing the incorporation of viral DNA into the host genome by inhibiting the metal-dependent activity (Mg^{2+}/Mn^{2+}) of the integrase-regulated strand transfer (ST) step.[66–68] The active site of IN adopts an active conformation in which the carboxylate groups of Asp64, Asp116, and Glu152 coordinate two Mg^{2+} ions near the reactive 3′-OH of the viral DNA. One metal ion, coordinated by Asp128 and Glu221, activates the 3′-OH group of the viral DNA for ST. Simultaneously, the other ion, bound by Asp128 and Asp185, destabilizes the scissile phosphodiester group in the target DNA. When used in highly active antiretroviral therapy (HAART), the pyrimidine-based integrase inhibitor raltegravir (**41a**) demonstrated significant and sustained suppression of viral RNA levels to fewer than 50 copies/mL accompanied by a substantial increase in CD4 immune cell counts.[69] Long-term therapy in HIV-1-infected subjects with **41a** induced mutations at amino acids 143, 148, and 155 in integrase together with associated secondary mutations. The Gly155His mutants emerge first and are eventually replaced by Gln148His mutants usually in combination with Gly140Ser. In addition to the above mutations, viral strains isolated from patients also harbor Tyr143Arg and Gln148Arg mutations. These mutations have become the primary cause of resistance to **41a** in HIV-1-

infected subjects. Elvitegravir (EVG, **41b**, Figure 18),[70] which contains a quinoline core and dolutegravir (DTG, **41c**, Figure 18),[71] which contains a pyrido[1′,2′:4,5]pyrazino[2,1-b][1,3]-oxazine core, were the next set of drugs approved which have displayed improved efficacy against RAL-resistant strains.[72–74] However, viral strains that are highly resistant to EVG and DTG demonstrated multiple mutations in the integrase protein.[75,76] Bictegravir, **41d** (2,5-methanopyrido[1′,2′:4,5]-pyrazino[2,1-b][1,3]oxazepine) and **41c** (Figure 18) share similar functional characteristics and have much higher genetic barriers to resistance.[77] **41d** displayed inhibitory activity against HIV-1 strains resistant to INSTI's as compared to **41c**. The double mutants Gly140Ser/Gln148Arg and Gly140Ser/Gln148His showed higher susceptibility to **41d** as compared to **41c**.[78]

Earlier literature showed that apart from metal-binding motifs, a hydrophobic aryl chain that coordinates to a proximal hydrophobic pocket via specific interactions is also necessary to inhibit the strand-transfer step.[79,80] Accordingly, different types of core moieties have been studied, including hydroxylated aromatics, diketo acids, naphthyridine carbox-amides, pyrrolloquinolones, dihydroxypyrimidine carboxa-mides, AI hydroxamic acids, 2-hydroxyisoquinoline-1,3-(2H,4H)-diones, 6,7-dihydroxy-1-oxoisoindolines, quinolone-3-carboxylic acids, and carbamoylpyridines. AI-based carbox-ylic acids **42a** and **42b** emerged from further SAR studies, but
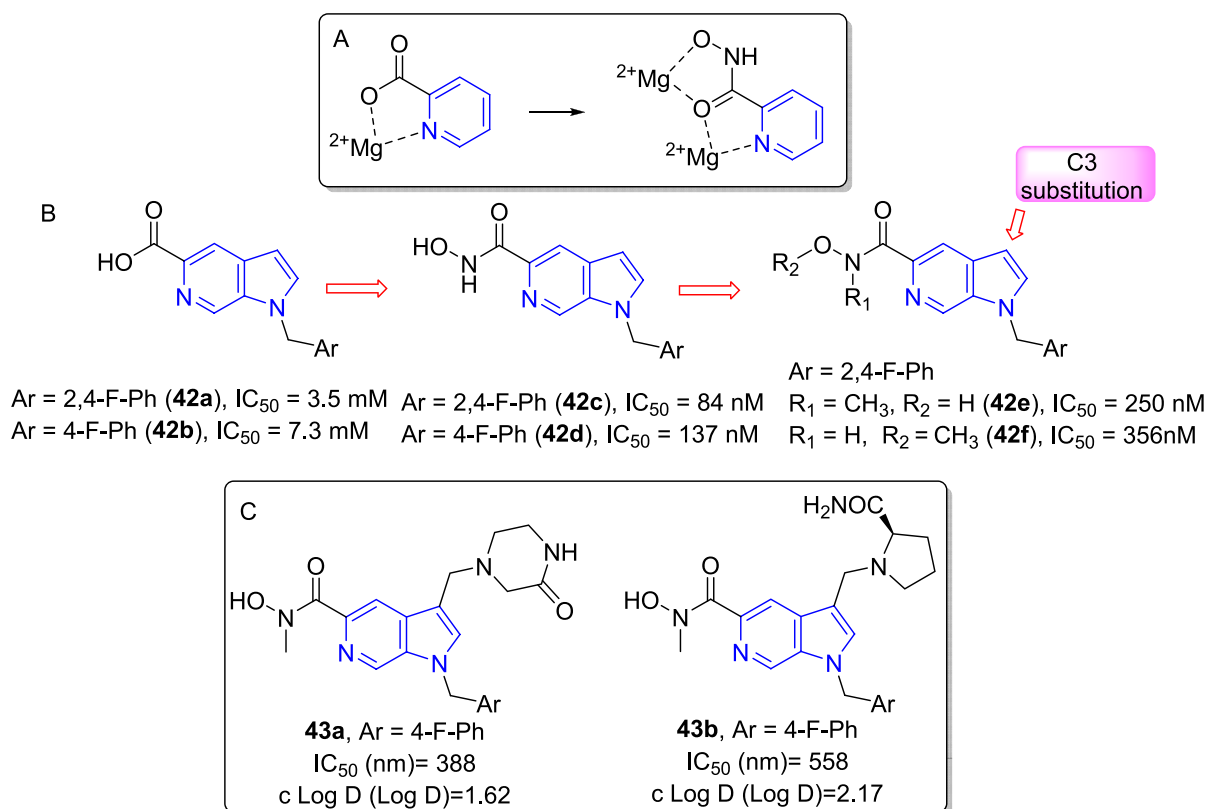
Figure 19. (A) Bidentate metal binding of picolinic acid and binding of two Mg^{2+} ions to picolinic hydroxamic acid. (B) Structural modification from AI carboxylic acids **42a** and **b** to the AI hydroxamic acids **42c** and **42d** and then to the N- and O-alkylated derivatives **42e** and **42f**. (C) Modification of the AI N-methyl hydroxamic acid core at the C3 position in the search for potent inhibitors **43a** and **43b** of the HIV-1 IN enzyme.
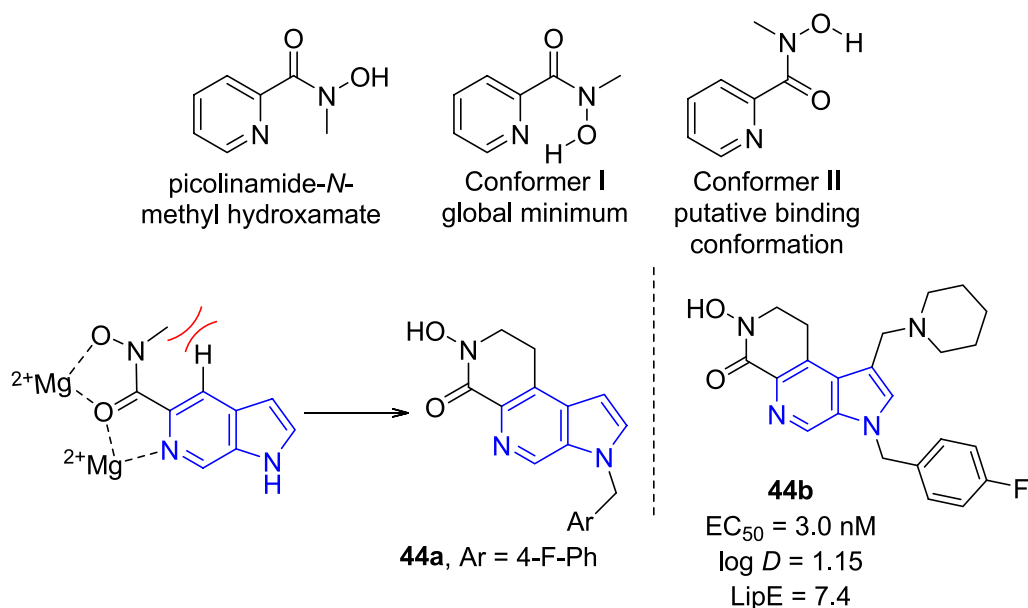

Figure 20. Structure of the 6-AI hydroxamate-based active molecule **44b** and its potency.

due to their modest activity and good ligand efficiencies (Figure 19A), they were further modified to AI−hydroxamic acids **42c** and **42d** (Figure 19B).[81]

These hydroxamic acids have shown a 40-fold increase in potency in enzymatic assays as compared to carboxylic acid-containing compounds and offered structurally simple scaffolds as novel HIV-1 IN inhibitors (Figure 19B).[81] However,

following metabolic modification that can lead to activation, these compounds can undergo a Lossen rearrangement to yield potentially mutagenic isocyanates. Therefore, to prevent this reaction process, alkylation of either the NH or the OH was explored; however, this resulted in a small loss in potency for **42e** and **42f**. The N-methylated compound **42e** showed stability against oxidative metabolism in human liver micro-
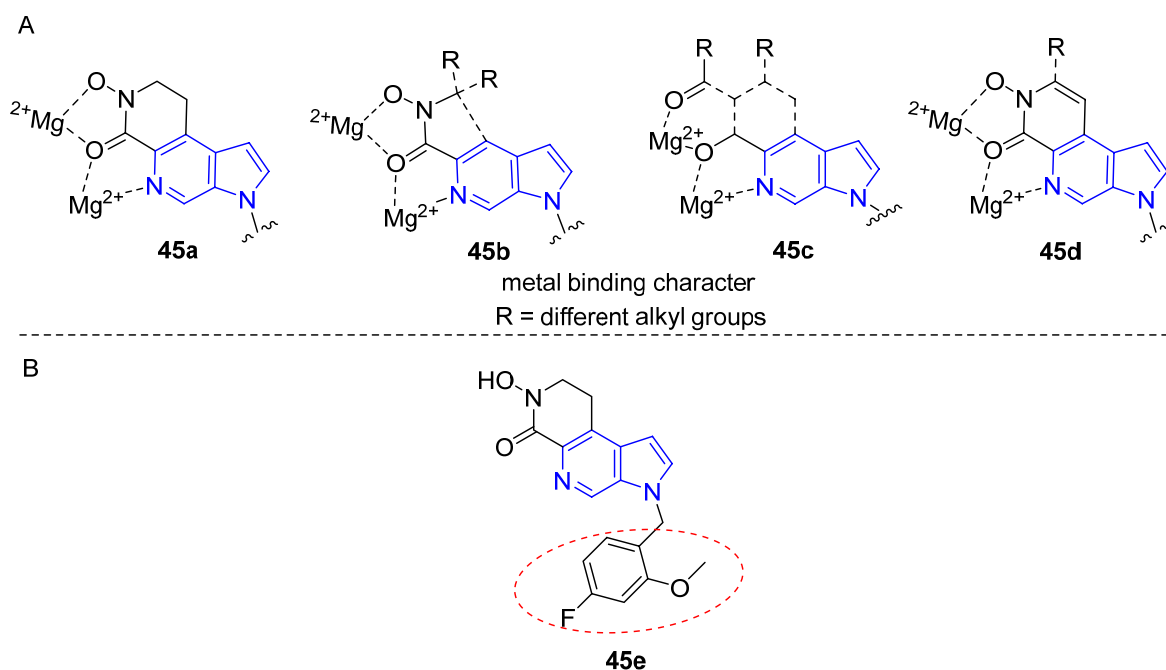
Figure 21. (A) Generalized structures with a metal-binding character from the 6-AI series targeted to lower phase 2 metabolism. (B) Dihydronaphthyridinone system containing the active molecule **45e**.

somes but was rapidly cleared by phase 2 metabolism via glucuronidation in dogs (Figure 19B). Here, increasing the size of the alkyl group did not modify the turnover rate in human hepatocytes and a reduction in antiviral activity was observed. When both N and O-atoms in the AI hydroxamic acid were alkylated, there was a complete loss of HIV-1 integrase inhibitory activity.

Attempting to attenuate glucuronidation rates and improve the metabolic stability, the β position (C-3) of the pyrrolyl ring of the AI nucleus was substituted with amines, ethers, amides, and acyclic C chains.[82] The substitution patterns of a piperazin-2-one (**43a**) and (S)-pyrrolidine-2-carboxamide (**43b**) at the C-3 position of 6-AI derivatives (Figure 19C) emerged as active molecules with half-lives of 1.2 and 6.2 h, respectively, in a dog PK experiment. Further, human PK parameters for the N-methyl hydroxamate (**42b**) were projected from dog PK data, which suggested low blood clearance (Cl_b = 5.5 mL/min/kg) and moderate bioavailability (F = 41%) and a reasonable half-life (4.5 h). This core showed lower log D values as compared to earlier hydroxamic acid analogs, resulting in an attenuated clearance rate in human hepatocytes.

Since the N-methyl AI hydroxamates **43a** and **43b** were found to have an allylic-type steric interaction between the eclipsed hydroxamate N-methyl group and the 4-H atom of the pyridine ring of bicyclic systems (Figure 20), conformational analysis of simplified picolinamide-N-methyl hydroxamate was performed in order to evaluate the impact of this interaction on the viral inhibition activity.[83] The global minimum calculated for picolinamide-N-methyl hydroxamate (Figure 20) was found to be a pyridine N−H-bonded conformer **I** (NCCO torsion = −179.42°, ONCO torsion = −178.77°) in which all relevant atoms from the pyridine N to the hydroxamate O were essentially in the same plane. Conformer **I** was assigned to have ΔE = 0.0 kcal/mol. Among the five possible conformers, the best conformer **II**, with a constrained

coplanar metal-binding domain, showed a very high ΔE value of 5.926 kcal/mol that was higher in energy than **I** (NCCO torsion = 0.34°, ONCO torsion = 0.32°). Therefore, to overcome this issue, conformational restriction by the introduction of a ring was explored as an approach to restraining the metal-binding motif, resulting in N-hydroxy-dihydronaphthyridinone **44a**. This molecule exhibited higher potency and a lower log D value which translated into an improved LipE value. In addition to the six-membered N-hydroxy-dihydronaphthyridinone **44a**, the seven-membered ring retained nanomolar biochemical and cellular inhibitory potencies with an IC$_{50}$ value of 23 nM and EC$_{50}$ value of 18 nM, respectively. The five-membered ring homologue lost significant potency, presumably due to the modified "bite" angles which would differentially reduce the metal-binding ability (Figure 20). Hence, the six-membered ring was pursued further.[83] The above data showed that the locked conformation of the metal-binding motifs contributed significantly to the formation of a stable $M(HL^2)_2$ complex (where M = Mg^{2+}, Mn^{2+} and L = ligand) and thus was more beneficial for coordination with the catalytic core of the enzyme.

In the substituted class, the C3-piperidine **44b** exhibited a better combination of antiviral potency, membrane permeability, and clearance in both human liver microsomes and human hepatocytes (Figure 20).

Compound **44b** showed human PK predictions that were comparable to **43b** but offered 300-fold higher antiviral potency, resulting in a significantly lower projected human dose of 32 mg bid that would offer improved safety margins.

Further, substitution of three carbon chains at the C-3 position confirmed tolerance within the pharmacophore but poor bioavailability following oral administration. Therefore, considering each subseries of substitution at C-3, the general trend toward higher LipE values at lower log D was observed, which is of interest and perhaps counterintuitive. The β-substituent is solvent exposed and does not require extensive
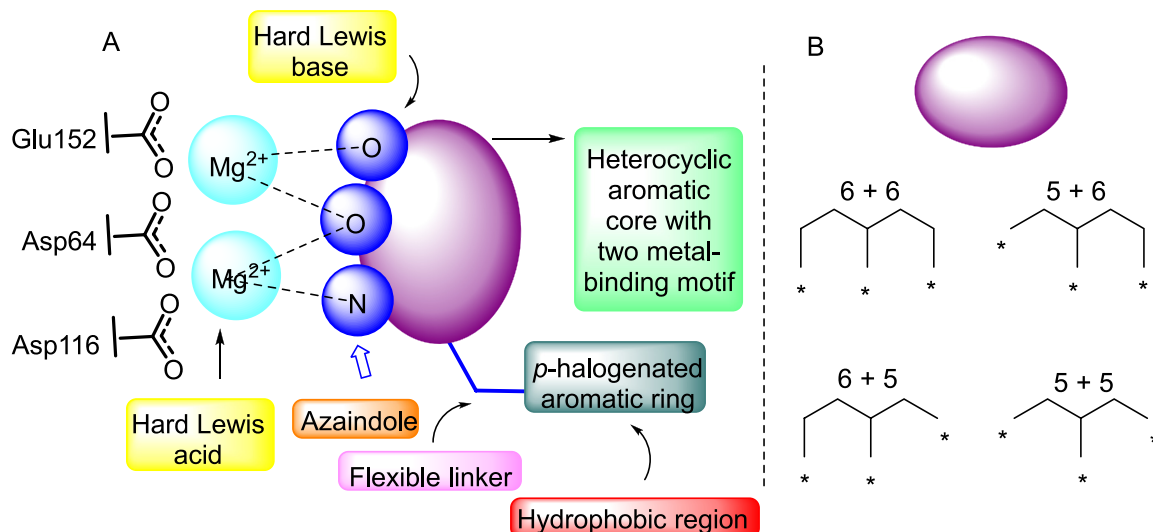
Figure 22. (A) Two metal-binding pharmacophore model of the IN inhibitor. (B) Planar heteroaromatic pharmacophore can be of 6 + 6, 5 + 6, 6 + 5, and 5 + 5 fused ring system.

desolation for binding; however, additional interactions with the protein or metal bound to the protein cannot be discounted. Finally, placing a sulfonamide substituent at C-3 afforded the desired virus inhibition and LipE properties but led to poor absorption, a possible effect of low permeability due to the polar sulfonamide moiety. All of the C3-substituted derivatives were able to attenuate clearance rates in human hepatocytes.

In further study, a medicinal chemistry strategy was applied that largely retained the naphthyridinone ring system that efficiently coordinated to bound metal ions (**45a**) while introducing structural changes that can be effective for improving the extent and rate of conjugation of the *N*-hydroxyl group (**45b** and **45d**), such as steric hindrance of a hydroxyl group and electronic deactivation or removal of this group (**45c**, Figure 21A).[84] On the basis of these points, substitutions around the dihydronaphthyridinone and benzyl systems were made.

In this series, **45e** (Figure 21B) was designated a potent ST inhibitory candidate (IC_{50} = 40.5 nM) that showed no activity against DNA polymerase α/β, targeted human liver microsome stability, and appreciable aqueous solubility. Compound **45e** successfully inhibited laboratory strains and patient viral isolates cultured in peripheral blood mononuclear cells.

No significant inhibition of ion channels, receptors, enzymes, or transporters in a CEREP broad ligand-screening panel was observed with **45e**. In addition, an advantage in terms of potency over the approved ST inhibitors **41a** and **41b** was found compared with that of the wild type for all of the mutants tested. Compound **45e** (Figure 21B) exhibited a <10-fold difference in potency compared with that of the wild type for all of the mutants tested with one exception, the double-mutant Gly140Ser/Gln148Lys virus.

The projected pharmacokinetic profile of **45e** in humans suggested a clearance rate of 18 mL/min/kg, a volume of distribution of 5.7 L kg^{-1}, 2 mL/min/kg in vivo hepatic clearance from liver microsomes, 5 mL/min/kg in vivo hepatic clearance from liver microsomes + UDPGA (uridine-diphospho-glucuronic acid), 6 mL/min/kg in vivo hepatic clearance from hepatocytes, and a short half-life of 2.8 h.

However, due to its projected short half-life, **45e** was not further pursued for clinical development.

On the basis of the studies explained above, we propose a 6-AI-containing planar heteroaromatic two-metal-binding pharmacophore model to design potent integrase inhibitors (Figure 22). The additional nitrogen atom of the 6 AI nucleus interacts with the Mg^{2+} or Mn^{2+} ions through coordinate bond formation present at the active site of IN enzyme. The nitrogen and oxygen atoms are known to be hard Lewis bases, while Mg^{2+} is a hard Lewis acid.[66,85] The hard Lewis bases act as donors, and the acids acts as acceptors. At the N-1 position, a flexible linker of 2−3 carbon atoms and an aromatic group that extends into an adjacent hydrophobic space are crucial for designing a potent inhibitor chemotype.

HUMAN ORTHOPNEUMOVIRUS/RESPIRATORY SYNCYTIAL VIRUS (RSV)

Respiratory syncytial virus (RSV) is a respiratory pathogen that belongs to the *Paramyxoviridae* family with a single-stranded, negative-sense RNA (15.2 kb) genome.[86,87] RSV is the main cause of bronchiolitis and acute lower respiratory tract infection (ALRTI) in infants, adults, and immunocompromised patients.[88] The viral envelope is comprised of three proteins: the fusion protein (F), attachment glycoprotein (G), and small hydrophobic (SH) protein.[89] The virulence of RSV occurs mainly through the surface proteins F and G. The initial step of RSV attachment to the host is carried out by the G protein, while the F protein mediates RSV envelope fusion, which releases the viral genome into the host cell, while the role of the SH protein in either process is somewhat enigmatic. There are two subtype strains, RSV-A (629 bp) and RSV-B (724−762 bp), which are defined by the nucleotide sequences in the ectodomain of the F protein. As the RSV F protein is a key player in viral infection, it is imperative to discuss the structure and mechanism of this protein.

RSV Fusion Protein. The RSV F protein is a glycoprotein that after proteolysis is comprised of two subunits, a 55 kDa, carboxy-terminal F_1 subunit (137−574 residues) and a 15 kDa amino-terminal F_2 subunit (26−109 residues).[90] The F_1 and F_2 elements are covalently connected via disulfide bonds to form a heterodimeric protomer. Three F_1/F_2 heterodimers associate
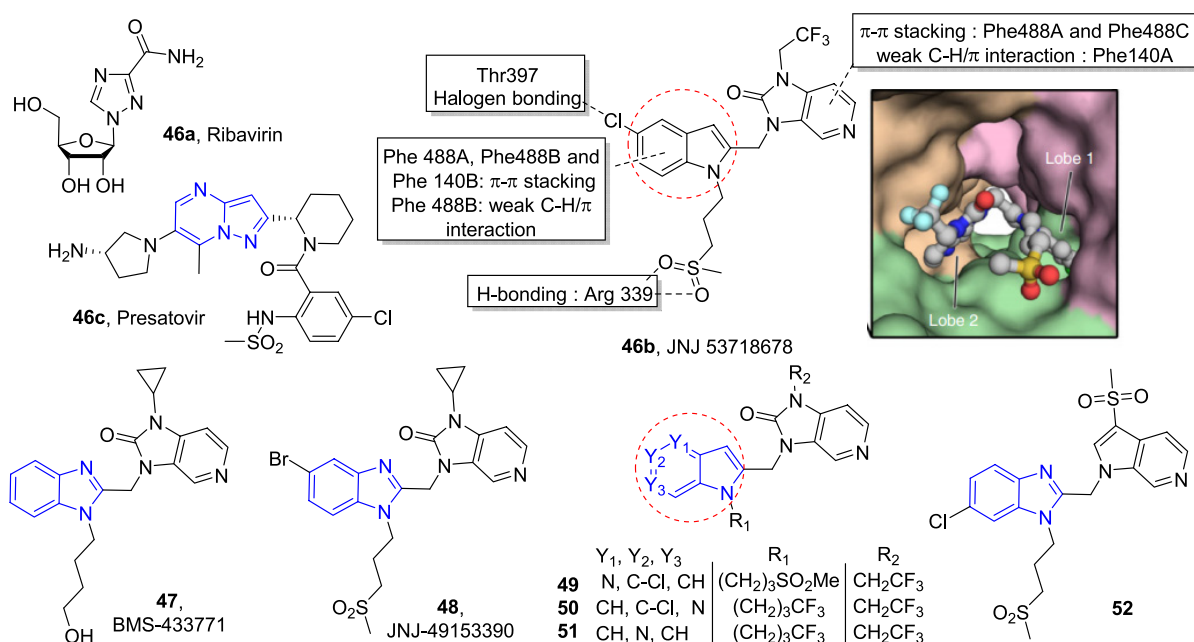
Figure 23. Simplified 2D ligand interaction of JNJ 53718678 (**46b**) with prefusion RSV F. RSV F is shown as a molecular surface with three identical protomers, each shown in a different color (F$_A$, green; F$_B$, pink; F$_C$, tan). JNJ53718678 is shown as a ball-and-stick representation with carbon atoms colored in gray, nitrogen atoms in blue, oxygen atoms in red, chlorine atoms in dark green, fluorine atoms in light blue, and sulfur atoms in orange. (Inset) Magnified view of the binding of JNJ53718678 into the central cavity. Conversion of **46b** into different benzimidazoles (**47**, **48**, and **52**) and AI isomers accommodating respiratory syncytial virus (RSV) fusion inhibitors (**49**−**51**).

to form the mature trimeric form of the F protein. The trimerization results in a spheroidal-shaped prefusion conformation of the F protein heterodimer. The unstable prefusion conformation of F is refolded into the postfusion conformation. During the refolding, the fusion peptides are withdrawn from the central cavity and projected away from the viral membrane. If another membrane, such as a host cell membrane, is in close proximity, the fusion peptides will insert into the membrane with the F protein thus binding to both membranes. The prefusion confirmation is highly unstable and proceeds to refold via association of the heptad repeats present in the amino and carboxyl termini of the F$_1$ subunit. Once again, a trimer of hairpins is created that helps to pull the viral membrane and host membrane together to promote membrane fusion.

The postfusion conformation of F is highly stable and melts at >90 °C. From the literature, it is well known that at some basal rate the unstable prefusion conformation of RSV F converts into postfusion confirmation. It was observed that both longer incubation times and incubation at elevated temperatures increase the conversion to the postfusion conformation.[91,92] This process of refolding is irreversible, giving a stable postfusion confirmation of F protein.

There have been a number of mechanisms proposed for the entry of RSV in host cells. RSV-infected cells fuse with neighboring cell membranes to generate multinucleated cells called syncytia. A more recent report indicated that the initial steps of RSV fusion occur at cholesterol-rich microdomains in the plasma membrane.[93] A subsequent study demonstrated that RSV utilizes macropinocytosis as an initial entry mechanism followed by fusion in endosomes.[94] Thus, the evidence now suggests either a two-step fusion event or fusion in endosomes after macropinocytosis. However, it may be the case that RSV can fuse at both the plasma membrane and in endocytic vesicles with different efficiencies depending on the

environmental conditions and target cells. Other options for the fusion mechanism, i.e., provocation by a second viral glycoprotein[95,96] and a clamp model,[97] were also not reassuring.

The current belief is that the infectious cycle RSV starts with virion attachment to the apical surface of polarized, ciliated airway epithelial host cells. Subsequently, the viral fusion (F) glycoprotein causes fusion of the viral and host cell membranes by undergoing a drastic conformational change. After fusion, the helical ribonucleoprotein complex (RNP) is released into the host cell cytoplasm followed by replication and transcription which occur in the cytoplasm in viral inclusion bodies that produce viral products. The viral RNA-dependent RNA polymerase (RdRp) complex is responsible for transcribing viral mRNA and synthesizing positive-sense nongenome intermediates required for replication of new negative-sense genomes for packaging into virions.

Clinical Intervention To Inhibit RSV Infection. There has been a persistent attempt to develop an effective treatment regimen to control RSV infection since the discovery of the virus in the 1950s. Palivizumab (Synagis) is a humanized IgG-1 mAb that binds the RSV-F protein A epitope and is administered as an intramuscular injection.[86,98] IgG antibodies, which are involved in the secondary immune response, have a half-life of approximately 20 days. Palivizumab offers greater activity against RSV and the relative ease of administration of a smaller volume of drug as an injection, compared with RSV-IGIV (RSV immune globulin intravenous, a polyclonal IgG product with a high content of anti-RSV IgG). This drug was approved for the treatment of infants aged less than 2 years who are suffering from RSV with hemodynamically significant congenital heart disease (HSCHD). It provides immunoprophylaxis against serious lower respiratory tract infections (LRTIs) caused by respiratory syncytial virus (RSV).[86] Ribavirin (**46a**), discovered in 1972 by Witkowski and co-
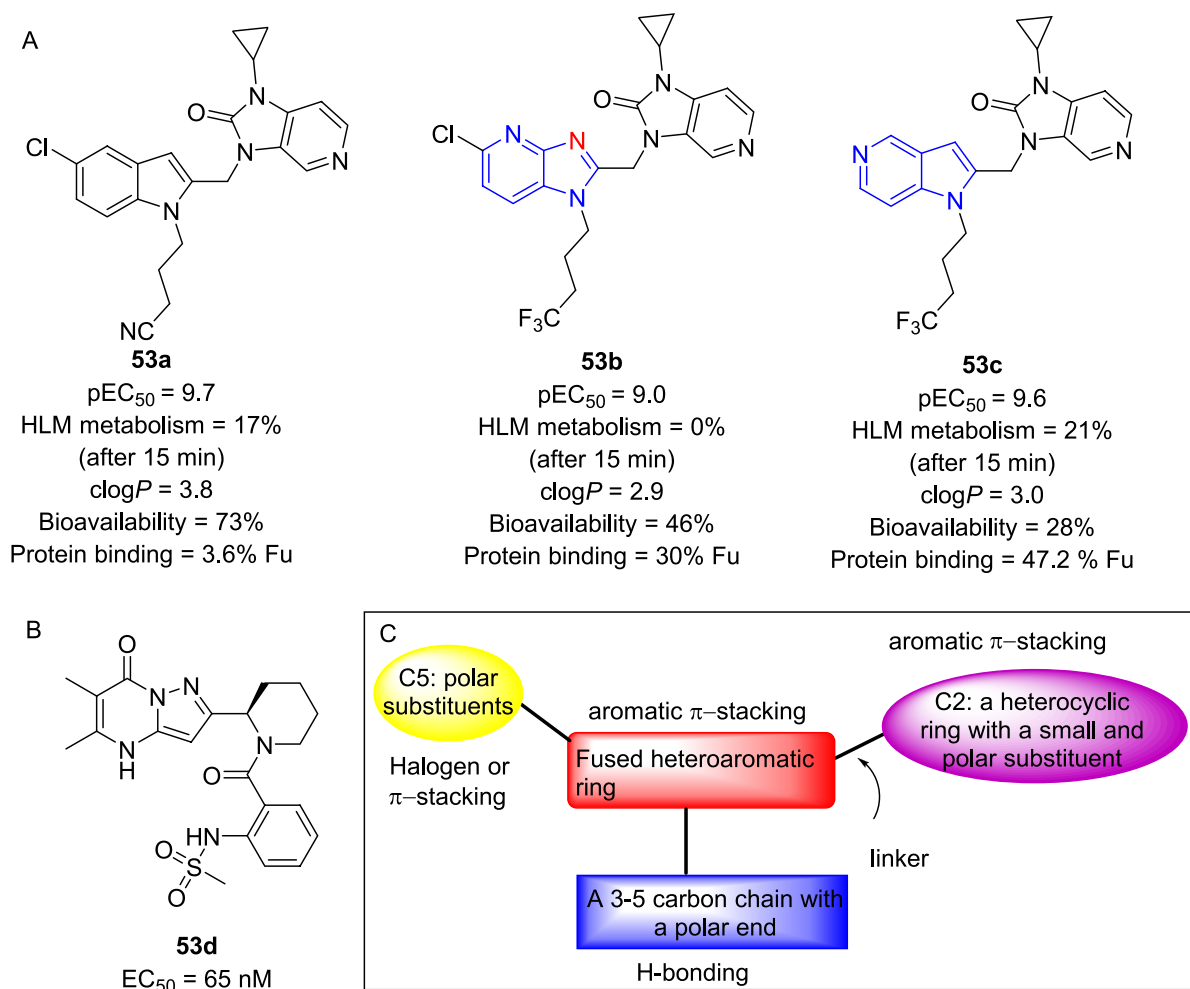
Figure 24. (A) Structures of RSV inhibitors containing indole (**53a**), azabenzimidazole (**53b**), and AI (**53c**). (B) Pyrazolo[1,5-*a*]pyrimidin-2-yl analog of RSV inhibitors (**53d**). (C) Model for the design of RSV F inhibitors.

workers,[99] is a guanosine analog that exhibits broad-spectrum activity against several RNA and DNA viruses (Figure 23).[100] Although originally approved only for the treatment of severe RSV infection in children,[101] it was later used for the treatment of other viruses. Ribavirin (**46a**) suffers from low efficacy and requires an aerosol/intravenous (IV) mode of administration. It is also teratogenic so poses a threat to healthcare workers who may be exposed to ribavirin aerosols.

On the basis of phenotypic screening of chemical libraries, several novel small-molecule-based RSV fusion inhibitors have been identified.[90] Subsequently, on the basis of crystallographic investigations, it was observed that these small molecules bound to a fusion intermediate of F and prevented the formation of the postfusion conformation. To date, all known RSV small-molecule fusion inhibitors bind in the same pocket and have the same mechanism of action. Two fusion inhibitors, JNJ 53718678 (**46b**) and GS-5806/presatovir (**46C**), have been advanced into phase II clinical trials and performed well in these studies. RSV inhibitor **46b** binds to a pocket inside the trimeric ectodomain of the RSV F protein. This molecule asymmetrically occupies two out of three identical lobes of the binding pocket and forms aromatic stacking interactions between the inhibitor and the RSV F residues Phe488 and Phe140 (Figure 23).[102] The 5-chloroindole heterocycle is involved in π–π stacking interactions with Phe488A, Phe488B, and Phe140B and in a weak C–H/π interaction with Phe140B,

which are present between RSV F protomers A and B (FA and FB, respectively) of lobe 1. Similarly, the 1,3-dihydroimidazo-[4,5*c*]pyridin-2-one group also forms a π–π stacking interaction with Phe488A and Phe488C and a weak C–H/π interaction with Phe140A, which are present between RSV F protomers A and C (FA and FC, respectively) of lobe 2 (Figure 23). The formation of these aromatic protein–ligand stacking interactions seems to be a commonality between all known RSV fusion inhibitors and may lock the central heterocyclic moieties of these inhibitors in a fixed conformation. In addition to stacking interactions, other interactions between the protein and **46b** were observed. The 5-Cl group of **46b** interacts with the carbonyl oxygen of Thr397[103] through a halogen bond along with a water-mediated H-bonding interaction between the O atoms of the sulfone and the side chain of Arg339. In addition to the above, it has been observed that rearrangement of the side chains of Phe140, Phe488, and Phe137 is required to make a hydrophobic environment to trap the CF_3 group of **46b**.[102] The C3 substitution in the benzimidazolone with a CF_3 group in **46b**, instead of the cyclopropyl moiety in **47**, contributed to improved metabolic stability and decreased susceptibility to reactive metabolite formation. Compound **46b** exhibited a mean EC_{50} = 0.46 nM against recombinant rgRSV224 virus in HeLa cells, whereas it showed an $EC_{50} \approx 0.2–20$ nM against 8
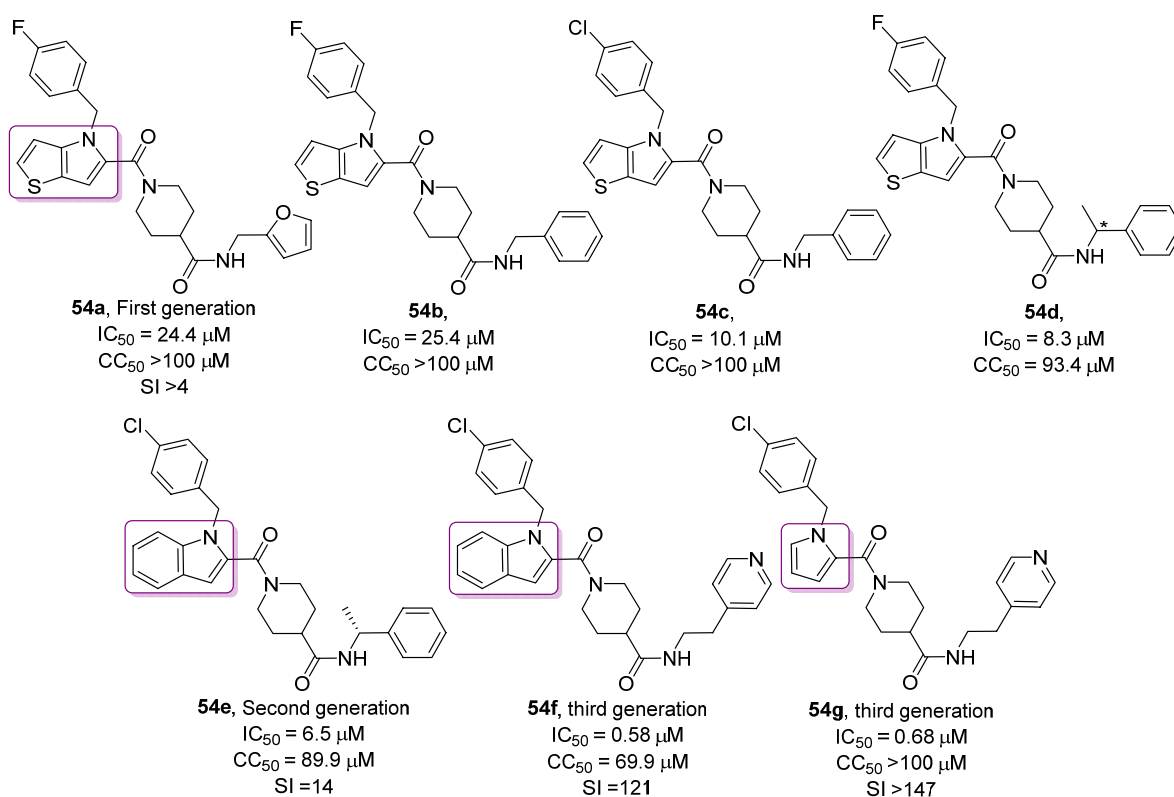
Figure 25. Structures, inhibitory concentration (IC_{50}), and cytotoxicity concentration (CC_{50}) of neurotropic alphavirus inhibitors: thienopyrrole(s) (**54a−d**), indole-2-carboxamides (**54e** and **54f**), and pyrrole-2-carboxamide (**54g**). IC_{50} and CC_{50} values were calculated from a WEEV replicon assay.

nonrecombinant RSV-A and RSV-B strains in plaque reduction assays.[86]

Structural comparison of JNJ 53718678 (**46b**), which possesses an indole moiety, with BMS-433771 (**47**) and JNJ-49153390 (**48**), both of which have a benzimidazole core (Figure 23), implied that the central heterocyclic core could be replaced without any loss of antiviral activity provided that the heterocycle offered an opportunity for π-stacking.[102] Encouraged by this finding, 4-, 5-, and 6-azaindole cores were explored as part of the optimization process (Figure 23). While offering similar antiviral potency (~EC_{50} = 1 nM), the 5-chloro azaheterocyclic compounds **49** and **50** displayed very different PK profiles, especially with regard to their distribution to the lungs. However, installing a nitrogen atom at C5 in the indole renders **51** more basic, which alters the pK_a and lipophilicity, resulting in improved pulmonary permeability and distribution.[104] According to a reported tissue distribution model, basic amines with a pK_a value of >8 show better uptake,[105] which may be the reason for increased uptake of **51**.

Compound **51**, a 5-azaindole analog of **46b**, showed high binding affinity to the RSV F protein, indicating that the introduction of a nitrogen atom at C-5 may compensate for halogen bonding. The azaindole moiety exhibited improved π-stacking with Phe488/Phe140.[102] Compound **52** was synthesized having 3-(methylsulfonyl)-6-azaindole as a C-2 substituent instead of the benzimidazolone in **46b** (Figure 23) and found to have 8−10-fold lower potency (EC_{50} = 78 nM) when compared to **46b**.[106]

Furthermore, a survey of pharmacophores of RSV inhibitors indicated that indole **53a**, azabenzimidazole **53b**, and 5-azaindole **53c** exhibited almost comparable EC_{50} values in the

RSV cell-based assay,[107] similar metabolic stability in human liver microsomes (Figure 24A), and similar membrane permeability in human cell lines. A significant difference in their plasma protein-binding profiles was observed reflecting their differential lipophilicity. The indole analog **53a** exhibited high protein binding in human plasma (3.6% free fraction), whereas azabenzimidazole (**53b**) and 5-azaindole (**53c**) were distinctly less protein bound (30% and 47.2% free fractions, respectively). The reduced plasma protein binding of azabenzimidazole **53b** and AI **53c** could be attributed to the combined effect of the lipophilic modulation caused by trifluorination at the terminal carbon of the N-1 propyl chain and the newly installed nitrogen atoms in the core ring compared with indole **53a**.[107] In addition, **53c** was well distributed to the lungs since it has a basic character. Another synthetic analog, **53d**, showed an EC_{50} value in the nanomolar range in an RSV A2 assay hosted by HEp-2 cells (Figure 24B). Subsequently, the X-ray cocrystallographic structure of **53d** in complex with RSV-A2 suggested that the presence of allylic strain induced by the amide bond forces the C-2 heteroaryl substituent on the piperidine ring, i.e., pyrazolopyrimidine, to formation of a dihedral angle of 95°.[108]

On the basis of the above results, we propose a pharmacophore model having a central fused heterocyclic core system that engages in aromatic stacking interactions with the prefusion conformation of the RSV F protein as necessary for optimum inhibitory activity against the virus (Figure 24C). In addition, a heteroaromatic ring at the C-2 position of the core system that imparts conformational flexibility should be attached through a linker (Figure 24C).[108]
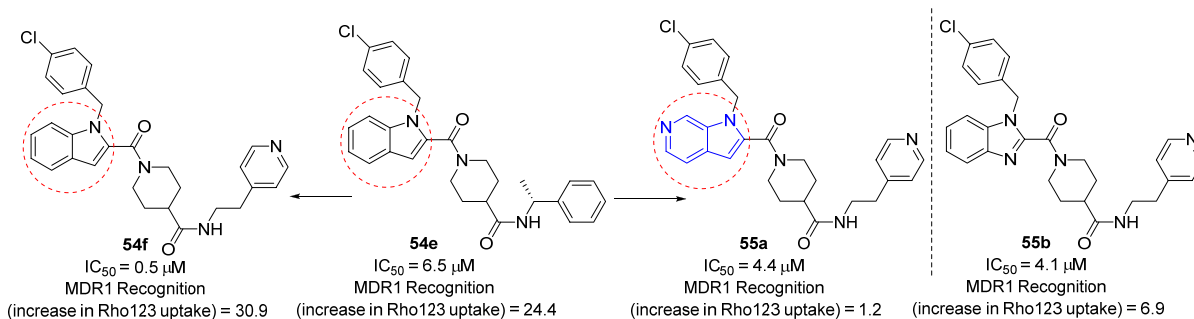
Figure 26. Scaffold hopping from an indole-derived inhibitor (**54e**) to a 6-azaindole core (**55a**) and benzimidazole core (**55b**) as neurotropic alphavirus replication inhibitors. MDR1 recognition was assessed by measuring rhodamine uptake in the presence of the MDR inhibitor tariquidar (5 μM) and either 30 μM of the test compound or vehicle and calculating $(C_{av} - C_{veh}) \times 100/(C_{tar} - C_{veh})$, where C_{av} is the concentration of rhodamine 123 in the presence of an antiviral inhibitor, C_{veh} is the concentration in the presence of a vehicle, and C_{tar} is the concentration of rhodamine 123 in the presence of tariquidar.

NEUROTROPIC ALPHAVIRUSES

Neurotropic alphaviruses or encephalitis viruses, including Western equine encephalitis virus (WEEV), are transmitted by mosquitoes and infect neurons present in animals and the human CNS.[109] The positive-stranded m-RNA (12 kb) alphavirus is enclosed in an icosahedral nucleocapsid that is surrounded by a lipid envelope coated by a viral envelope containing two glycoproteins, E1 and E2. These two proteins form a stable heterodimer, and three E2–E1 heterodimers interact to form the spike required for viral infection. The alphavirus normally enters through endocytosis in clathrin-coated vesicles followed by transfer to endosomes, where the low pH results in a conformational change in the E1–E2 heterodimer such that the fusion domain in E1 is exposed and the virus envelope fuses with the endosomal membrane.[109]

In the alphavirus class, Semliki Forest virus (SFV) and Sindbis virus (SIN) are widely used as models to study different steps of pathogenicity, including virus entry, endosomal release, and budding inside the host cells.[110] According to recent studies; neurotropic alphaviruses can also propagate without capsids. Neurotropic alphaviruses are considered category B priority pathogens by the National Institute of Allergy and Infectious Diseases (NIAID) because they can be aerosolized and released into a population center as potential bioterrorism agents, causing CNS infections that lead to potentially fatal encephalitis. Another study showed that WEEV activates transcription factor, interferon regulatory factor 3 (IRF-3) mediated neuronal innate immune pathways, and any revocation in IRF-3 will cause enhanced virus-mediated injury.[111] Compounds carrying thienopyrrole (**54a–d**),[112] indole-2-carboxamides (**54e** and **54f**),[113,114] and pyrrole-2-carboxamide (**54g**)[115] have been reported to act as alphavirus replication inhibitors (Figure 25). The thieno[3,2-b]pyrroles were identified as a class of potent antiviral agents via a high-throughput screening (HTS) campaign. The replicon-based assay used for the HTS and subsequent validation steps implicated viral replicase proteins as potential targets of these thieno–pyrroles. In the study, the analogues were evaluated with the cell-based WEEV replicon assay in which the majority of the WEEV structural genes are replaced with the firefly luciferase gene as a reporter for viral RNA replication. An MTT assay was performed to evaluate their effects on cell viability (Figure 25). This study produced **54a** which exhibited an IC$_{50}$ of 24.4 μM and a CC$_{50}$ of >100 μM. Further, structural optimization of **54a** started from sub-

stitution of the equipotent benzyl amide instead of the 2-furanylmethyl amide to obtain **54b**.[113] The 4-fluorobenzyl group of **54b** was changed to a 4-chlorobenzyl group to afford **54c**. The chiral molecule **54d** was synthesized using (R)-α-methylbenzylamine and inhibited the virus with an IC$_{50}$ of 8.3 μM. Replacement of the thieno[3,2-b]pyrrole core with an indole core yielded **54e**. Compound **54e** demonstrated moderate potency, stability toward oxidative metabolism, and protective effects that correlate with both in vitro and in vivo antiviral activity. The indole analog **54e** with chirality at the benzylamide expressed the same eudismic ratio difference in pharmacological activity between the two enantiomers as observed with the thieno[3,2-b]pyrroles with the (R)-enantiomer having a superior IC$_{50}$ value compared to the (S)-enantiomer. Interestingly, **54f** and **54g** showed a 10-fold improvement in IC$_{50}$ values, suggesting that an ethylene linker along with the pyridine ring plays a major role in the inhibitory activity of these molecules.[114] Furthermore, upon moving the nitrogen of the pyridine ring from the para to the ortho position, a 40-fold decrease in potency was observed. The pyrrole in **54g** is a viable substitute for the indole core of **54f** and reduced the molecular weight and actually diminished the cytotoxicity compared with that of **54f**.

Subsequently, bioisosteric replacement of the indole core in **54e** with an AI to provide **55a** was examined. The 6-azaindole derivative **55a** exhibited reduced lipophilicity and enhanced solubility while retaining antiviral potency (Figure 26).[114] The major efflux transporter at the blood–brain barrier (BBB), P-glycoprotein (P-gp/MDR1), facilitates xenobiotic efflux from the CNS. The degree to which P-gp interacts with the molecules was measured using a rhodamine 123 uptake assay conducted in MDCK cells transfected with human P-gp (MDR1-MDCKII). Rhodamine-123 is a known P-gp substrate that is actively effluxed from MDR1-MDCKII cells. Significantly, the 6-azaindole-derived **55a** was found to be more effective in attenuating P-glycoprotein (P-gp/MDR1) recognition. The MDR recognition value was reduced to 1, suggesting minimal efflux of **55a** from cells.

Compound **55a** exhibited moderate antiviral activity, IC$_{50}$ = 4.4 μM, and was not able to effectively reduce the viral load (69.4 pfu/mL) as compared with **54e** (39.3 pfu/mL).[114] Moreover, an eroded metabolic stability and increase in solubility was observed upon replacement of the indole ring of **54f** with the pyrrole in **54g**, suggesting that the central aromatic ring is a major site of metabolism. In addition, the improved metabolic stability shown by replacement of the

indole of **54f** with the more electron-deficient benzimidazole ring in **55b** is also consistent with this proposal. A 5-fold decrease in potency was noted when a propyl linker was used with a pyridine ring instead of an ethylene linker of **54f**.[114] This suggests that the optimum distance between the amide group and the pyridine ring may be a significant structural requirement for potent antiviral molecules.

A complete loss of antiviral activity was observed upon removal of the aromatic core from any molecule, which indicates the necessity of an aromatic core. The *p*-halogenated benzyl ring at the N-1 position of the aromatic core and a linker connecting it to the aromatic core are important to achieve significant inhibitory potency. Considering all of the above findings, we propose the general concept for a pharmacophore model to develop a potent neurotropic alphavirus inhibitor depicted in Figure 27.
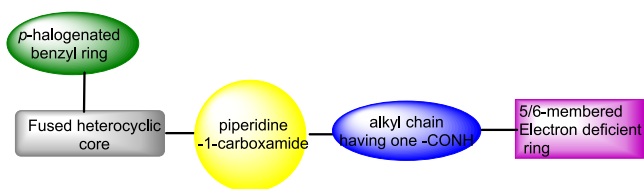

Figure 27. Proposed pharmacophore model for neurotropic alphavirus inhibitor.

DENGUE AND EBOLA VIRUSES

Dengue virus (DENV) belongs to the *Flaviviridae* family and is classified as an "arbovirus" since it is transmitted by arthropod vectors, particularly mosquitoes, such as *Aedes aegypti* and to a lesser extent *Aedes albopictus*.[116,117] The genome of DENV is a single-stranded and positive-sense RNA. There are four serotypes, DENV-1, DENV-2, DENV-3, and DENV-4, and each interacts distinctly with antibodies in human blood serum.[117] Currently, no specific antiviral drugs are available to treat DENV. A live-attenuated tetravalent vaccine, Dengvaxia (CYD-TDV), has been developed by Sanofi-Aventis Pasteur Limited, Paris, France, and approved in endemic countries; however, it exhibits suboptimal protection against DENV-1 and DENV-2.[118] The vaccine's varying efficacy across different ages and serostatus as well as a clear safety signal in seronegative recipients, i.e., that Dengvaxia enhanced subsequent disease in some seronegative individuals, raised a number of questions against other dengue vaccine candidates also. Therefore, new therapeutics against DENV are needed. Ebola virus (EVD) belongs to the *Filoviridae* family and has a single-stranded, negative-sense RNA genome. To date, no specific antiviral medications or approved vaccines are available for EVD.[116]

Adaptor-Associated Kinase 1 (AAKI Inhibitors). Originally, AAK1 inhibitors were developed to treat neurological disorders and only later emerged as antiviral agents. Verdonck and co-workers developed AAK1 inhibitors with broad-spectrum antiviral properties.[119] Their work is based on targeting the host kinases used by viruses for intracellular membrane trafficking aiding their entry into host cells. Intracellular trafficking of many RNA viruses is regulated by clathrin-associated host adaptor proteins controlled by AAK1 and cyclin G-associated kinase (GAK). Both are serine-threonine kinases belonging to the NUMB-associated kinase (NAK) family. Anticancer drugs such as sunitinib and erlotinib inhibit AAK1 and exhibit broad-spectrum in vitro antiviral activity against different viruses, including HCV, DENV, Zika virus, and West Nile virus. Compound **56**, a 7-AI derivative (Figure 28), was used as the basis to develop a series of potent AAK1 inhibitors.

Compound **56** was 3-fold more selective for AAK1 than GAK and 8- and 22-fold more selective for AAK1 than bone
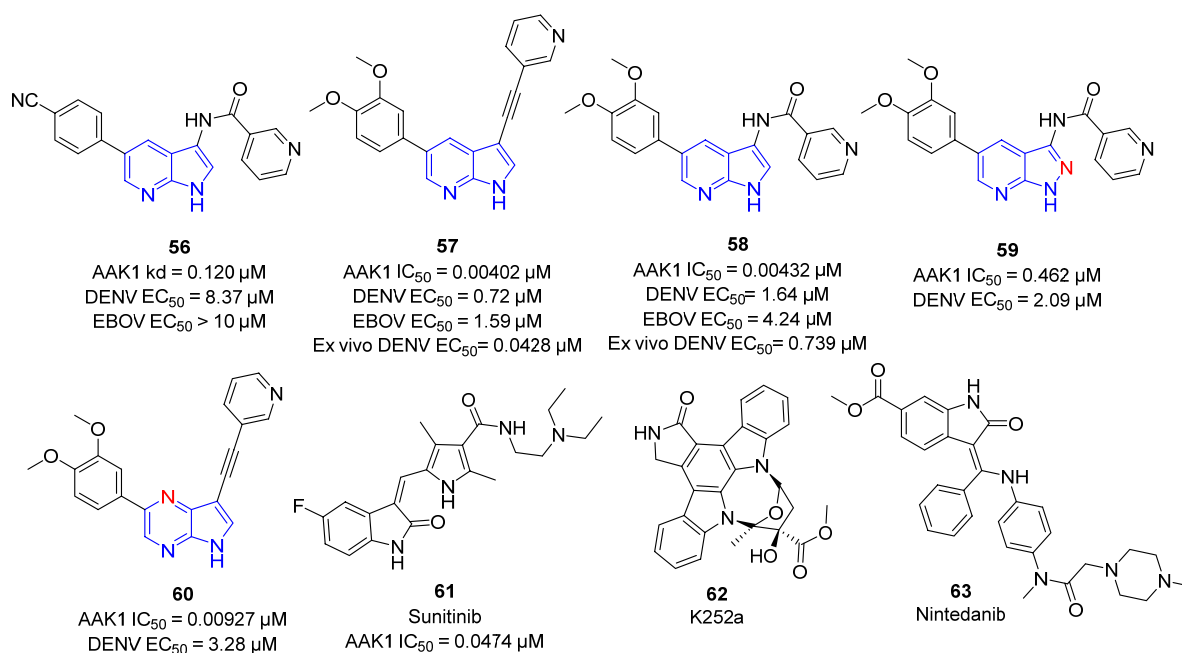

Figure 28. Structures of known adaptor-associated kinase 1 inhibitors **56** and **61**, broad-spectrum kinase inhibitor K252a (**62**), and tyrosine kinase inhibitor nintedanib **63**. Terminal cyano group and C3 position of **56** were optimized to afford 7-azaindole analogs **57** and **58**. Replacement of C-2 and C-4 with a N atom in analogs **59** and **60**.

morphogenetic protein 2 inducible kinase-2 (BMP2K) and serine/threonine-protein kinase 16 (STK16), respectively. Furthermore, the binding mode of **56** to AAK1 based on X-ray studies showed that its 7-AI ring directly bound between the side chain of Ala72 from β2 on the kinase N-lobe and Leu183 of the C-lobe. N-1 and N-7 of **56** engaged in H-bonding interactions with Asp127 and Cys129 at the kinase hinge region. Similarly, the terminal aromatic nitrogen of the pyridine moiety formed a H bond with the side chain of Lys74; however, the nitrogen atom of the terminal cyano group interacted with the side chain of Asn136 (Figure 29).
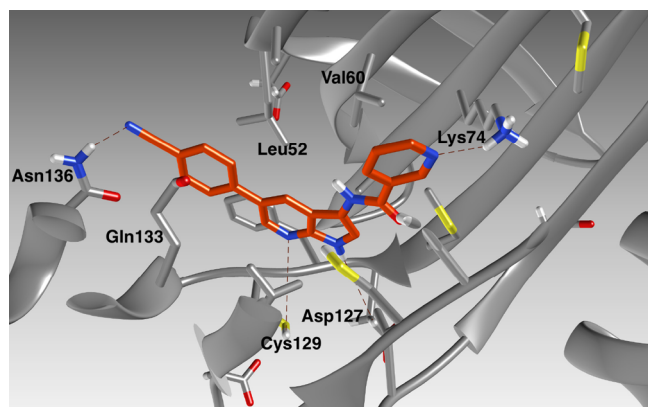

Figure 29. Binding interactions of compound **56** in the ATP-binding pocket of AAK1. Terminal cyano group, pyridine nitrogen, N-1, and N-7 of AI are involved in hydrogen-bonding interactions with amino acid residues Asn136, Lys74, Asp127, and Cys129, respectively, around the ATP-binding pocket.

The SAR studies with **56** first explored the effect of replacing the 5-(4-cyanophenyl) group with a phenyl, thienyl, and substituted phenyl ring carrying electron-donating and -withdrawing groups and a halogen. Compounds carrying a 3,4-dimethoxy phenyl ring at the C-5 position (**58**) showed stronger AAK1 affinity (IC_{50} = 0.00432 μM) than the positive control sunitinib (**61**) (IC_{50} = 0.0474 μM) (Figure 28) and exhibited good activity against DENV-2 (EC_{50} = 1.64 μM). Further focus was given to replacing the N-acyl moiety of **58** with aromatic, heteroaromatic, and cycloalkyl groups. It was observed that the 3-pyridyl moiety **58** was critical for AAK1 binding as other N-acyl analogs showed a 100-fold decrease in AAK1 affinity compared with **58**. However, the amide bond of the N-acyl group in **58** could be replaced with aryl keto, phenyl, and alkynyl groups without a significant loss in AAK1 affinity. The 3-ethynylpyridine analog **57** was found to exhibit excellent AAK1 binding (IC_{50} = 0.00402 μM) and antiviral potency against DENV-2 (EC_{50} = 0.72 μM). Scaffold modification of 7-AI (**57**) to pyrrolo[2,3-b]pyrazine (**60**) showed potent AAK1 binding with an IC_{50} = 0.00927 μM; however, it also demonstrated greater cytotoxicity.

In parallel, scaffold modification of the 7-AI **58** to the pyrazolo[3,4-b]pyridine **59** resulted in a 100-fold reduction in AAK1 binding affinity (IC_{50} = 0.462 μM) compared with **58**. This study suggested that **57** (AAK1 IC_{50} = 0.00402 μM; DENV-2 EC_{50} = 0.72 μM; EBOV EC_{50} = 1.59 μM) and **58** (AAK1 IC_{50} = 0.00432 μM; DENV EC_{50} = 1.64 μM; EBOV EC_{50} = 4.24 μM) were the optimized analogs of **56**. However, **56** did not show any significant inhibitory activity toward EBOV (EC_{50} > 10 μM). Furthermore, **56** and **57** were advanced to studies in human primary dendritic cells, which are physiologically more relevant models for DENV infection. Compounds **57** and **58** showed dose-dependent inhibition of
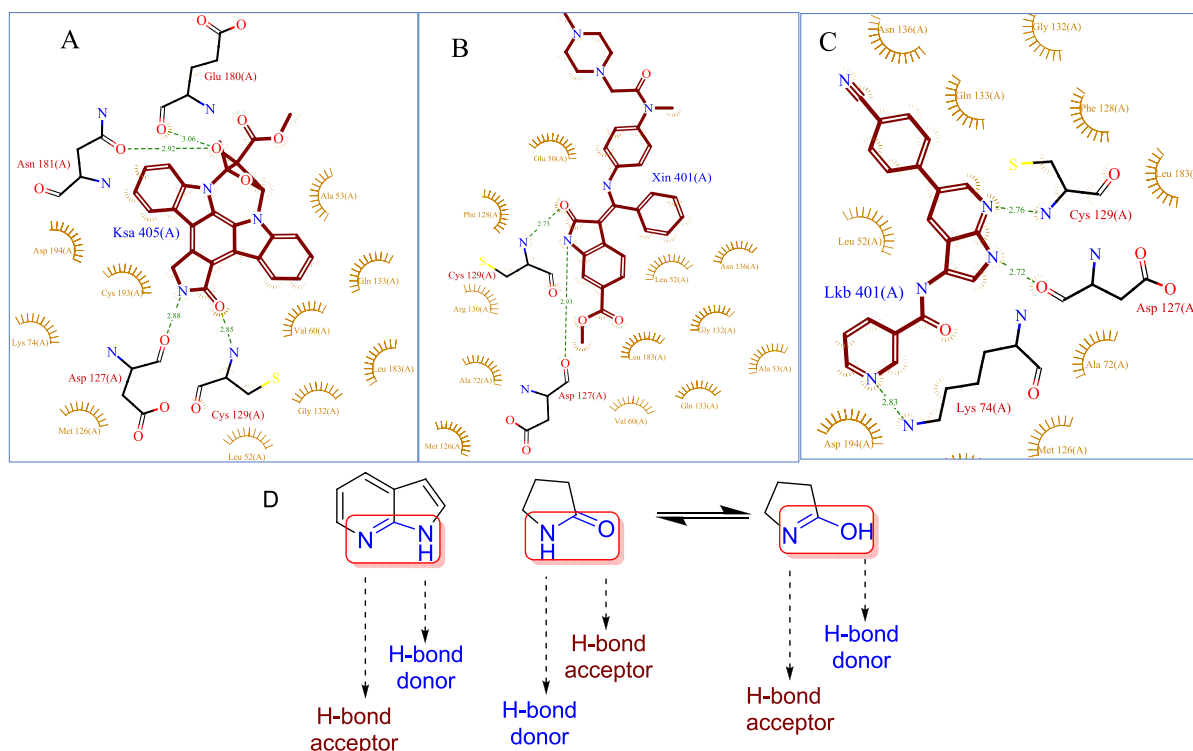
Figure 30. Comparison of the 2D interaction diagrams of the AAK1 binding pocket with (A) K252a (**62**), (B) nintedanib (**63**), and (C) compound **56**. (D) Hydrogen bonding in the 7-azaindole versus pyrole-2-one moiety.

Figure 31. Representative examples of reported AAK1 inhibitors.

Figure 32. (A) Modification of the acylaminothiazole moiety with heterocycles carrying a common H-bonding motif in the bicyclic core (except in compound **73**). (B) Two-dimensional interaction diagram of PI3Kγ inhibitor **69**.

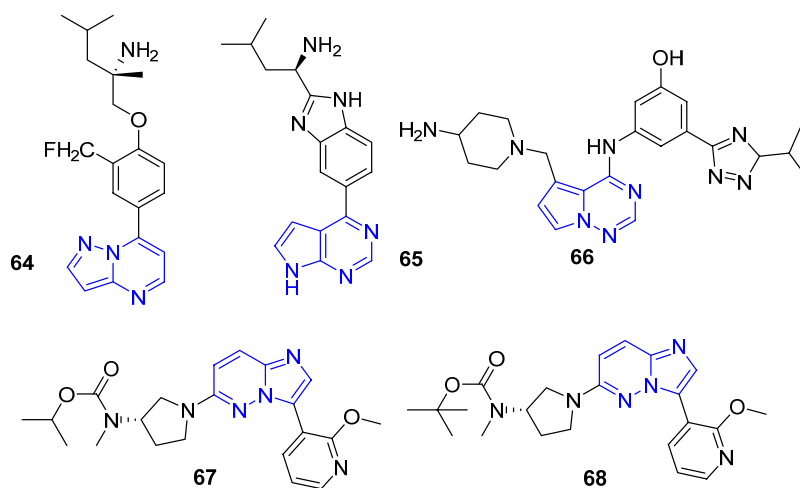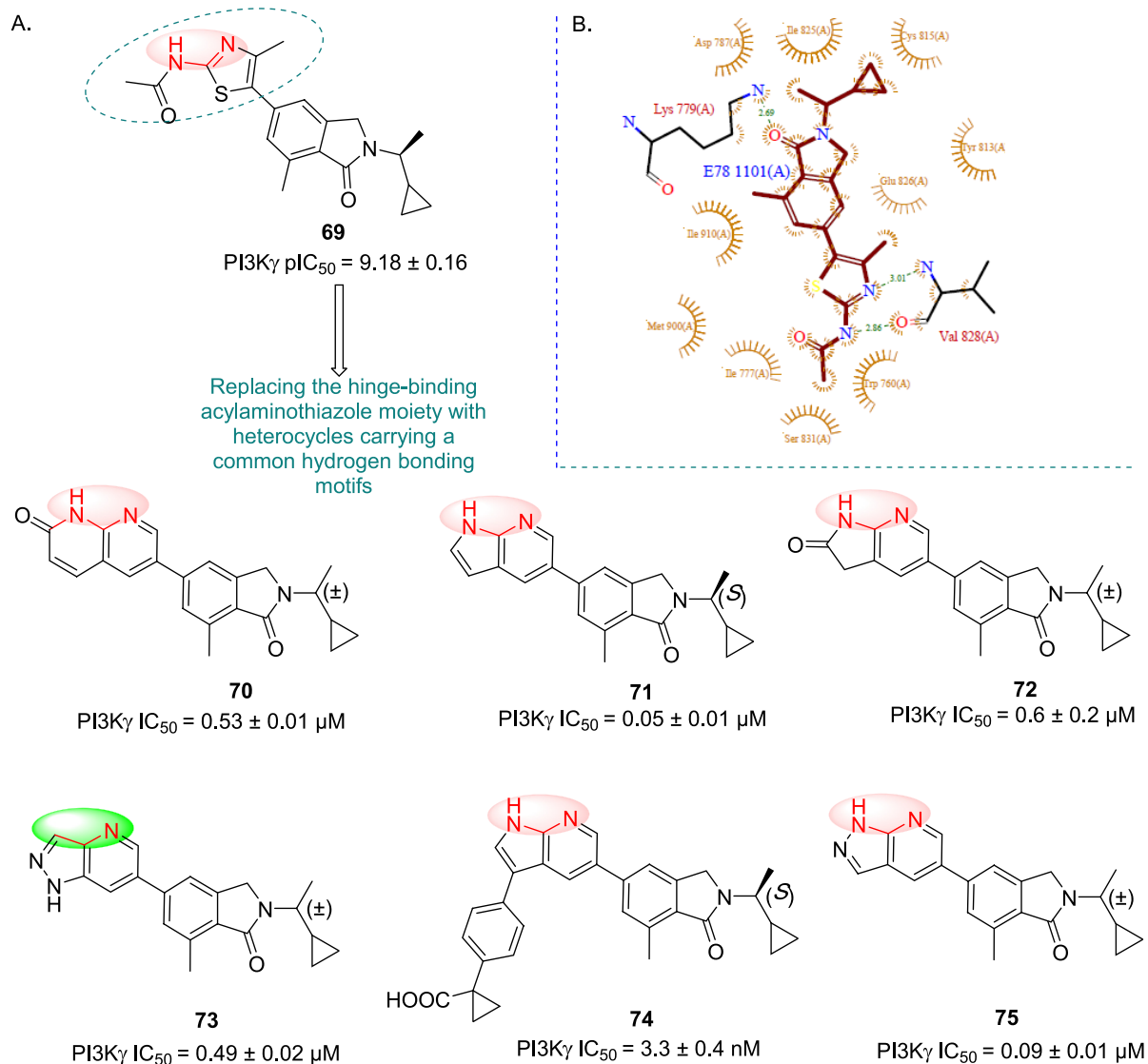DENV-2 infection with EC_{50} values of 0.0428 and 0.739 μM, respectively. Finally, in the kinase selectivity experiment against 468 kinases, **57** displayed binding with multiple kinases, including NAK family members, which may explain the broad-spectrum antiviral effect of **57**. Compound **57** showed lower cytotoxicity ($CC_{50} > 20$ μM) toward Huh7 mammalian cells in *in vitro* in cell viability assays. Overall, this work demonstrated that the development of cellular AAK1 inhibitors may represent a promising broad-spectrum antiviral strategy..

7-AI is a well-established hinge-binding scaffold that can adopt different orientations in the folding cleft of the hinge region of the kinase.[120] The capacity of 7-AI to engage in H bonding and its amide isosteric characteristics can be tactically applied in drug discovery studies. For example, the binding interaction of the broad-spectrum kinase inhibitor K252a (**62**), the tyrosine kinase inhibitor nintedanib (**63**), and **56** with the AAK1 binding pocket demonstrated the versatility of AIs (Figures 28 and 30).[121] Despite the differences in their chemical structures, the pyrrole-2-one moieties of **62** and **63** interact with Cys129 and Asp127 of the AAK1 binding site. Similarly, 7-azaindole **56** exhibits the same interaction pattern, engaging Asp127 and Cys129 residues through N-1 and N-7, respectively (Figure 30). Hence, two different molecules having similar functional groups at the correct position may bind similarly to a protein.

A few AAK1 inhibitors that are non-7-azaindole chemotypes carrying pyrazolopyrimidine (**64**), pyrrolopyrimidine (**65** and **66**), and imidazolopyridazine (**67** and **68**) pharmacophores are shown in Figure 31. These isomeric pharmacophores incorporate three nitrogen atoms that are positioned differently, and these nitrogens may be (no X-ray data available) interacting with different amino acid residues at the ATP-binding pocket depending on their substituents to afford a signatory H-bonding pattern of AAK1 inhibitors.

A few phosphoinositide-3-kinase γ(PI3Kγ) inhibitors share common H-bonding donor and acceptor motifs (Figure 32).[122] The bicyclic ring in inhibitors engages in a bidentate manner with Val882, a hinge motif of PI3Kγ. Hence, this bidentate interaction is a determining factor of the potency of different substituted isoindolenones (Figure 32).[123,124] Replacement of the acylaminothiazole ring of **69** with a 7-AI yielded **71** and **74**. Both of these compounds exhibited excellent inhibitory potency with IC_{50} values of 0.05 and 3.3 nM, respectively, as compared to the naphthyridinone **70**, the azaindole-2-one **72**, and the pyrazolopyridines **73** and **75**. The NH in the azaindazole **73** is not suitably oriented for interaction with Val882, and this molecule displayed 5.4-fold lower potency ($IC_{50} = 0.49$ μM) than the isomeric analog **75** ($IC_{50} = 0.09$ μM). Subsequently, the 7-AI analog **71** was found to exhibit greater potency ($IC_{50} = 0.05$ μM) than reference compound **69**. Substituting a benzyl acetic acid derivative at the C-3 position in **71** provided very potent PI3Kγ inhibition ($IC_{50} = 3.3$ nM), and this molecule exhibited an acceptable pharmacokinetic profile in rats (in vivo CL = 1.8 L/h/kg). Thus, the combination of C-3 substitution and the versatility of the N1 and N7 nitrogen in forming bidentate interactions with the target sites allows for facile optimization.

Currently, AAK1 inhibitors are envisioned to be beneficial in countering SARS-CoV-2 entry into host cells. Compounds **56**−**58** and their derivatives can be further optimized and tested against various virus families, including SARS-CoV-2. Repurposing kinase inhibitors as broad-spectrum antiviral agents is a recent and ongoing endeavor.[125−128] It has been suggested that kinase inhibition may significantly surpass viral resistance because the virus does not genetically control the host kinases. However, toxicity is a major concern associated with kinase inhibition since host kinases play essential roles in mediating other cellular functions.[119]

■ HEPATITIS C VIRUSES

Hepatitis C virus (HCV) is a small enveloped RNA virus composed of 9.6 kb RNA having a long open reading frame (ORF) flanked by a 5′- and 3′-nontranslated region. It belongs to the *Flaviviridae* family, and its genome consists of single-stranded, positive-sense RNA.[129] The 3′-nontranslated region contains a poly U/UC tract and a highly conserved 98-nucleotide element that is required for viral RNA synthesis. The 5′-nontranslated region is the most conserved among the different genotypes and contains the internal ribosomal entry site (IRES) element which is essential for a direct Cap-independent translation of the ORF region. Translation results in a precursor polyprotein containing ∼3000 amino acids (aa). The precursor polyprotein gets processed by the host cell and viral proteases into both structural (S) and nonstructural (NS) proteins, respectively. The S proteins are comprised of a nucleocapsid core (C) and the glycosylated transmembrane proteins E1 and E2 required for the attachment of HCV to host cell receptors and the viroporin p7 that likely forms ion channels essential for assembly and release of infectious virions. The other precursor protein contains the NS proteins NS2, NS3, NS4A, NS4B, NS5A, and NS5B. The nonstructural proteins play a major role in replication of the HCV virus. Out of all of the above-mentioned nonstructural proteins, NS4B represents a druggable and appealing antiviral target, thus making NS4B the last entry target in the HCV drug discovery process. Although a number of direct antivirus agents were approved against HCV, none of the drugs have been approved against NS4B to date.[130,131]

HCV NS4B Inhibitors. Chen and co-workers developed 7-azaindole-based compounds that target the nonstructural, membrane-bound protein NS4B, an integral hydrophobic membrane protein that plays a pivotal but undefined role in the HCV RNA replication mechanism.[132] All of these compounds were evaluated for activity against the genotype 1b HCV replicon by measuring mRNA levels with respect to cellular GAPDH mRNA in Huh-7 cells. Briefly, quantitative RT-PCR was performed to quantify the amount of intracellular HCV RNA, and the concentration of a compound inhibiting HCV RNA replication by 50% (EC_{50}) is indicated. The indolylpyridine-sulfonamide **76**, which exhibited an EC_{50} of 7 nM,[133] was chosen as the lead compound, and a SAR study was performed by replacing the indole ring with isomeric 4-, 5-, 6-, and 7-azaindoles to explore anti-HCV activity (Table 4).[132]

The SAR exploration revealed that the 7-azaindole series with an electronegative CF_3 substituent at C-5 (**77**) exhibited more potent anti-HCV activity than the indole analog **76**.[132] Analogs **78** and **81** carrying small lipophilic substituents on the azaindole ring were also found to exhibit good HCV inhibition. However, the unsubstituted 7-azaindole analog **80** was less active (Table 4). Similarly, attaching propoxy (**85**) and isopropoxy (**86**) substituents at the C-5 position on the 7-azaindole core was found to be inferior for anti-HCV activity. Shifting the nitrogen around the aromatic ring to form isomeric AIs **82**−**84** with a small lipophilic methyl group at either C-5 (**82**) or C-6 (**83**, **84**) resulted in a significant drop in potency. In pharmacokinetic screening, oral administration

Table 4. Structure of Indole Analog 76 (Selective Inhibitor of HCV RNA replication) and Its AI Analogs 77−86[a]

Compd No	Structure	EC50 (gt 1b) HCV subgenomic RNA replication assay	Ring type
76		EC50 = 7 nM	Indole
77		EC50 = 2 nM	7-azaindole
78		EC50 = 13 nM	7-azaindole
79		EC50 = 87 nM	7-azaindole
80		EC50 = 217 nM	7-azaindole
81		EC50 = 15 nM	7-azaindole
82		EC50 = 1400 nM	6-azaindole
83		EC50 = 230 nM	5-azaindole
84		EC50 = 119 nM	4-azaindole
85		EC50 = 2150 nM	7-azaindole
86		EC50 = 7600 nM	7-azaindole

[a]EC50 values are the averages of at least two independent determinations. Huh7 cells harboring genotype 1b (gt 1b) HCV bicistronic replicons were plated at 5000 cells/well in 96-well plates. Compounds were added to the wells with a final DMSO concentration of 0.5%.

of a single 10 mpk dose of the 5-CF3 analog 77 to rats showed excellent exposure (AUC$_{0-6h}$ = 5833 nM·h) of the compound. It also exhibited higher exposure (AUC$_{0-24h}$ = 8162 and 5440 nM·h, respectively) in dogs (PO, 2 mpk) and monkeys (PO, 3 mpk) than 76 (AUC$_{0-24h}$ = 6858 and 7568 nM·h, respectively). Notably, the C-2 position of AI has been reported to be vulnerable to oxidative metabolism, leading to C-2 hydroxy metabolites.[142] However, the C-2 position is occupied in optimized compound 77; thus, C-2 oxidative metabolism may be avoided.

Reports of different chemical classes targeting HCV NS4B, including benzimidazole 87, pyrozolopyrimidine 88, pyrozolo-pyridines 89 and 90, and imidazolothiazole 91 have emerged (Figure 33). The suggestion of a common ligand-binding site at NS4B is unclear due to the lack of crystal structure data on the NS4B protein, which hinders structure-based drug discovery.

■ INFLUENZA A VIRUSES

Influenza virus belongs to the *Orthomyxoviridae* family of viruses, which have a negative-sense, single-stranded, and segmented RNA genome with diverse antigenic character-istics.[134] Current subtypes of influenza A viruses that routinely circulate in humans include A(H1N1) and A(H3N2) types. Although vaccination represents the best way to lessen the impact of the disease, the virus varies continuously due to antigenic drift that can evade pre-existing immunity.[135] Thus, influenza vaccines are reformulated every year to match circulating strains. Currently, oseltamivir 92 (oral), zanamivir 93 (inhalation), peramivir 94, and baloxavir-marboxil 95 (oral) are FDA-approved antiviral drugs that are recommended for the treatment of influenza virus infection (Figure 34). At the same time, zanamivir and oseltamivir are also recommended for chemoprophylaxis.

Generally, anti-influenza drugs work best only when they are administered in a timely manner within 48 h of the onset of infection. The current antiviral standard of care (SOC) for the treatment of influenza is the neuraminidase inhibitors, oseltamivir, 92 (Figure 34), and zanamivir, 93.[136] Zanamivir, 93, has low oral bioavailability; hence, it is given via the topical route by inhaler, but 92 is administered orally. These drugs are effective against a variety of type A and B influenza viruses, but there are three major limitations to these molecules that have emerged in recent years. First, the neuraminidase inhibitors have only a moderate impact on the severity of symptoms as well as the duration of illness, and they must be administered within 24−48 h of the onset of infection. Second, infants suffering with influenza in a few countries have recently shown the emergence of viruses with mutations in the neuraminidase gene that encode for drug-resistant neuraminidase proteins. If this frequent emergence of resistant mutants is found to be a general occurrence in children, it represents a serious concern, especially since children are an important source of the spread of influenza in the community. Third, recent reports about H5N1 influenza virus have shown resistance to oseltamivir. Hence, new anti-influenza therapeutics with a novel mecha-nism of action are required.

Novel Polymerase Basic Protein 2 (PB2) Inhibitors of Influenza A Virus. The discovery of alternative therapeutic options for the treatment of influenza virus are still a challenge, and phenotypic-assay-based drug discovery efforts have been made by a number of research groups in an effort to identify novel chemotypes. The viral polymerase is made up of three different subunits, i.e., PB1, PB2, and PA. The heterotrimeric viral polymerase synthesizes viral mRNAs via a cap-snatching mechanism where it utilizes host pre-mRNA as a primer for transcription. The PB2 subunit contains a cap-binding domain that recognizes 7-methyl GTP (m7 GTP) on the 5′-end of the host pre-mRNA. Once host pre-mRNA is bound to PB2, the PA endonuclease subunit cuts the host RNA strand, leaving behind a 10−13-nucleotide primer. The PB1 subunit contains the conserved polymerase domain and utilizes the primer for RNA elongation. In the phenotypic-assay-based drug discovery
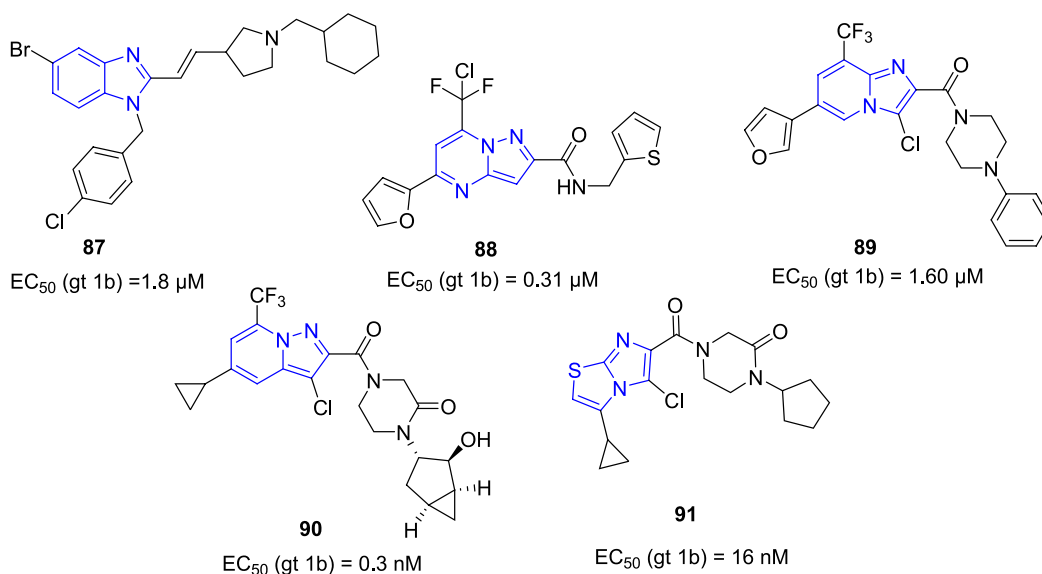
Figure 33. Representative examples of different chemical classes of reported HCV NSB4 inhibitors.
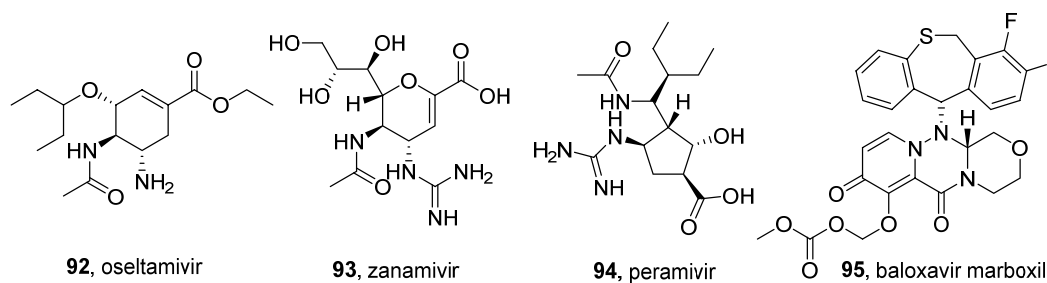

Figure 34. FDA-approved antiviral drugs recommended for the treatment of recently circulating influenza viruses.
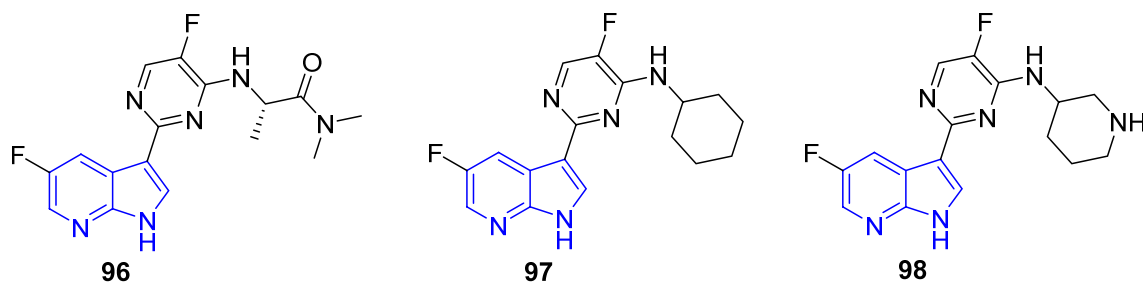

Figure 35. Structures of 7-azaindole analogs bearing a dimethyl alanine side chain 96, cyclohexylamine analog 97, and piperidine analog 98.

effort, the 7-azaindole-based inhibitors target the PB2 cap-binding domain of the viral polymerase of influenza. Principally, 7-azaindole influenza inhibitors bind to the PB2 cap-binding domain and interfere with the replication and transcription of the viral RNA genome to exert pharmacological inhibitory activity.[137]

The discovery of 7-azaindole-based anti-influenza compounds emerged from early work by Clark et al., who first identified a set of 7-azaindole analogs with considerable in vitro antiviral activity using branched DNA (bDNA) viral replication assay in cells and PB2 fluorescent polarization competition binding assay (Figure 35).[138]

A 96-well bDNA assay detects the negative-strand RNA of the influenza A virus (A/PR/8/34 strain) using a set of oligonucleotides designed for the A/PR/8/34 nucleoprotein transcript.[139] A cell-based antiviral assay was developed that

depends on the multiplication of virus RNA in the infected cells with negative strand RNA levels being directly measured using the branched-chain DNA (bDNA) hybridization method. Cells were initially infected with the virus and incubated in the presence of test compound for approximately 20 h. Viral replication was quantified by determination of negative strand RNA levels by bDNA assay. The concentrations of the test compound resulting in viral RNA levels equal to that of 10% of the control wells were reported as EC_{90}.

The binding affinity of compounds for the cap-binding domain of PB2 was determined using a competition binding fluorescence polarization (FP) assay. PB2 binding was examined using a 165 amino acid fragment of PB2 that had been identified as the cap-binding domain portion of the full-length protein. This PB2 domain was incubated with test compounds and with a 5′-FITC-labeled probe for 60 min at
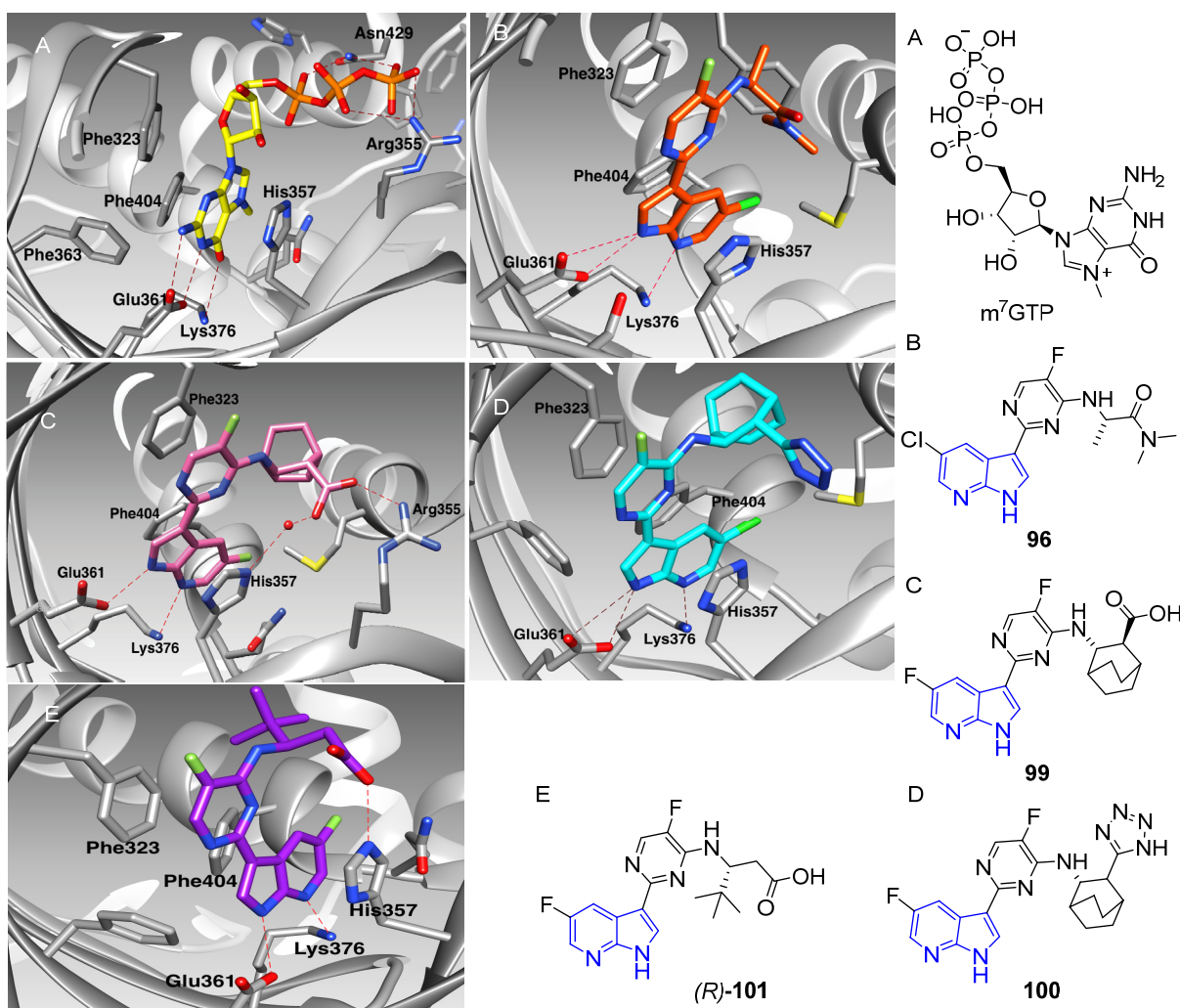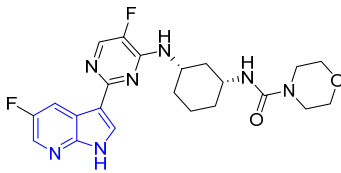
Figure 36. Comparison of the binding interactions of m[7]GTP and 7-azaindole analogs at the cap-binding domain of PB2. (A) m[7]GTP complexed with the PB2 cap-binding domain (PDB 4NCE). N-1,2-NH$_2$ and O-6 of the guanine ring are involved in binding interactions with Glu361 and Lys376. (B, C, D, and E) Compounds **96**, **99**, **100**, and (*R*)-**101** complexed with the PB2 cap-binding domain, respectively. Compounds **93** (PDB 4NCM), **99** (PDB 4P1U), **100** (PDB 4YD0), and (*R*)-**101** (PDB 5JUR) occupied the same binding site of m[7]GTP and exhibited similar binding interactions with Glu361 and Lys376 residues; however, N-1 and N-7 of the AI ring were involved in H-bonding interactions.

room temperature to reach equilibrium. Values for probe-only wells were used as the background. PB2 K_d values were determined by fitting the background-subtracted data to an equation for competitive displacement of a fluorescent probe.

The X-ray cocrystal structure of **96** complexed with the PB2 cap-binding domain (165 amino acid fragments) suggested that **96** and m[7]GTP (a known binder to PB2) displayed similar hydrogen-bonding interactions with the side-chain residues of PB2, engaging Glu361 and Lys376. The N-1 NH$_2$, O-6 of m[7]GTP and N-1 and N-7 elements of **96** were involved in H bonding (Figure 36B).[138] The AI core of **96** was sandwiched between the aromatic side chains of His357 and Phe404, while the pyrimidine ring was π-stacked against Phe323. Although the dimethylalanyl moiety of **96** occupied the region to which the sugar phosphate group of m[7]GTP was bound, no direct polar interactions were observed with positively charged residues, such as Lys-339, Arg-355, and His-357. It was postulated that optimization of the amino substituent at the 4 position of the pyrimidine ring in **96** formed polar interactions with amino acids present around the sugar phosphate-binding region of m[7]GTP. To extend the structure toward the sugar

phosphate-binding region of PB2, a series of compounds was synthesized by appending cycloalkyl, piperidine, diaminocyclohexyl, and cyclohexyl carboxylate functionalities on the amino substituent at the 4 position of the pyrimidine ring in compound **96** (Figure 36). Consequently, the binding interactions of the cyclohexyl carboxylate-bearing [2,2,2]-bicyclooctane analog **99** with PB2 were similar to those of m[7]GTP (Figure 36C). In addition, the carboxylic group of **99** showed water-mediated interactions with the nitrogen of His357 and Gln406 as well as with the carbonyl group of Arg355. Overall, this study confirmed that 7-methylguanine and 7-azaindole occupy the same binding site in PB2. Furthermore, **99** demonstrated potent antiviral activity against a broad range of influenza type A strains in in vitro studies, Table 5. This study describes the emergence of several potent compounds; among them, **99** and the diaminocyclohexyl-based analog **102** were advanced to in vivo studies. Compound **99** provided 100% protection against influenza-induced death in mice when the test compound was administered at three doses (10, 3, or 1 mpk b.i.d. for 10 days) starting 48 h postinfection. However, **102** demonstrated only 75% survival when dosed at

Table 5. In Vitro bDNA-Binding Assay and PB2 Fluorescence Competitive Binding Assay of Compounds 96, 99, and 102

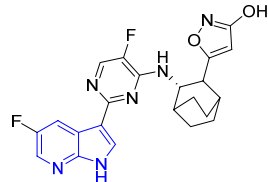| Structure and No.	bDNA EC$_{90}$[a] (μM)	PB2 K$_d$[b] (μM)
96	1.13	0.10
99	0·004	<0.003
102	0.012	0.40

[a]Concentration of the test compound resulting in viral RNA levels equal to 10% of the control wells is reported as the EC$_{90}$. [b]Affinity of the cap-binding domain of the PB2 subunit as measured in a fluorescence polarization competition binding assay.

30 mpk b.i.d for 10 days beginning 48 h postinfection. The standard drug oseltamivir, a neuroaminidase inhibitor when administered at the clinically relevant human equivalent dose (10 mpk b.i.d.) in the same animal model after 48 h of infection, did not provide any survival benefits.

Boyd and co-workers performed SAR studies on 99 by replacing the COOH group with different isosteres.[140] One of the resulting compounds 100, which incorporates a tetrazole ring in place of the COOH moiety, exhibited 13- and 16-fold lower viral potency in the CPE and bDNA assays when compared to 99. However, the isoxazole analog 103 was equipotent to 99 in the CPE assay and only 3-fold less potent than 99 in the bDNA assay (Table 6).

The crystal structure data and computational studies suggested that 100 retained the H-bonding interactions with Lys376 and Glu361 of PB2 similar to 99. The carboxylic acid group of 99 exhibited two water-mediated interactions with the ε nitrogens of His357 and Gln406 and the backbone carbonyl

Table 6. In Vitro Cytopathic Effect (CPE) Viral Assay and bDNA Assay of Compounds 99, 100, and 103

Structure and No.	CPE[a] IC$_{50}$ (μM)	bDNA[b] EC$_{99}$ (μM)
99	0.002	0.011
100	0.025	0.18
103	0.001	0.033

[a]MDCK cells were incubated with the test compounds and influenza A virus (A/PR/8/34 strain) for 72 h, and the concentration of the test compound resulting in 50% cell protection is reported as the IC$_{50}$. [b]Concentration of the test compound resulting in viral RNA levels equal to 1% of the control wells is reported as the EC$_{99}$.

group of Arg355. However, 100 did not show any such water-mediated interactions between PB2 and the tetrazole ring, which might be the reason behind the loss of antiviral potency. The antiviral profile of the isoxazole analog 103 was appreciable and comparable to that of 99, barring the 3-fold lower potency in the bDNA assay (Table 6). In general, these studies indicated that a negative charge is required for in vitro antiviral potency. However, none of the compounds were advanced for preclinical studies.

Farmer and co-workers[141] replaced the alanine dimethylamide side chain of 96 with an acyclic β-amino acid fragment bearing a nonpolar tert-butyl group (Figure 37) to form

Compound No.	R	bDNA[a] EC$_{90}$ (μM)	PB2[b] K$_d$ (μM)
(R)-101	F	0.03	0.003
(R)-104	Cl	0.023	<0.003
(S)-101	F	>6.65	0.15
(S)-104	Cl	>3.3	0.2

[a]The concentration of test compounds resulting in viral RNA levels equal to that of 10% of the control wells was reported as EC$_{90}$. [b] Affinity for cap-binding domain of the PB2 subunit as measured in a fluorescence polarization competition binding assay.

Figure 37. Structure of enantiomeric pairs of (R,S)-101 and (R,S)-104 of 7-azaindole analogs bearing a tert-butyl-substituted beta amino acid side chain; in vitro bDNA and PB2 fluorescence competition binding assay of enantiomeric pairs.

enantiomeric pairs. It was envisaged that attaching a nonpolar group at the β position may afford potential hydrophobic interactions with the aromatic amino acid residues Phe323, Phe325, and Phe404 present in the phosphate-binding region of PB2 while retaining the key-interactions, i.e., interaction of 7-azaindole core with Glu361 and Lys376. First, to validate this assumption, a docking analysis of compound (R)-101 into the active site of PB2 followed by superimposition of the X-ray structure of 96 complexed with PB2 was conducted (Figure 36). The overlay of 96 and (R)-101 at the cap-binding region of PB2 revealed good superimposition, and the tert-butyl group occupied the same area as the α-methyl dimethyl amide functionality. Encouraged by these findings, two enantiomeric pairs, namely, (R)-101, (S)-101 and (R)-104, (S)-104, were synthesized and evaluated for their binding affinity and antiviral potency. In support of the docking studies, the (R)-enantiomers (R)-101 and (R)-104 exhibited excellent binding affinity to PB2 (K$_d$ = 0.003 and <0.003 μM, respectively) and antiviral potency (EC$_{90}$ = 0.03 and 0.023 μM, respectively), whereas the (S)-enantiomers (S)-101 and (S)-104 were less potent (Figure 37). Furthermore, the X-ray cocrystal structure data for (R)-101 bound to PB2 suggested that N-1 and N-7 of the AI ring formed a H bond with Glu361 and Lys376 (Figure 36E), the AI ring was sandwiched between His357 and Phe404, while the pyrimidine ring was engaged in a π-stacking interaction with Phe323. The X-ray data also demonstrated that the hydrophobic pocket defined by the three phenylalanine residues Phe323, Phe325, and Phe404 could be utilized to forge stronger interactions with larger side chains (Figure 36E).

On the basis of the above findings, additional schemes were designed to develop a series of compounds having branched carbon chains (Figure 38).[141] This study suggested that interactions with the hydrophobic pocket of PB2 could be
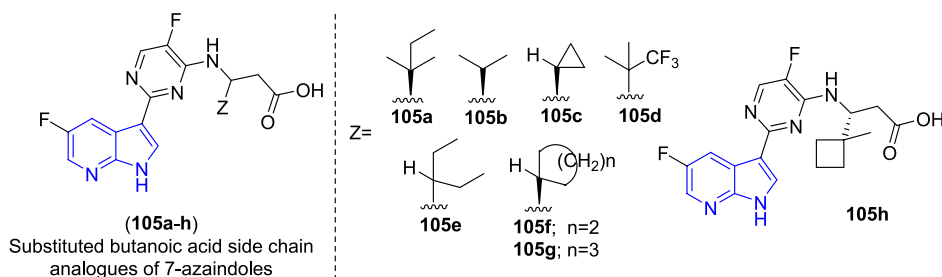
Figure 38. Structures of 7-azaindole analogs bearing substituted butanoic acids as side chains and their optimized spirocyclobutane analog **105h**.
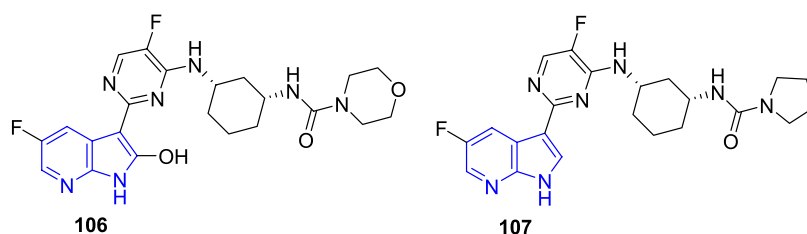

Figure 39. Structures of the 2-hydroxy metabolite of 1,3-diaminocyclohexyl morpholine urea analog **106** and 1,3-diaminocyclohexyl pyrrolidine urea analog **107**.
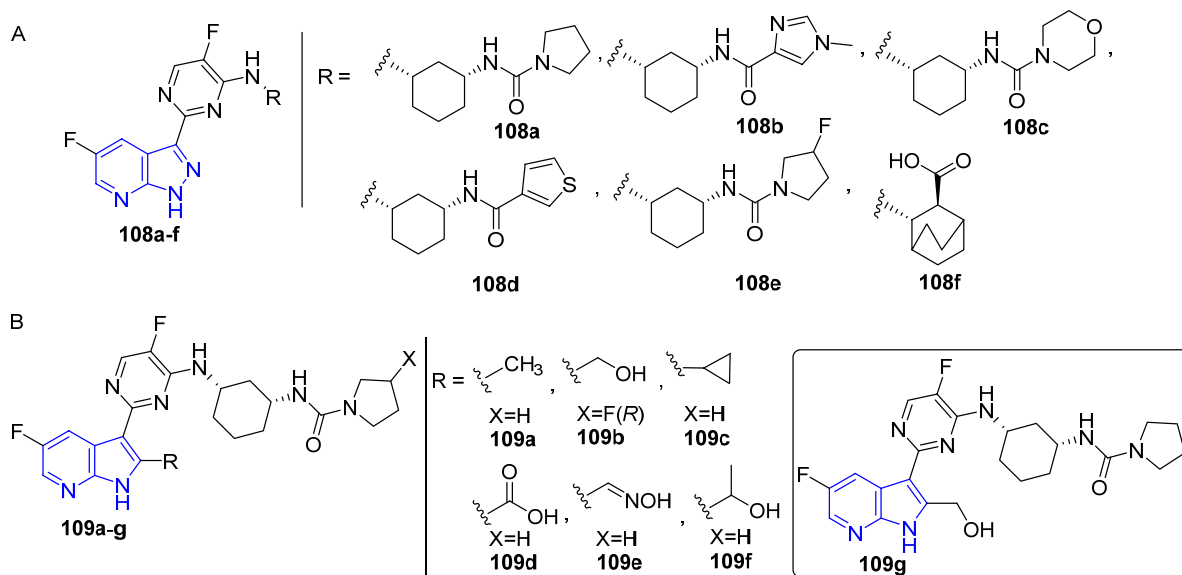

Figure 40. (A) Substituted 7-azaindazoles (**108a–f**). (B) C-2-Substituted 7-azaindoles (**109a–g**) and optimized analog 2-hydroxy methyl-substituted pyrrolidine urea **109g**.

increased by the incorporation of hydrophobic groups on the side chain of the pyrimidine ring in AI analogs.

Among the analogs **105a–h**, the spiro cyclobutane analog **105h** exhibited the highest anti-influenza activity. The overall cellular potency and target affinity of (*R*)-**101** (bDNA EC$_{90}$ = 0.03 μM and PB2 K_d = 0.003) and **105h** (bDNA EC$_{90}$ = 0.01 μM and PB2 $K_d \leq$ 0.003) led to further study to assess the antiviral activity against a broad range of influenza type A strains. Interestingly, (*R*)-**101** demonstrated potent antiviral activity against a broad range of influenza type A strains, including oseltamivir carboxylate-resistant isolates and the pandemic-causing H1N1 and H5N1 strains. In addition, the PK profiles of (*R*)-**101** and **105h** showed desirable iv and oral exposure in animal studies. (*R*)-**101** provided complete protection at all three tested doses with all animals surviving (10, 30, and 60 mpk b.i.d for 10 days). Similarly, **105h** also

showed a complete survival benefit but only when dosed at 3, 10, and 30 mpk b.i.d beginning at 48 h postinfection. Thus, (*R*)-**101** and **105h** showed efficacy even giving it after 48 h in an influenza mouse model. However, the standard drug oseltamivir was devoid of efficacy in this mouse model when tested at the clinically relevant human equivalent dose (10 mpk b.i.d).

Notably, the primary metabolite observed for **102** (Table 5) in human hepatocytes was due to oxidation at the C-2 position of the 7-azaindole ring to form the 2-hydroxy-substituted metabolite **106** (Figure 39) mediated by the cytosolic enzyme aldehyde oxidase (AO), which catalyzes the oxidation of aza-heterocycles and aldehydes, amide hydrolysis, and diverse reductions.[142]

To bypass the AO-mediated metabolism of 7-azaindoles, C-2-substituted compounds were synthesized incorporating a
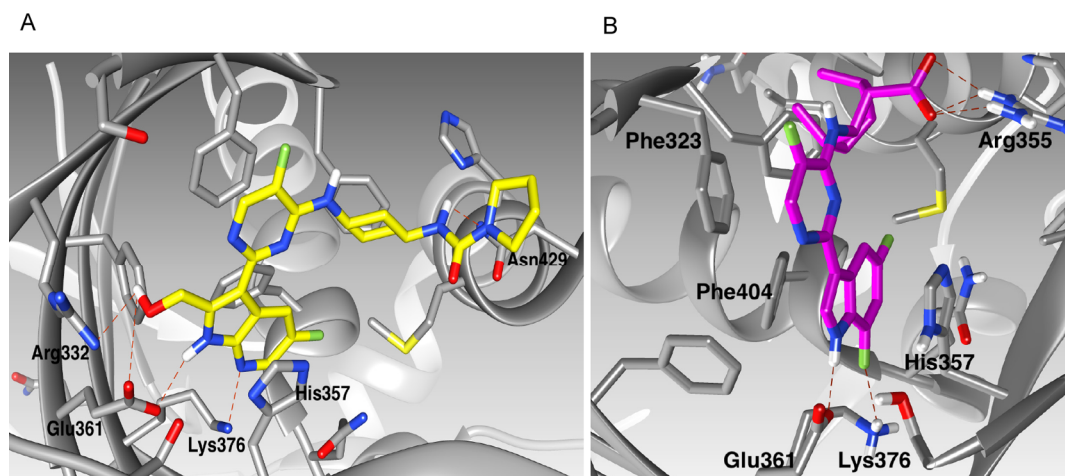
Figure 41. Binding interactions of the 7-azaindole-based 2-hydroxymethyl-substituted 1,3-diaminocyclohexyl pyrrolidine urea **109g** and indole analog **110** at the cap-binding domain of PB2. (A) Binding interactions of compound **109** at the m^{7}GTP binding site (PDB 5BUH), and involvement of N-1 and N-7 in the H-bonding interaction with Glu361 and Lys376 and 2-hydroxy methyl group interaction with Arg332 and Glu361. (B) Binding mode of compound **110** at the same binding site (PDB 6S5V). Fluorine at C7 interacts with Lys376, whereas N-1 interacts with Glu361. In addition, the terminal carboxylic acid group interacts with Arg355.

range of functionalities, including the addition of hydroxy methyl, methyl, cyclopropyl, carboxylic acid, oxime, and secondary alcohol groups (Figure 40B). This strategy was applied to **109**, which has a pyrrolidine urea moiety and was found to be 12-fold more potent than **102** in the bDNA assay.[142] In parallel, replacement of the C-2 carbon atom with a nitrogen atom to form an azaindazole ring (**108a–h**) was also envisioned as an approach to counter AO-mediated metabolism (Figure 40A).

Human liver cytosol stability studies have indicated that **109a**, **109b**, **109f**, and **109g** (Figure 40B) bypass AO-mediated metabolism at the C-2 position compared with compounds **102** and **107**. The PK profiles of **107**, **109g**, and **108a** in both mice and rats were favorable. Furthermore, the X-ray cocrystal structure of the complex of **109g** bound to the PB2 subunit revealed that the interaction between the PB2 domain and **109g** was similar to that of earlier molecules. An additional interaction was observed between the C-2 hydroxy methyl group through H bonds with Glu 361 and Arg 332 (Figure 41A).

McGowan and collaborators envisaged that 5,7-difluoroindoles could be effective bioisosteres of the 7-azaindole ring system in which the fluorine atom at the 7 position could mimic an aromatic nitrogen atom and adopt a similar binding mode.[143] In view of this, the 5,7-difluoroindole analog **110** of **99** was synthesized (Figure 42). In addition, substituents with similar sizes or electronic characteristics to fluorine, such as methyl, cyano, and chloro groups at the C-5 position, were also prepared.

X-ray cocrystal studies of **110** (Figure 41B) indicated that the indole ring formed π-stacking interactions with Phe404 and His357 and ionic interactions with Glu361 and Lys376, similar to earlier 7-azaindole congeners. A few additional interactions were observed, including π−π stacking between the pyrimidine ring of **110** and Phe323 and an interaction between the positively charged guanidino group of Arg355 and the negatively charged carboxylate group of **110**.

As anticipated, the C-7 fluorine atom of **110** interacted with Lys376, and the longer electronegative C−F bond length shifted **110** approximately 0.8 Å out of the binding pocket.
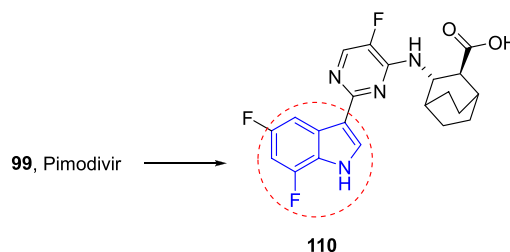

Figure 42. Bioisosteric replacement of 5-fluoroazaindole with 5,7-difluoroindole.

Thus, **110** adopted a slightly different conformation, allowing the carboxylic group to gain two additional ionic interactions with Arg355. This observation confirmed that 7-fluoroindole could act as a bioisostere of 7-azaindole. Compound **110** showed excellent in vitro metabolic stability (Cl$_{int}$ < 7.7 μL/min/mg protein) in human liver microsomes and was not susceptible to AO metabolism. The presence of fluorine atoms at the C-5 and C-7 positions of **110** may also be responsible for the enhanced metabolic stability.[144] In vivo studies with **110** were performed at a dose of 30 mpk b.i.d. for 10 days in the mouse influenza model, where 75% survival was observed in animals administered the drug beginning at 48 h postinfection, whereas oseltamivir yielded only 38% survival at its therapeutic equivalent dose in mice (10 mpk b.i.d. for 10 days).

Given the above findings, we postulate the important structural features of a probable potent PB2 inhibitor, as shown in Figure 43. A coplanar heterocycle at the C-3 position of the AI core will be beneficial for π-stacking with a protein. A hydrophobic linker connecting a C-3-substituted heterocycle ring with another aromatic ring might provide better binding with PB2 connected through ionic and H-bonding interactions.

Taken together, AI and its isomers continue to serve as a core potential template with which to design new antiviral agents against HIV-1, HCV, DENV, RSV, and influenza. Replacing CH with N atoms in the AI/indole core was the most successful approach to attain multiparameter optimization in antiviral drug research. We created a summary of the reported bioisosteric replacements of AIs/indoles along with
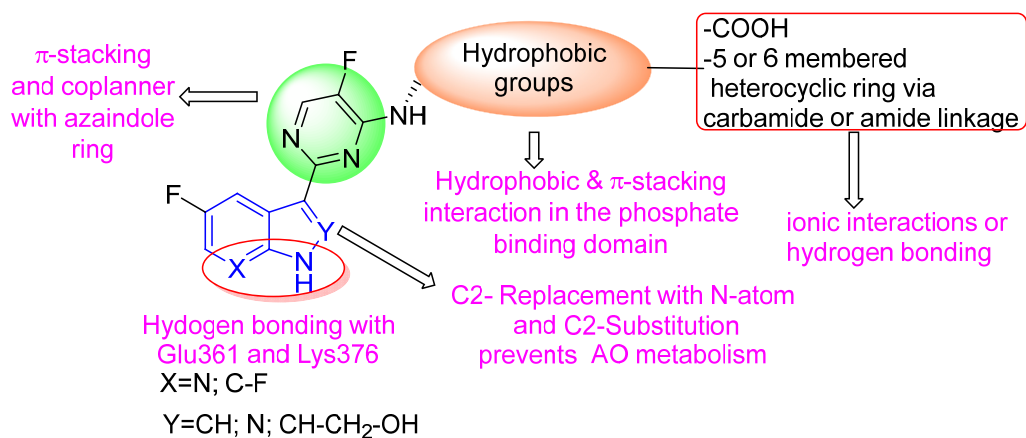
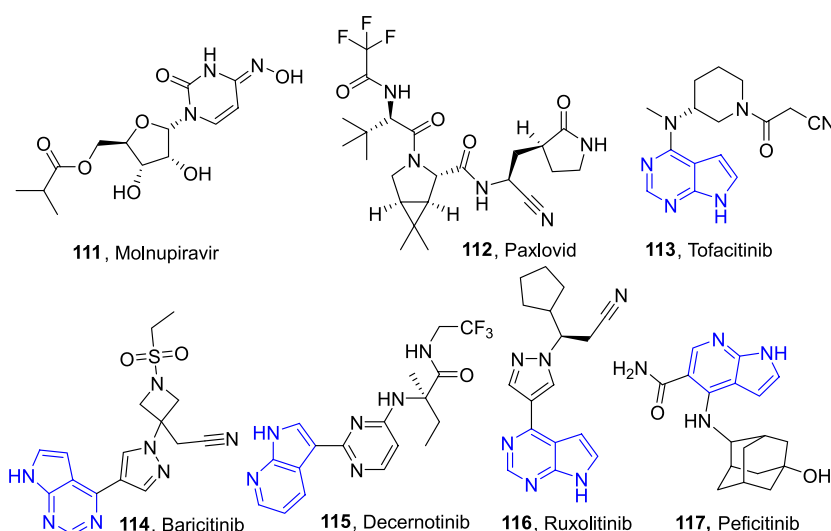**Figure 43.** Structural features of the 7-azaindole-based PB2 inhibitor design.

Figure 44. FDA-approved oral antiviral drugs, molnupiravir and paxlovid (**111** and **112**) against COVID-19, and chemical structures of AI-based JAK inhibitors.

the C-2 and C-3 substitution in antiviral drug discovery (Table 7).

FUTURE PERSPECTIVES OF AI ANALOGUES IN REGULATING COVID-19-INDUCED CYTOKINE STORM OR HYPERINFLAMMATORY SYNDROME IN PATIENTS

The coronavirus disease 2019 (COVID-19) pandemic, caused by severe acute respiratory syndrome coronavirus 2 (SARS-CoV-2), continues to spread globally despite unprecedented social isolation and restrictions resulting in widespread economic decline. More than 3.2 million people have been infected, and more than 230 000 of them have died. To date, no treatments have been definitively shown to be effective; however, a multipronged approach to mitigate transmission, morbidity, and mortality is ongoing. While upstream prevention strategies such as vaccination are ideal, these strategies are unlikely to be available in time to address current clinical need. Instead, fast tracking of drug development and repurposing of approved drugs has facilitated and expedited clinical trials that might hasten effective therapeutics. Many of these drugs act, at least in part, to directly limit viral replication. By contrast, the use of interleukin-6 (IL-6)

inhibition might have benefits by controlling the pathological immune response to the virus. Here, we expand on the theoretical basis of IL-6 inhibition and propose potential benefits from other immunomodulators that could, in theory, prove more efficacious.

For the latter phase of convalescence, hospitalized patients with COVID-19 can develop a syndrome of dysregulated and systemic immune over activation described as a cytokine storm or hyperinflammatory syndrome that worsens acute respiratory distress syndrome and can lead to multisystem organ failure. The scarce systematic data available have shown an association between ferritin, lactate dehydrogenase, IL-6, IL-1, d-dimer, and C-reactive protein and severe disease. If this group can be identified before decompensation, early and aggressive immunomodulatory treatment might prevent the need for intubation and extracorporeal membrane oxygenation. To date, observational studies suggest a possible benefit, but results of placebo-controlled randomized clinical trials are not yet available. Given the methodological limitations of existing studies, more evidence is needed. With the rapidly expanding number of critically ill patients, there is an urgent need to identify multiple putative biological targets. While IL-6 inhibition attenuates key aspects of the cytokine cascade, we
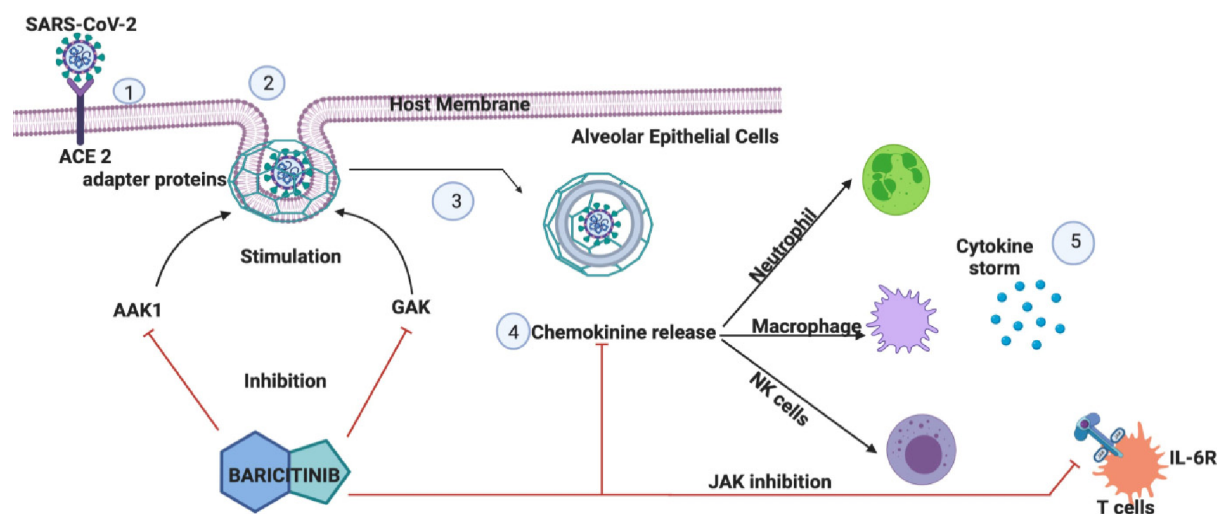
Figure 45. Proposed dual mechanism (anticytokine activity and inhibitors of host cell viral propagation) of the action of baricitinib (**114**) in COVID-19: (1) SARS-CoV-2 binds to host ACE 2 through the spike proteins (2) upon entry; SARS-CoV-2 induces clathrin-mediated endocytosis. AAK1 and GAK mediate the assembly of clathrin adapter proteins to form clathrin cages surrounding the virus before it is trafficked to endosomes (3) upon virus entry; activation of immune cells and release of chemokines (4) result in the recruitment of neutrophils, macrophages, NK cells, and T cells, which further damage alveolar epithelial cells via a process called the cytokine storm (5) baricitinib (**114**); AI analog has been proposed to inhibit 2 checkpoints, i.e., inhibit viral entry via AAK1- and GAK-mediated endocytosis and inhibit cytokine storms via JAK-STAT-dependent cytokine receptors.

posit other immune targets of inhibition to be considered and their potential to be more efficacious in the setting of COVID-19, specifically IL-1 inhibitors and Janus kinase (JAK) inhibitors.

Recently, molnupiravir (**111**) and paxlovid (**112**) have been approved by the FDA for emergency use as oral antiviral drugs against COVID-19 (Figure 44). However, the WHO has not yet recommended the use of these drugs for the treatment of COVID-19. The WHO recommended baricitinib, an oral drug, and sotrovimab, the monoclonal antibodies against COVID-19, but still a lot of deliberations are going on, and most of the countries have not included it as a part of the therapeutic regimen against COVID-19. However, the available treatment options for COVID-19 are essentially based on symptoms, and oxygen therapy is the main option for severely infected patients. In cases of respiratory failure, artificial ventilation may be necessary.[145] The symptomatic treatment modalities of COVID-19 are based mainly on three different mechanisms, i.e., reducing the viral load by drugs targeting viral entry, drugs inhibiting viral replication, and management of the hyperinflammatory state by immunomodulating drugs.

Novel virus-based structural proteins have been identified as drug targets in COVID-19, such as the nucleocapsid N protein, spike S glycoprotein, and several virus-based nonstructural proteins. Similarly, host-based targets, such as the ACE2 receptor, AAK1/GAK, JAK, transmembrane serine protease 2, furin, cathepsin L, phosphatidylinositol 3-phosphate 5-kinase, and two-pore channels, have also been identified as potential host targets.[146,147]

More than 100 drugs from diverse therapeutic classes were proposed for their potential to be repurposed for COVID-19 by taking advantage of current information on their safety pharmacology to enable rapid clinical trials and regulatory review.[148] Recently, the potential role of AI-based JAK inhibitors **114** and **116** (Figure 44) in combating cytokine storms or hyperinflammatory syndrome in COVID-19 patients has been explored. Hyperinflammatory syndrome is one of the

primary causes of multiple organ failure and death.[149,150] ACE2 and CD147 (cluster of differentiation 147) are the two important receptors that are thought to be involved in SARS-CoV-2 invasion and dissemination into the host cells.[151] In the early stages of SARS-CoV-2 infection, the positive role of the transmembrane protein ACE2 has been confirmed in alveolar epithelial cells in conjunction with the cellular protease TMPRSS2.[152] ACE2 binds to the spike proteins on the capsid of SARS-CoV-2 (Figure 45), which subsequently initiates clathrin-dependent endocytosis of SARS-CoV-2.[151]

Following SARS-CoV-2 infection, a reciprocal state tends to be established in which downregulation of the renin−angiotensin system affords a natural protective effect along with an upregulation of proinflammatory cytokines.[153] From the clinical data, higher serum levels of many cytokines, such as IL 6, IL 2, IL-1b, IL-8, IL-17, IFN-g, TNF-a, IP 10, MCP-1, IL-10, and IL-4, have been documented in COVID-19 patients.[154]

Therefore, targeting JAK-STAT-dependent signaling with JAK inhibitors to reduce the production of IL-6 and other cytokines was thought to be a direct approach to mitigate the cytokine storms associated with COVID-19 (Figure 45). Five clinical trials were explored which were designed to address the safety and efficacy of **114** in COVID-19-infected patients at clinical doses of 2−4 mg daily for 7−14 days.[149] Moreover, **114** has been reported to block the intracellular trafficking of SARS-CoV-2 virus, which is regulated by clathrin-associated host adaptor proteins controlled by AAK1 and cyclin G-related kinases (GAK).[155] Molecule **114** binds with high affinity to AAK1 (17 nM), JAK1 (6 nM), and JAK2 (6 nM), affording a potential advantage in countering SARS-CoV-2 COVID-19 infectivity.[156] In addition, **114** has been reported for treating inflammatory conditions, such as rheumatoid arthritis and myelofibrosis. Recently, in 2021, the FDA issued warnings for the use of the JAK inhibitors against chronic inflammatory conditions. The FDA advisory highlighted the increased risk of heart-related events such as heart attack, stroke, blood clots, and death of few patients. There is higher risk involved with
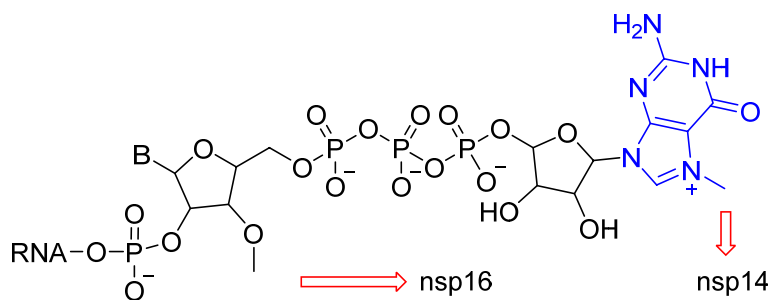
Figure 46. Methylation of N-7 of GTP and the C2 hydroxyl group of the adjacent nucleotide by nsp14 and nsp16, respectively. B = base.
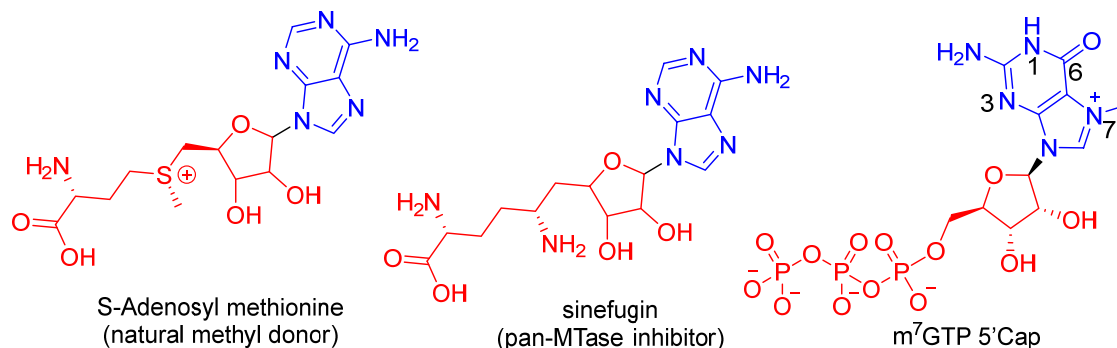

Figure 47. N-1,2-NH$_2$ and O-6 of the guanine ring and N-1 and N-7 of the AI ring recognize the same binding pocket due to the observed bioisosterism.

these drugs for current or past smoking patients or who had a heart attack. It was advised that all of the clinical health care professionals must consider the benefits and risks for the individual patient prior to initiating or continuing therapy using JAK inhibitors against COVID-19 infection.

Next, it was proposed that **114** may be effective against the elevated levels of cytokines at its therapeutic dose in COVID-19 patients.[156,157] Fine tuning of the selectivity of AI toward JAK and AAK1 may yield multitargeted molecules against COVID-19. JAK-targeting compounds may be developed as anticytokine medicines against various inflammation-associated diseases, including COVID-19. In contrast, compounds selective for AAK1 can be established as early-phase medication agents in SARS-CoV-2 and other viral infections.

Virus-based nonstructural proteins (nsps) serve an essential function in the lifecycle of SARS-CoV-2.[158] The eukaryotic mRNA 5′-cap structure is considered necessary for RNA stability by affording a molecular signature for self- or nonself-mRNA distinction.[159] To escape innate host immunity, the 5′-end of the viral RNA gets modified by forming an m^{7}GTP cap and a C2′-O methyl cap on the adjacent nucleotide (Figure 46).[160] In eukaryotes, 5′ capping is introduced on newly transcribed host mRNA already present within the nucleus to which SARS-CoV-2 does not have access. To overcome this inaccessibility, the virus has evolved to synthesize its own cap-forming protein machinery in the cytoplasm.

In particular, nsp14 and nsp16 are responsible for methylation of the guanine of the GTP and the C2′ hydroxyl group of the nucleotides (Figure 46).[160]

Both nsp14 and nsp16 are *S*-adenosyl methionine (SAM)-dependent methyltransferases (MTases) and seem to be essential for the viral lifecycle.[158] In SARS-CoV-2, nsp16 in conjunction with nsp10 methylates the 5′-end of virally

encoded mRNAs to mimic cellular mRNAs, thus protecting the virus from host innate immune restriction. nsp16 seems to be a very promising molecular target for drug discovery, and the crystal structure of SARS-CoV-2 nsp10 and nsp16 in complex with the purine analogs sinefungin (pan-MTase inhibitor) and SAM (natural methyl donor) provides a strong foundation for structure-based inhibitor design for COVID-19 (Figure 47).[158,160] The binding pattern of the 7-azaindole analogs **96**, **99**, (*R*)-**101**, **103**, **109g**, and **110** includes N-1 and N-7 of AI, which undergo H-bonding interactions similar to the purine ring of m^{7}GTP (N-1, 2-N1, 2-H$_2$, O-6) and occupy the purine-binding domain at the Pb2 cap-binding site (Figures 36 and 41). These features confirm the bioisostere nature of 7-azaindole with purine in the PB2 binding pocket. The anti-influenza activity of 7-azaindole results from its inhibition of the influenza virus cap-snatching mechanism. SARS-CoV-2 also exhibits a similar capping mechanism for its RNA stability with the help of nsp14 and nsp16.[160]

Therefore, we believe that structure-guided optimization to form 7-azaindole-based nucleosides could generate promising scaffolds. Alternately, the incorporation of carbocyclic/heterocyclic mimics of sugar amino acids at the C-3, C-4, or C-5 position of 7-azaindole could be a rational structural design strategy to develop AI-based inhibitors to combat COVID-19 and other viral diseases.

■ CONCLUSION

Our in-depth and critical survey of a decade of work on AIs and their analogs reinforces the perspectives of remarkably successful antiviral agents against a wide spectrum of RNA viruses. It is thus imperative to modify AI-containing compounds to attenuate the H-bonding capacity, physiological profile, pharmacological characteristics, and physicochemical

Table 7. Summary of Bioisosteric Replacements of AIs/Indoles and C-2 and C-3 Substitutions on AIs in the Design of Antiviral Agents

Transformation	Example	Pharmacological profile
C-3 substitution	**43b**	1) Readily hydrolyzed and stable 2) Low blood clearance in humans 3) Moderate bioavailability humans and $t_{1/2}$ = 4.5 h 4) No inhibition of CYP isoforms, HCV polymerase and Mg-dependent protein kinase 5) Attenuated clearance rates in human hepatocytes
C-3, C-5 substitution	**44b**	1) 300-fold improvement in antiviral potency, clearance in both human liver microsomes and human hepatocytes 2) Improved *in vitro* permeability 3) Reduction in glucuronidation rates *in vitro* 4) Comparable *in vivo* human PK parameters
CH → N	**49=** Y_1, Y_2, Y_3 = N, C-Cl, CH; R_1 = (CH₂)₃SO₂Me; R_2 = CH₂C **50=** Y_1, Y_2, Y_3 = CH, C-Cl, N; R_1 = (CH₂)₃CF₃; R_2 = CH₂C **51=** Y_1, Y_2, Y_3 = CH, N, CH; R_1 = (CH₂)₃CF₃; R_2 = CH₂C	1) Similar potent activity for **49-50**, but variable PK profile 2) N at C-5 (**51**) yielded refined π-stacking, thus increasing the solubility and lung distribution of the compounds
CH → N	**52**	N at C-6 in **52** yielded lower potency (8-10-fold)
CH → N	**53b**	1) Substantial permeability and similar metabolic stability in rats 2) Less protein bound, excellent plasma exposure, moderate clearance after iv dosing and low distribution to the lung in rats
CH → N	**53c**	1) Beneficial for both permeability and potency, acceptable metabolic stability in rats 2) Less protein binding, moderate plasma exposure, high clearance, and well distributed to the lung in rats
CH → N	**54f** py = pyridine	1) Decreased lipophilicity (enhanced solubility), and a decrease in antiviral potency 2) Effective in attenuating Pgp recognition
Identical binding at PB2 binding site	**99**	H-bonding interaction of N-1 and N-7 of **99** and N-1,2-N1,2-H₂, O-6 of the m⁷GTP ring are similar at the PB2 binding site.

Table 7. continued

Transformation	Example	Pharmacological profile
Identical binding at AAK1 binding site	56	A pyrrole-2-one moiety of kinase inhibitor K252a, nintedanib, and a 7-azaindole moiety of compound **56** exhibit identical binding at the AAK1 binding site.
C-2 substitution	109g	C-2 substitution of 7-azaindole bypasses AO-mediated metabolism.
N → C-F	110	Metabolic stability and a marked increase in *in vivo* antiviral potency
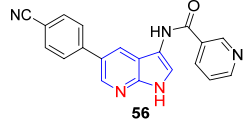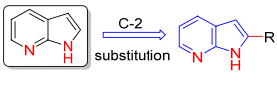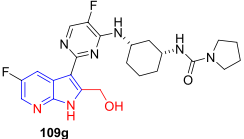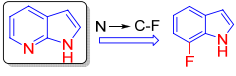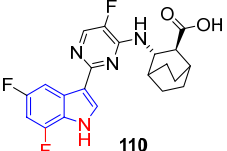
properties of AIs to obtain lead compounds against different viruses.

AUTHOR INFORMATION

Corresponding Author

Vibha Tandon − *Drug Discovery Laboratory, Special Centre for Molecular Medicine, Jawaharlal Nehru University, New Delhi 110 067, India;* orcid.org/0000-0001-6146-937X; Email: vtandon@mail.jnu.ac.in

Authors

Urvashi − *Department of Chemistry, University of Delhi, New Delhi 110007, India; Drug Discovery Laboratory, Special Centre for Molecular Medicine, Jawaharlal Nehru University, New Delhi 110 067, India*

J. B. Senthil Kumar − *Drug Discovery Laboratory, Special Centre for Molecular Medicine, Jawaharlal Nehru University, New Delhi 110 067, India*

Parthasarathi Das − *Department of Chemistry, Indian Institute of Technology (ISM), Dhanbad 826004, India;* orcid.org/0000-0002-9306-4956

Complete contact information is available at:
https://pubs.acs.org/10.1021/acs.jmedchem.2c00444

Notes

Biographies

Vibha Tandon received her Ph.D. degree from Allahabad University, India in 1991. She has 27 years of research experience in Medicinal Chemistry. She is a full professor at the Special Centre for Molecular Medicine, Jawaharlal Nehru University. Before moving to JNU, she was a professor at the Department of Chemistry, Delhi University. She received a Fulbright Nehru Senior Fellowship by the USFEI and Royal Society of UK by the Indian National Science Academy to visit the United States and United Kingdom for a research collaboration for one year each. She pursues translational research in her lab to bring small molecules from the bench to the bed side. Her research interests involve synthesis of libraries of small molecules and multiscale approaches to combat the mechanisms of antimicrobial resistance through PPEF (small molecule) as a bacterial topoisomerase IA inhibitor. Prof. Tandon's group has developed one bisbenzimidazole as radioprotector to protect normal cells.

Urvashi received her B.Sc. degree in 2011 and M.Sc. degree in Organic Chemistry from Delhi University in 2013. She joined the Special Centre for Molecular Medicine, Jawaharlal Nehru University as a junior research fellow for a few months. She received her Ph.D. degree from Delhi University in 2021, and her doctoral thesis title was "Transition-Metal-Catalyzed C−C/C−S Coupling and C−N Bond Formation: Synthesis of N-Heterocyclic Compounds and their Biological Evaluation". Briefly, her research interests include finding a flexible route to access heteroaromatic frameworks (C−C/C−S/C−N) with challenging substitution patterns using transition-metal-catalyzed cyclization, condensation, coupling, and addition reactions and to evaluate them for medicinal purposes.

J. B. Senthil Kumar obtained his Ph.D. degree in Medicinal Chemistry in 2014 from the University of Delhi, North Campus. The main focus of his Ph.D. thesis was to identify a newer class of dopamine agonists by structural modification of a natural product ergoline ring to obtain promising compounds with in vivo efficacy animal models of Parkinsonism. Currently, he is working as a DS Kothari Postdoctoral Fellow (UGC) at the Special Centre for Molecular Medicine, Jawaharlal Nehru University. His research interest includes the design and synthesis of neuroprotective agents for the mitigation of oxidative stress associated with neurological disorders.

Parthasarathi Das received his Ph.D. degree in 1999 from NCL Pune, India. After completing postdoctoral studies (1999−2003) at RWTH Aachen, Germany, Tohoku University, Japan, and Harvard University, United States, he joined Dr. Reddy's Laboratories Ltd., India (2004) and worked in the medicinal chemistry group with a research focus on various therapeutic areas. In 2012, he joined the CSIR-Indian Institute of Integrative Medicine Jammu, India. Currently, he is a faculty member at the Indian Institute of Technology (ISM). His research interests include medicinal chemistry, the development of new synthetic tools, and the synthesis of biologically active natural products. He has received the Chemical Research Society of India (CRSI) Bronze Medal for his contribution to research in chemistry.

ABBREVIATIONS USED

AAK1, adaptor-associated kinase 1; ACE2, angiotensin-converting enzyme 2; ADCC, antibody-dependent cellular cytotoxicity; ADME, absorption, distribution, metabolism, and excretion; AI, azaindole; ALRT, acute lower respiratory tract infection; AMLV, amphotropic murine leukemia virus; AO, aldehyde oxidase; BBB, blood−brain barrier; BCS, Biopharmaceutics Classification System; bDNA, branched DNA; BIF, bioisostere factor; BMP2K, bone morphogenetic protein 2 inducible kinase; BMS, Bristol Myers Squibb; CART, combination antiretroviral therapy; CD147, cluster of differentiation 147; CDC, complement-dependent cytotoxicity; cDNA, complementary DNA; CNS, central nervous system; CPE, cellular protection assay; CPR, cytopathic effect; CYP3A4, cytochrome P450 3A4; DENV, dengue virus; DNP, 1,3-dinitrophenyl; DTG, dolutegravir; HLM, human liver microsomes; EBOV, ebola virus; ESPT, excited-state proton transfer; EVD, ebola virus; EVG, elvitegravir; FP, fusion peptides; GAK, cyclin G-associated kinase; GIT, gastrointestinal tract; HCV, hepatitis C virus; hERG, Human Ether-à-go-go-Related Gene; HIV, human immunodeficiency virus; HSCHD, hemodynamically significant congenital heart diseases; IN, integrase; IRF-3, interferon regulatory factor-3; JAK, Janus kinase; JAK-STAT, Janus kinase signal transduction and transcription; LipE, lipophilic efficacy; mAb, monoclonal antibody; m^7GTP, 7-methylguanosine 5′-triphosphate; MLM, mouse liver microsomes; MTases, methyl transferase; NAKs, NUMB-associated kinases family; nsps, nonstructural proteins; NIAID, National Institute of Allergy and Infectious Disease; NNRTIs, non-nucleoside reverse transcriptase inhibitors; NRTIs, nucleoside reverse transcriptase inhibitors; NS4B, nonstructural membrane bound protein; PBMC, peripheral blood mononuclear cells; PIs, protease inhibitors; PI3Kγ, phosphoinositide-3-kinase γ inhibitors; PK, pharmacokinetics; RAL, raltegravir; RdRp, RNA-dependent RNA polymerase; RSV, respiratory syncytial virus; RT, reverse transcriptase; SAM, S-adenosyl methionine; SAR, structure−activity relationship; SARS, severe acute respiratory syndrome; SFV, Semliki Forest; SIN, Sindbis virus; STK16, serine/threonine protein kinase16; TM, transmembrane anchor; WEEV, Western equine encephalitis virus

REFERENCES

(1) Dua, R.; Shrivastava, S.; Sonwane, S. K.; Srivastava, S. K. Pharmacological significance of synthetic heterocycles scaffold: A review. *Adv. Biol. Res.* **2011**, *5*, 120−144.

(2) Jampilek, J. Heterocycles in medicinal chemistry. *Molecule* **2019**, *24*, 3839−3842.

(3) Vitaku, E.; Smith, D. Y.; Njardarson, J. T. Analysis of the structural diversity, substitution patterns, and frequency of nitrogen heterocycles among U.S. FDA approved pharmaceuticals. *J. Med. Chem.* **2014**, *57*, 10257−10274.

(4) Horton, D. A.; Bourne, G. T.; Smythe, M. L. The combinatorial synthesis of bicyclic privileged structures or privileged substructures. *Chem. Rev.* **2003**, *103*, 893−930.

(5) de Sa Alves, F.; Barreiro, E.; Manssour Fraga, C. From nature to drug discovery: The indole scaffold as a 'privileged structure. *Mini Rev. Med. Chem.* **2009**, *9*, 782−793.

(6) Sharma, V.; Kumar, P.; Pathak, D. Biological importance of the indole nucleus in recent years: A comprehensive review. *J. Heterocycl. Chem.* **2010**, *47*, 491−502.

(7) Welsch, M. E.; Snyder, S. A.; Stockwell, B. R. Privileged scaffolds for library design and drug discovery. *Curr. Opin. Chem. Biol.* **2010**, *14*, 347−361.

(8) Walker, S. R.; Carter, E. J.; Huff, B. C.; Morris, J. C. Variolins and related alkaloids. *Chem. Rev.* **2009**, *109*, 3080−3098.

(9) Pennington, L. D.; Moustakas, D. T. The necessary nitrogen atom: A versatile high-impact design element for multiparameter optimization. *J. Med. Chem.* **2017**, *60*, 3552−3579.

(10) Kalil, A. C.; Patterson, T. F.; Mehta, A. K.; Tomashek, K. M.; Wolfe, C. R.; Ghazaryan, V.; Marconi, V. C.; Ruiz-Palacios, G. M.; Hsieh, L.; Kline, S.; Tapson, V.; Iovine, N. M.; Jain, M. K.; Sweeney, D. A.; El Sahly, H. M.; Branche, A. R.; Regalado Pineda, J.; Lye, D. C.; Sandkovsky, U.; Luetkemeyer, A. F.; Cohen, S. H.; Finberg, R. W.; Jackson, P. E.H.; Taiwo, B.; Paules, C. I.; Arguinchona, H.; Erdmann, N.; Ahuja, N.; Frank, M.; Oh, M.-d.; Kim, E.-S.; Tan, S. Y.; Mularski, R. A.; Nielsen, H.; Ponce, P. O.; Taylor, B. S.; Larson, L.; Rouphael, N. G.; Saklawi, Y.; Cantos, V. D.; Ko, E. R.; Engemann, J. J.; Amin, A. N.; Watanabe, M.; Billings, J.; Elie, M.-C.; Davey, R. T.; Burgess, T. H.; Ferreira, J.; Green, M.; Makowski, M.; Cardoso, A.; de Bono, S.; Bonnett, T.; Proschan, M.; Deye, G. A.; Dempsey, W.; Nayak, S. U.; Dodd, L. E.; Beigel, J. H. Baricitinib plus remdesivir for hospitalized adults with Covid-19. *N. Engl. J. Med.* **2021**, *384*, 795−807.

(11) Blaazer, A. R.; Lange, J. H. M.; van der Neut, M. A. W.; Mulder, A.; den Boon, F. S.; Werkman, T. R.; Kruse, C. G.; Wadman, W. J. Novel indole and azaindole (pyrrolopyridine) cannabinoid (CB) receptor agonists: Design, synthesis, structure-activity relationships, physicochemical properties and biological activity. *Eur. J. Med. Chem.* **2011**, *46*, 5086−5098.

(12) Irie, T.; Sawa, M. 7-azaindole: A versatile scaffold for developing kinase inhibitors. *Chem. Pharm. Bull.* **2018**, *66*, 29−36.

(13) Mérour, J.-Y.; Buron, F.; Plé, K.; Bonnet, P.; Routier, S. The azaindole framework in the design of kinase inhibitors. *Molecules* **2014**, *19*, 19935−19979.

(14) Daydé-Cazals, B.; Fauvel, B.; Singer, M.; Feneyrolles, C.; Bestgen, B.; Gassiot, F.; Spenlinhauer, A.; Warnault, P.; Van Hijfte, N.; Borjini, N.; Chevé, G.; Yasri, A. Rational design, synthesis, and biological evaluation of 7-azaindole derivatives as potent focused multi-targeted kinase inhibitors. *J. Med. Chem.* **2016**, *59*, 3886−3905.

(15) Koyama, T.; Wakisaka, A. Molecular self-assembly composed of aromatic hydrogen-bond donor-acceptor complexes. *J. Chem. Soc., Faraday Trans.* **1997**, *93*, 3813−3817.

(16) Luo, G. G.; Gao, S. Global health concerns stirred by emerging viral infections. *J. Med. Virol.* **2020**, *92*, 399−400.

(17) Wu, Y.-J. Heterocycles and medicine: A survey of the heterocyclic drugs approved by the U.S. FDA from 2000 to present. *Progr. Heterocycl. Chem.* **2012**, *24*, 1−53.

(18) Taylor, A. P.; Robinson, R. P.; Fobian, Y. M.; Blakemore, D. C.; Jones, L. H.; Fadeyi, O. Modern advances in heterocyclic chemistry in drug discovery. *Org. Biomol. Chem.* **2016**, *14*, 6611−6637.

(19) Adler, T. K.; Albert, A. The biological and physical properties of the azaindoles. *J. Med. Chem.* **1963**, *6*, 480−483.

(20) Bochvar, D. A.; Bagatur'yants, A. A. The electronic structure of protonated forms of azaindoles. *Theor. Exp. Chem.* **1972**, *5*, 529−532.

(21) Mérour, J.-Y.; Routier, S.; Suzenet, F.; Joseph, B. Recent advances in the synthesis and properties of 4-, 5-, 6- or 7-AIs. *Tetrahedron* **2013**, *69*, 4767−4834.

(22) Ishikita, H.; Saito, K. Proton transfer reactions and hydrogen-bond networks in protein environments. *J. R. Soc. Interface* **2014**, *11*, 20130518.

(23) Gensch, T.; Heberle, J.; Viappiani, C. Proton transfer in biological systems. *Photochem. Photobiol. Sci.* **2006**, *5*, 529−530.

(24) Ross, J. B.; Szabo, A. G.; Hogue, C. W. Enhancement of protein spectra with tryptophan analogs: fluorescence spectroscopy of protein-protein and protein nucleic acid interactions. *Methods Enzymol.* **1997**, *278*, 151−190.

(25) Cornish, V. W.; Benson, D. R.; Altenbach, C. A.; Hideg, K.; Hubbell, W. L.; Schultz, P. G. Site-specific incorporation of biophysical probes into proteins. *Proc. Natl. Acad. Sci. USA* **1994**, *91*, 2910−2914.

(26) Scott, D. J.; Leejeerajumnean, S.; Brannigan, J. A.; Lewis, R. J.; Wilkinson, A. J.; Hoggett, J. G. Quaternary re-arrangement analysed by spectral enhancement: the interaction of a sporulation repressor with its antagonist. *J. Mol. Biol.* **1999**, *293*, 997−1004.

(27) Blouse, G. E.; Perron, M. J.; Thompson, J. H.; Day, D. E.; Link, C. A.; Shore, J. D. A concerted structural transition in the plasminogen activator inhibitor-1 mechanism of inhibition. *Biochemistry* **2002**, *41*, 11997−12009.

(28) De Filippis, V.; De Boni, S.; De Dea, E.; Dalzoppo, D.; Grandi, C.; Fontana, A. Incorporation of the fluorescent amino acid 7-azatryptophan into the core domain 1−47 of hirudin as a probe of hirudin folding and thrombin recognition. *Protein Sci.* **2004**, *13*, 1489−1502.

(29) Richmond, M. H. The effect of amino acid analogues on growth and protein synthesis in microorganisms. *Bacteriol. Rev.* **1962**, *26*, 398−420.

(30) Chen, Y.; Rich, R. L.; Gai, F.; Petrich, J. W. Fluorescent species of 7-azaindole and 7-azatryptophan in water. *J. Phys. Chem.* **1993**, *97*, 1770−1780.

(31) Hsieh, C.-C.; Jiang, C.-M.; Chou, P.-T. Recent experimental advances on excited-state intramolecular proton coupled electron transfer reaction. *Acc. Chem. Res.* **2010**, *43*, 1364−1374.

(32) Twine, S. M.; Murphy, L.; Phillips, R. S.; Callis, P.; Cash, M. T.; Szabo, A. G. The photophysical properties of 6-azaindole. *J. Phys. Chem. B* **2003**, *107*, 637−645.

(33) Shen, J.-Y.; Chao, W.-C.; Liu, C.; Pan, H.-A.; Yang, H.-C.; Chen, C.-L.; Lan, Y.-K.; Lin, L.-J.; Wang, J.-S.; Lu, J.-F.; Chun-Wei Chou, S.; Tang, K.-C.; Chou, P.-T. Probing water micro-solvation in proteins by water catalysed proton-transfer tautomerism. *Nat. Commun.* **2013**, *4*, 2611.

(34) Gordon, M. S. Hydrogen transfer in 7-azaindole. *J. Phys. Chem.* **1996**, *100*, 3974−3979.

(35) Yu, W.-S.; Cheng, C.-C.; Cheng, Y.-M.; Wu, P.-C.; Song, Y.-H.; Chi, Y.; Chou, P.-T. Excited-state intramolecular proton transfer in five-membered hydrogen-bonding systems: 2-pyridyl pyrazoles. *J. Am. Chem. Soc.* **2003**, *125*, 10800−10801.

(36) Duong, M. P. T.; Park, K.; Kim, Y. Excited state double proton transfer of a 1:1 7-azaindole: H_2O complex and the breakdown of the rule of the geometric mean: Variational transition state theory studies including multidimensional tunnelling. *J. Photochem. Photobiol., A* **2010**, *214*, 100−107.

(37) Watts, J. M.; Dang, K. K.; Gorelick, R. J.; Leonard, C. W.; Bess, J. W., Jr; Swanstrom, R.; Burch, C. L.; Weeks, K. M. Architecture and secondary structure of an entire HIV-1 RNA genome. *Nature* **2009**, *460*, 711−716.

(38) Barré-Sinoussi, F.; Ross, A. L.; Delfraissy, J.-F. Past, present and future: 30 years of HIV research. *Nat. Rev. Microbiol.* **2013**, *11*, 877−883.

(39) Freed, E. O. HIV-1 assembly, release and maturation. *Nat. Rev. Microbiol.* **2015**, *13*, 484−496.

(40) Rücker, E.; Grivel, J. C.; Münch, J.; Kirchhoff, F.; Margolis, L. Vpr and Vpu are important for efficient human immunodeficiency virus type 1 replication and CD_4^+ T-cell depletion in human lymphoid tissue *ex vivo*. *J. Virol.* **2004**, *78*, 12689−12693.

(41) Li, G.; De Clercq, E. HIV genome-wide protein associations: a review of 30 years of research. *Microbiol. Mol. Biol. Rev.* **2016**, *80*, 679−731.

(42) Offering information on HIV/AIDS treatment, prevention, and research; https://aidsinfo.nih.gov/understanding-hiv-aids/infographics/25/fda-approval-of-hiv-medicines (accessed on July 4, 2020).

(43) Haqqani, A. A.; Tilton, J. C. Entry inhibitors and their use in the treatment of HIV1 infection. *Antivir. Res.* **2013**, *98*, 158−170.

(44) Tilton, J. C.; Doms, R. W. Entry inhibitors in the treatment of HIV-1 infection. *Antiviral Res.* **2010**, *85*, 91−100.

(45) Kuritzkes, D. R. HIV-1 entry inhibitors: an overview. *Curr. Opin. HIV AIDS* **2009**, *4*, 82−87.

(46) Engelman, A.; Cherepanov, P. The structural biology of HIV-1: mechanistic and therapeutic insights. *Nat. Rev. Microbiol.* **2012**, *10*, 279−290.

(47) Qian, K.; Morris-Natschke, S. L.; Lee, K. H. HIV entry inhibitors and their potential in HIV therapy. *Med. Res. Rev.* **2009**, *29*, 369−393.

(48) Meanwell, N. A.; Wallace, O. B.; Fang, H.; Wang, H.; Deshpande, M.; Wang, T.; Yin, Z.; Zhang, Z.; Pearce, B. C.; James, J.; Yeung, K.-S.; Qiu, Z.; Wright, J. J. K.; Yang, Z.; Zadjura, L.; Tweedie, D. L.; Yeola, S.; Zhao, F.; Ranadive, S.; Robinson, B. A.; Gong, Y.-F.; Wang, H. -G. H.; Blair, W. S.; Shi, P.-Y.; Colonno, R. J.; Lin, P.-F. Inhibitors of HIV-1 attachment. Part 2: An initial survey of indole substitution patterns. *Bioorg. Med. Chem. Lett.* **2009**, *19*, 1977−1981.

(49) Lu, L.; Yu, F.; Cai, L.; Debnath, A. K.; Jiang, S. Development of small-molecule HIV entry inhibitors specifically targeting gp120 or gp41. *Curr. Top. Med. Chem.* **2015**, *16*, 1074−1090.

(50) Meanwell, N. A.; Krystal, M. R.; Nowicka-Sans, B.; Langley, D. R.; Conlon, D. A.; Eastgate, M. D.; Grasela, D. M.; Timmins, P.; Wang, T.; Kadow, J. F. Inhibitors of HIV-1 attachment: The discovery and development of temsavir and its prodrug fostemsavir. *J. Med. Chem.* **2018**, *61*, 62−80.

(51) Wang, T.; Zhang, Z.; Wallace, O. B.; Deshpande, M.; Fang, H.; Yang, Z.; Zadjura, L. M.; Tweedie, D. L.; Huang, S.; Zhao, F.; Ranadive, S.; Robinson, B. S.; Gong, Y.-F.; Ricarrdi, K.; Spicer, T. P.; Deminie, C.; Rose, R.; Wang, H. -G. H.; Blair, W. S.; Shi, P.-Y.; Lin, P.-F.; Colonno, R. J.; Meanwell, N. A. Discovery of 4-benzoyl-1-[(4-methoxy-1*H*- pyrrolo[2,3-*b*]pyridin-3-yl)oxoacetyl]-2-(*R*)-methylpiperazine (BMS-378806): A novel HIV-1 attachment inhibitor that interferes with CD4-gp120 interactions. *J. Med. Chem.* **2003**, *46*, 4236−4239.

(52) Pancera, M.; Lai, Y. T.; Bylund, T.; Druz, A.; Narpala, S.; O'Dell, S.; Schön, A.; Bailer, R. T.; Chuang, G. Y.; Geng, H.; Louder, M. K.; Rawi, R.; Soumana, D. I.; Finzi, A.; Herschhorn, A.; Madani, N.; Sodroski, J.; Freire, E.; Langley, D. R.; Mascola, J. R.; McDermott, A. B.; Kwong, P. D. Crystal structures of trimeric HIV envelope with entry inhibitors BMS-378806 and BMS-626529. *Nat. Chem. Biol.* **2017**, *13*, 1115−1122.

(53) Wang, T.; Yang, Z.; Zhang, Z.; Gong, Y. F.; Riccardi, K. A.; Lin, P. F.; Parker, D. D.; Rahematpura, S.; Mathew, M.; Zheng, M.; Meanwell, N. A.; Kadow, J. F.; Bender, J. A. Inhibitors of HIV-1 attachment. Part 10. The discovery and structure-activity relationships of 4-azaindole cores. *Bioorg. Med. Chem. Lett.* **2013**, *23*, 213−217.

(54) Kadow, J. F.; Ueda, Y.; Meanwell, N. A.; Connolly, T. P.; Wang, T.; Chen, C. P.; Yeung, K. S.; Zhu, J.; Bender, J. A.; Yang, Z.; Parker, D.; Lin, P. F.; Colonno, R. J.; Mathew, M.; Morgan, D.; Zheng, M.; Chien, C.; Grasela, D. Inhibitors of human immunodeficiency virus type 1 (HIV-1) attachment 6. Preclinical and human pharmacokinetic profiling of BMS-663749, a phosphonooxymethyl prodrug of the HIV-1 attachment inhibitor 2-(4-benzoyl-1-piperazinyl)-1-(4,7-dimethoxy-1H-pyrrolo[2,3-*c*]pyridin-3-yl)-2-oxo ethanone (BMS-488043). *J. Med. Chem.* **2012**, *55*, 2048−2056.

(55) Yeung, K.-S.; Qiu, Z.; Xue, Q.; Fang, H.; Yang, Z.; Zadjura, L.; D'Arienzo, C. J.; Eggers, B. J.; Riccardi, K.; Shi, P.-Y.; Gong, Y.-F.; Browning, M. R.; Gao, Q.; Hansel, S.; Santone, K.; Lin, P.-F.; Meanwell, N. A.; Kadow, J. F. Inhibitors of HIV-1 attachment. Part 7: Indole-7-carboxamides as potent and orally bioavailable antiviral agents. *Bioorg. Med. Chem. Lett.* **2013**, *23*, 198−202.

(56) Yeung, K.-S.; Qiu, Z.; Yin, Z.; Trehan, A.; Fang, H.; Pearce, B.; Yang, Z.; Zadjura, L.; D'Arienzo, C. J.; Riccardi, K.; Shi, P.-Y.; Spicer, T. P.; Gong, Y.-F.; Browning, M. R.; Hansel, S.; Santone, K.; Barker, J.; Coulter, T.; Lin, P.-F.; Meanwell, N. A.; Kadow, J. F. Inhibitors of HIV-1 attachment. Part 8: The effect of C7-heteroaryl substitution on the potency, and in vitro and in vivo profiles of indole-based inhibitors. *Bioorg. Med. Chem. Lett.* **2013**, *23*, 203−208.

(57) Regueiro-Ren, A.; Xue, Q. M.; Swidorski, J. J.; Gong, Y. F.; Mathew, M.; Parker, D. D.; Yang, Z.; Eggers, B.; D'Arienzo, C.; Sun, Y.; Malinowski, J.; Gao, Q.; Wu, D.; Langley, D. R.; Colonno, R. J.;

Chien, C.; Grasela, D. M.; Zheng, M.; Lin, P. F.; Meanwell, N. A.; Kadow, J. F. Inhibitors of human immunodeficiency virus type 1 (HIV-1) attachment. 12. Structure-activity relationships associated with 4-fluoro-6-azaindole derivatives leading to the identification of 1-(4-benzoylpiperazin-1-yl)-2-(4-fluoro-7-[1,2,3]triazol-1-yl-1H-pyrrolo[2,3-c]pyridin-3-yl)ethane-1,2-dione (BMS-585248). *J. Med. Chem.* **2013**, *56*, 1656–1669.

(58) Wang, T.; Ueda, Y.; Zhang, Z.; Yin, Z.; Matiskella, J.; Pearce, B. C.; Yang, Z.; Zheng, M.; Parker, D. D.; Yamanaka, G. A.; Gong, Y. F.; Ho, H. T.; Colonno, R. J.; Langley, D. R.; Lin, P. F.; Meanwell, N. A.; Kadow, J. F. Discovery of the Human Immunodeficiency Virus Type 1 (HIV-1) Attachment inhibitor temsavir and its phosphonooxymethyl prodrug fostemsavir. *J. Med. Chem.* **2018**, *61*, 6308–6327.

(59) Sato, S.; Inokuma, T.; Otsubo, N.; Burton, D. R.; Barbas, C. F., 3rd Chemically programmed antibodies as HIV-1 attachment inhibitors. *ACS Med. Chem. Lett.* **2013**, *4*, 460–465.

(60) Tuyishime, M.; Danish, M.; Princiotto, A.; Mankowski, M. K.; Lawrence, R.; Lombart, H. G.; Esikov, K.; Berniac, J.; Liang, K.; Ji, J.; Ptak, R. G.; Madani, N.; Cocklin, S. Discovery and optimization of novel small-molecule HIV-1 entry inhibitors using field-based virtual screening and bioisosteric replacement. *Bioorg. Med. Chem. Lett.* **2014**, *24*, 5439–5445.

(61) Lai, Y. T.; Wang, T.; O'Dell, S.; Louder, M. K.; Schon, A.; Cheung, C. S. F.; Chuang, G. Y.; Druz, A.; Lin, B.; McKee, K.; Peng, D.; Yang, Y.; Zhang, B.; Herschhorn, A.; Sodroski, J.; Bailer, R. T.; Doria-Rose, N. A.; Mascola, J. R.; Langley, D. R.; Kwong, P. D. Lattice engineering enables definition of molecular features allowing for potent small-molecule inhibition of HIV-1 entry. *Nat. Commun.* **2019**, *10*, 47.

(62) Rockstroh, J. K. Integrase inhibitors: Why do we need a new drug class for HIV therapy? *Eur. J. Med. Res.* **2009**, *14*, 1.

(63) Wong, E.; Trustman, N.; Yalong, A. HIV pharmacotherapy: A review of integrase inhibitors. *J. Am. Acad. Phys.* **2016**, *29*, 36–40.

(64) Messiaen, P.; Wensing, A. M. J.; Fun, A.; Nijhuis, M.; Brusselaers, N.; Vandekerckhove, L. Clinical use of HIV integrase inhibitors: A systematic review and meta-analysis. *PLoS One* **2013**, *8*, No. e52562.

(65) Summa, V.; Petrocchi, A.; Bonelli, F.; Crescenzi, B.; Donghi, M.; Ferrara, M.; Fiore, F.; Gardelli, C.; Gonzalez Paz, O.; Hazuda, D. J.; Jones, P.; Kinzel, O.; Laufer, R.; Monteagudo, E.; Muraglia, E.; Nizi, E.; Orvieto, F.; Pace, P.; Pescatore, G.; Scarpelli, R.; Stillmock, K.; Witmer, M. V.; Rowley, M. Discovery of raltegravir, a potent, selective orally bioavailable HIV-integrase inhibitor for the treatment of HIV-AIDS infection. *J. Med. Chem.* **2008**, *51*, 5843–5855.

(66) Agrawal, A.; DeSoto, J.; Fullagar, J. L.; Maddali, K.; Rostami, S.; Richman, D. D.; Pommier, Y.; Cohen, S. M. Probing chelation motifs in HIV integrase inhibitors. *Proc. Natl. Acad. Sci. U.S.A.* **2012**, *109*, 2251–2256.

(67) Kawasuji, T.; Fuji, M.; Yoshinaga, T.; Sato, A.; Fujiwara, T.; Kiyama, R. A platform for designing HIV integrase inhibitors. Part 2: A two-metal binding model as a potential mechanism of HIV integrase inhibitors. *Bioorg. Med. Chem.* **2006**, *14*, 8420–8429.

(68) Tandon, V.; Urvashi; Yadav, P.; Sur, S.; Abbat, S.; Tiwari, V.; Hewer, R.; Papathanasopoulos, M. A.; Raja, R.; Banerjea, A. C.; Verma, A. K.; Kukreti, S.; Bharatam, P. V. Design, synthesis, and biological evaluation of 1,2-dihydroisoquinolines as HIV-1 integrase inhibitors. *ACS Med. Chem. Lett.* **2015**, *6*, 1065–1070.

(69) Steigbigel, R. T.; Cooper, D. A.; Kumar, P. N.; Eron, J. E.; Schechter, M.; Markowitz, M.; Loutfy, M. R.; Lennox, J. L.; Gatell, J. M.; Rockstroh, J. K.; Katlama, C.; Yeni, P.; Lazzarin, A.; Clotet, B.; Zhao, J.; Chen, J.; Ryan, D. M.; Rhodes, R. R.; Killar, J. A.; Gilde, L. R.; Strohmaier, K. M.; Meibohm, A. R.; Miller, M. D.; Hazuda, D. J.; Nessly, M. L.; DiNubile, M. J.; Isaacs, R. D.; Nguyen, B. Y.; Teppler, H. Raltegravir with optimized background therapy for resistant HIV-1 infection. *N. Engl. J. Med.* **2008**, *359*, 339–354.

(70) Sato, M.; Motomura, T.; Aramaki, H.; Matsuda, T.; Yamashita, M.; Ito, Y.; Kawakami, H.; Matsuzaki, Y.; Watanabe, W.; Yamataka, K.; Ikeda, S.; Kodama, E.; Matsuoka, M.; Shinkai, H. Novel HIV-1

integrase inhibitors derived from quinolone antibiotics. *J. Med. Chem.* **2006**, *49*, 1506–1508.

(71) Min, S.; Song, I.; Borland, J.; Chen, S.; Lou, Y.; Fujiwara, T.; Piscitelli, S. C. Pharmacokinetics and safety of S/GSK1349572, a next-generation HIV integrase inhibitor, in healthy volunteer. *Antimicrob. Agents Chemother.* **2010**, *54*, 254–258.

(72) Shimura, K.; Kodama, E. N. Elvitegravir: a new HIV integrase inhibitor. *Antivir. Chem. Chemother.* **2009**, *20*, 79–85.

(73) Ramkumar, K.; Neamati, N. Raltegravir: The evidence of its therapeutic value in HIV-1 infection. *Core. Evid.* **2009**, *4*, 131–147.

(74) Al-Mawsawi, L. Q.; Al-Safi, R. I.; Neamati, N. Anti-infectives clinical progress of HIV-1 integrase inhibitors. *Expert Opin. Emerging Drugs* **2008**, *13*, 213–225.

(75) Abram, M. E.; Hluhanich, R. M.; Goodman, D. D.; Andreatta, K. N.; Margot, N. A.; Ye, L.; Niedziela-Majka, A.; Barnes, T. L.; Novikov, N.; Chen, X.; Svarovskaia, E. S.; McColl, D. J.; White, K. L.; Miller, M. D. Impact of primary elvitegravir resistance-associated mutations in HIV-1 integrase on drug susceptibility and viral replication fitness. *Antimicrob. Agents Chemother.* **2013**, *57*, 2654–2663.

(76) Carganico, A.; Dupke, S.; Ehret, R.; Berg, T.; Baumgarten, A.; Obermeier, M.; Walter, H. New dolutegravir resistance pattern identified in a patient failing antiretroviral therapy. *J. Int. AIDS Soc.* **2014**, *17*, 19749.

(77) Barber, T. Integrase inhibitors go head-to-head. *Lancet HIV* **2017**, *4*, e142–e143.

(78) Max, B. Update on HIV integrase inhibitors for the treatment of HIV-1 infection. *Future Virol.* **2019**, *14*, 693–709.

(79) Singh, R.; Yadav, P.; Urvashi; Tandon, V. Novel dioxolan derivatives of indole as HIV-1 integrase strand transfer inhibitors active against RAL resistant mutant. *ChemistrySelect* **2016**, *1*, 5471–5478.

(80) Goldgur, Y.; Craigie, R.; Cohen, G. H.; Fujiwara, T.; Yoshinaga, T.; Fujishita, T.; Sugimoto, H.; Endo, T.; Murai, H.; Davies, D. R. Structure of the HIV-1 integrase catalytic domain complexed with an inhibitor: a platform for antiviral drug design. *Proc. Natl. Acad. Sci. U. S. A.* **1999**, *96*, 13040–13043.

(81) Plewe, M. B.; Butler, S. L.; Dress, K. R.; Hu, Q.; Johnson, T. W.; Kuehler, J. E.; Kuki, A.; Lam, H.; Liu, W.; Nowlin, D.; Peng, Q.; Rahavendran, S. V.; Tanis, S. P.; Tran, K. T.; Wang, H.; Yang, A.; Zhang, J. Azaindole hydroxamic acids are potent HIV-1 integrase inhibitors. *J. Med. Chem.* **2009**, *52*, 7211–7219.

(82) Tanis, S. P.; Plewe, M. B.; Johnson, T. W.; Butler, S. L.; Dalvie, D.; DeLisle, D.; Dress, K. R.; Hu, Q.; Huang, B.; Kuehler, J. E.; Kuki, A.; Liu, W.; Peng, Q.; Smith, G. L.; Solowiej, J.; Tran, K. T.; Wang, H.; Yang, A.; Yin, C.; Yu, X.; Zhang, J.; Zhu, H. Azaindole *N*-methyl hydroxamic acids as HIV-1 integrase inhibitors-II. The impact of physicochemical properties on ADME and PK. *Bioorg. Med. Chem. Lett.* **2010**, *20*, 7429–7434.

(83) Johnson, T. W.; Tanis, S. P.; Butler, S. L.; Dalvie, D.; Delisle, D. M.; Dress, K. R.; Flahive, E. J.; Hu, Q.; Kuehler, J. E.; Kuki, A.; Liu, W.; McClellan, G. A.; Peng, Q.; Plewe, M. B.; Richardson, P. F.; Smith, G. L.; Solowiej, J.; Tran, K. T.; Wang, H.; Yu, X.; Zhang, J.; Zhu, H. Design and synthesis of novel *N*-hydroxy-dihydronaphthyridinones as potent and orally bioavailable HIV-1 integrase inhibitors. *J. Med. Chem.* **2011**, *54*, 3393–3417.

(84) Pryde, D. C.; Webster, R.; Butler, S. L.; Murray, E. J.; Whitby, K.; Pickford, C.; Westby, M.; Palmer, M. J.; Bull, D. J.; Vuong, H.; Blakemore, D. C.; Stead, D.; Ashcroft, C.; Gardner, I.; Bru, C.; Cheung, W.-Y.; Roberts, I. O.; Morton, J.; Bissell, R. A. Discovery of an HIV integrase inhibitor with an excellent resistance profile. *Med. Chem. Commun.* **2013**, *4*, 709–719.

(85) Carayon, K.; Leh, H.; Henry, E.; Simon, F.; Mouscadet, J.-F.; Deprez, E. A cooperative and specific DNA-binding mode of HIV-1 integrase depends on the nature of the metallic cofactor and involves the zinc-containing *N*-terminal domain. *Nucleic Acids Res.* **2010**, *38*, 3692–3708.

(86) Cockerill, G. S.; Good, J. A. D.; Mathews, N. State of the art in respiratory syncytial virus drug discovery and development. *J. Med. Chem.* **2019**, *62*, 3206–3227.

(87) Griffiths, C.; Drews, S. J.; Marchant, D. J. Respiratory syncytial virus: infection, detection, and new options for prevention and treatment. *Clin. Microbiol. Rev.* **2017**, *30*, 277–319.

(88) Hynicka, L. M.; Ensor, C. R. Prophylaxis and treatment of respiratory syncytial virus in adult immunocompromised patients. *Ann. Pharmacother* **2012**, *46*, 558–566.

(89) Borchers, A. T.; Chang, C.; Gershwin, M. E.; Gershwin, L. J. Respiratory syncytial virus–a comprehensive review. *Clinic Rev. Allerg. Immunol.* **2013**, *45*, 331–379.

(90) Battles, M. B.; McLellan, J. S. Respiratory syncytial virus entry and how to block it. *Nat. Rev. Microbiol.* **2019**, *17*, 233–245.

(91) Killikelly, A. M.; Kanekiyo, M.; Graham, B. S. Pre-fusion F is absent on the surface of formalin-inactivated respiratory syncytial virus. *Sci. Rep.* **2016**, *6*, 34108.

(92) Yunus, A. S.; Jackson, T. P.; Crisafi, K.; Burimski, I.; Kilgore, N. R.; Zoumplis, D.; Allaway, G. P.; Wild, C. T.; Salzwedel, K. Elevated temperature triggers human respiratory syncytial virus F protein six-helix bundle formation. *Virology* **2010**, *396*, 226–237.

(93) San-Juan-Vergara, H.; Sampayo-Escobar, V.; Reyes, N.; Cha, B.; Pacheco-Lugo, L.; Wong, T.; Peeples, M. E.; Collins, P. L.; Castaño, M. E.; Mohapatra, S. S. Cholesterol-rich microdomains as docking platforms for respiratory syncytial virus in normal human bronchial epithelial cells. *J. Virol.* **2012**, *86*, 1832–1843.

(94) Krzyzaniak, M. A.; Zumstein, M. T.; Gerez, J. A.; Picotti, P.; Helenius, A. Host cell entry of respiratory syncytial virus involves macropinocytosis followed by proteolytic activation of the F protein. *PLOS Pathog.* **2013**, *9*, No. e1003309.

(95) Yuan, P.; Thompson, T. B.; Wurzburg, B. A.; Paterson, R. G.; Lamb, R. A.; Jardetzky, T. S. Structural studies of the parainfluenza virus 5 hemagglutinin-neuraminidase tetramer in complex with its receptor, sialyllactose. *Structure* **2005**, *13*, 803–815.

(96) Crennell, S.; Takimoto, T.; Portner, A.; Taylor, G. Crystal structure of the multifunctional paramyxovirus hemagglutinin-neuraminidase. *Nat. Struct. Biol.* **2000**, *7*, 1068–1074.

(97) Bose, S.; Jardetzky, T. S.; Lamb, R. A. Timing is everything: fine-tuned molecular machines orchestrate paramyxovirus entry. *Virology* **2015**, *479–480*, 518–531.

(98) Fenton, C.; Scott, L. J.; Plosker, G. L. Palivizumab: a review of its use as prophylaxis for serious respiratory syncytial virus infection. *Paediatr. Drugs.* **2004**, *6*, 177–197.

(99) Witkowski, J. T.; Robins, R. K.; Sidwell, R. W.; Simon, L. N. Design, synthesis, and broad spectrum antiviral activity of 1-D-ribofuranosyl-1, 2, 4-triazole-3-carboxamide and related nucleosides. *J. Med. Chem.* **1972**, *15*, 1150–1154.

(100) Sidwell, R. W.; Huffman, J. H.; Khare, G. P.; Allen, L. B.; Witkowski, J. T.; Robinset, R. K. Broad-spectrum antiviral activity of Virazole: 1-beta-D-ribofuranosyl-1, 2, 4-triazole-3-carboxamide. *Science* **1972**, *177*, 705–706.

(101) Krilov, L. R. Respiratory Syncytial Virus: Update on Infection, Treatment, and Prevention. *Curr. Infect. Dis. Rep.* **2001**, *3*, 242–246.

(102) Roymans, D.; Alnajjar, S. S; Battles, M. B; Sitthicharoenchai, P.; Furmanova-Hollenstein, P.; Rigaux, P.; Berg, J. V. d.; Kwanten, L.; Ginderen, M. V.; Verheyen, N.; Vranckx, L.; Jaensch, S.; Arnoult, E.; Voorzaat, R.; Gallup, J. M.; Larios-Mora, A.; Crabbe, M.; Huntjens, D.; Raboisson, P.; Langedijk, J. P.; Ackermann, M. R.; McLellan, J. S; Vendeville, S.; Koul, A. Therapeutic efficacy of a respiratory syncytial virus fusion inhibitor. *Nat. Commun.* **2017**, *8*, 167.

(103) Wilcken, R.; Zimmermann, M. O.; Lange, A.; Joerger, A. C.; Boeckler, F. M. Principles and Applications of Halogen Bonding in Medicinal Chemistry and Chemical Biology. *J. Med. Chem.* **2013**, *56*, 1363–1388.

(104) Boer, F. Drug handling by the lungs. *Br. J. Anaesth.* **2003**, *91*, 50–60.

(105) Yokogawa, K.; Ishizaki, J.; Ohkuma, S.; Miyamoto, K. Influence of lipophilicity and lysosomal accumulation on tissue distribution kinetics of basic drugs: a physiologically based pharmacokinetic model. *Methods Find Exp. Clin. Pharmacol.* **2002**, *24*, 81–93.

(106) Feng, S.; Li, C.; Chen, D.; Zheng, X.; Yun, H.; Gao, L.; Shen, H. C. Discovery of methylsulfonyl indazoles as potent and orally active respiratory syncytial virus (RSV) fusion inhibitors. *Eur. J. Med. Chem.* **2017**, *138*, 1147–1157.

(107) Vendeville, S.; Tahri, A.; Hu, L.; Demin, S.; Cooymans, L.; Vos, A.; Kwanten, L.; Van den Berg, J.; Battles, M. B.; McLellan, J. S.; Koul, A.; Raboisson, P.; Roymans, D.; Jonckers, T. Discovery of 3-({5 Chloro-1-[3-(methylsulfonyl)propyl]-1*H*-indol-2-yl}methyl)-1-(2,2,2-trifluoroethyl)-1,3-dihydro-2*H*-imidazo[4,5-*c*]pyridin-2-one(JNJ-53718678), a potent and orally bioavailable fusion inhibitor of respiratory syncytial virus. *J. Med. Chem.* **2020**, *63*, 8046–8058.

(108) Mackman, R. L.; Sangi, M.; Sperandio, D.; Parrish, J. P.; Eisenberg, E.; Perron, M.; Hui, H.; Zhang, L.; Siegel, D.; Yang, H.; Saunders, O.; Boojamra, C.; Lee, G.; Samuel, D.; Babaoglu, K.; Carey, A.; Gilbert, B. E.; Piedra, P. A.; Strickley, R.; Iwata, Q.; Hayes, J.; Stray, K.; Kinkade, A.; Theodore, D.; Jordan, R.; Desai, M.; Cihlar, T. Discovery of an oral respiratory syncytial virus (RSV) fusion inhibitor (GS-5806) and clinical proof of concept in a human RSV challenge study. *J. Med. Chem.* **2015**, *58*, 1630–1643.

(109) Strauss, J. H.; Strauss, E. G. The alphaviruses: gene expression, replication, and evolution. *Microbiol. Rev.* **1994**, *58*, 491–562.

(110) Ruiz-Guillen, M.; Abrescia, N. G. A.; Smerdou, C. Neurotropic alphaviruses can propagate without capsid. *Oncotarget* **2017**, *8*, 8999–9000.

(111) Peltier, D. C.; Lazear, H. M.; Farmer, J. R.; Diamond, M. S.; Miller, D. J. Neurotropic arboviruses induce interferon regulatory factor 3- mediated neuronal responses that are cytoprotective, interferon independent, and inhibited by western equine encephalitis virus capsid. *J. Virol.* **2013**, *87*, 1821–1833.

(112) Peng, W.; Peltier, D. C.; Larsen, M. J.; Kirchhoff, P. D.; Larsen, S. D.; Neubig, R. R.; Miller, D. J. Identification of thieno[3,2-*b*]pyrrole derivatives as novel small molecule inhibitors of neurotropic alphaviruses. *J. Infect. Dis.* **2009**, *199*, 950–957.

(113) Sindac, J. A.; Yestrepsky, B. D.; Barraza, S. J.; Bolduc, K. L.; Blakely, P. K.; Keep, R. F.; Irani, D. N.; Miller, D. J.; Larsen, S. D. Novel inhibitors of neurotropic alphavirus replication that improve host survival in a mouse model of acute viral encephalitis. *J. Med. Chem.* **2012**, *55*, 3535–3545.

(114) Sindac, J. A.; Barraza, S. J.; Dobry, C. J.; Xiang, J.; Blakely, P. K.; Irani, D. N.; Keep, R. F.; Miller, D. J.; Larsen, S. D. Optimization of novel indole-2-carboxamide inhibitors of neurotropic alphavirus replication. *J. Med. Chem.* **2013**, *56*, 9222–9241.

(115) Delekta, P. C.; Dobry, C. J.; Sindac, J. A.; Barraza, S. J.; Blakely, P. K.; Xiang, J.; Kirchhoff, P. D.; Keep, R. F.; Irani, D. N.; Larsen, S. D.; Miller, D. J. Novel indole-2-carboxamide compounds are potent broad-spectrum antivirals active against western equine encephalitis virus *in vivo*. *J. Virol.* **2014**, *88*, 11199–11214.

(116) Dhama, K.; Karthik, K.; Khandia, R.; Chakraborty, S.; Munjal, A.; Latheef, S. K.; Kumar, D.; Ramakrishnan, M. A.; Malik, Y. S.; Singh, R.; Malik, S. V. S.; Singh, R. K.; Chaicumpa, W. Advances in designing and developing vaccines, drugs, and therapies to counter ebola virus. *Front Immunol.* **2018**, *9*, 1803.

(117) Simmons, C. P.; Farrar, J. J.; van Vinh Chau, N.; Wills, B. Dengue. *N. Engl. J. Med.* **2012**, *366*, 1423–1432.

(118) Thomas, S. J.; Yoon, I. K. A review of dengvaxia: Development to deployment. *Hum. Vaccin. Immunother.* **2019**, *15*, 2295–2314.

(119) Verdonck, S.; Pu, S. Y.; Sorrell, F. J.; Elkins, J. M.; Froeyen, M.; Gao, L. J.; Prugar, L. I.; Dorosky, D. E.; Brannan, J. M.; Barouch-Bentov, R.; Knapp, S.; Dye, J. M.; Herdewijn, P.; Einav, S.; De Jonghe, S. Synthesis and structure-activity relationships of 3,5-disubstituted-pyrrolo[2,3-*b*]pyridines as inhibitors of adaptor-associated kinase 1 with antiviral activity. *J. Med. Chem.* **2019**, *62*, 5810–5831.

(120) Xing, L.; Klug-Mcleod, J.; Rai, B.; Lunney, E. A. Kinase hinge binding scaffolds and their hydrogen bond patterns. *Bioorg. Med. Chem.* **2015**, *23*, 6520–6527.

(121) Sorrell, F. J.; Szklarz, M.; Abdul Azeez, K. R.; Elkins, J. M.; Knapp, S. Family-wide structural analysis of human numb-associated protein kinases. *Structure* **2016**, *24*, 401–411.

(122) Miles, D. H.; Yan, X.; Thomas-Tran, R.; Fournier, J.; Sharif, E. U.; Drew, S. L.; Mata, G.; Lawson, K. V.; Ginn, E.; Wong, K.; Soni, D.; Dhanota, P.; Shaqfeh, S. G.; Meleza, C.; Chen, A.; Pham, A. T.; Park, T.; Swinarski, D.; Banuelos, J.; Schindler, U.; Walters, M. J.; Walker, N. P.; Zhao, X.; Young, S. W.; Chen, J.; Jin, L.; Leleti, M. R.; Powers, J. P.; Jeffrey, J. L. Discovery of potent and selective 7-azaindole isoindolinone-based PI3Kγ inhibitors. *ACS Med. Chem. Lett.* **2020**, *11*, 2244–2252.

(123) Drew, S. L.; Thomas-Tran, R.; Beatty, J. W.; Fournier, J.; Lawson, K. V.; Miles, D. H.; Mata, G.; Sharif, E. U.; Yan, X.; Mailyan, A. K.; Ginn, E.; Chen, J.; Wong, K.; Soni, D.; Dhanota, P.; Chen, P.-Y.; Shaqfeh, S. G.; Meleza, C.; Pham, A. T.; Chen, A.; Zhao, X.; Banuelos, J.; Jin, L.; Schindler, U.; Walters, M. J.; Young, S. W.; Walker, N. P.; Leleti, M. R.; Powers, J. P.; Jeffrey, J. L. Discovery of potent and selective PI3Kγ inhibitors. *J. Med. Chem.* **2020**, *63*, 11235–11257.

(124) Gangadhara, G.; Dahl, G.; Bohnacker, T.; Rae, R.; Gunnarsson, J.; Blaho, S.; Öster, L.; Lindmark, H.; Karabelas, K.; Pemberton, N.; Tyrchan, C.; Mogemark, M.; Wymann, M. P.; Williams, R. L.; Perry, M.; Papavoine, T.; Petersen, J. A class of highly selective inhibitors bind to an active state of PI3Kγ. *Nat. Chem. Biol.* **2019**, *15*, 348–357.

(125) Ji, X.; Li, Z. Medicinal chemistry strategies toward host targeting antiviral agents. *Med. Res. Rev.* **2020**, *40*, 1519–1557.

(126) Perwitasari, O.; Yan, X.; O'Donnell, J.; Johnson, S.; Tripp, R. A. Repurposing kinase inhibitors as antiviral agents to control influenza A virus replication. *Assay drug dev. techn.* **2015**, *13*, 638–649.

(127) Schor, S.; Einav, S. Repurposing of kinase inhibitors as broad-spectrum antiviral drugs. *DNA cell biol.* **2018**, *37*, 63–69.

(128) Weisberg, E.; Parent, A.; Yang, P. L.; Sattler, M.; Liu, Q.; Liu, Q.; Wang, J.; Meng, C.; Buhrlage, S. J.; Gray, N.; Griffin, J. D. Repurposing of kinase inhibitors for treatment of COVID-19. *Pharm. res.* **2020**, *37*, 167.

(129) Sheridan, C. New Merck and Vertex drugs raise standard of care in hepatitis C. *Nat. Biotechnol.* **2011**, *29*, 553–554.

(130) Cannalire, R.; Barreca, M. L.; Manfroni, G.; Cecchetti, V. A journey around the medicinal chemistry of hepatitis C virus inhibitors targeting NS4B: from target to preclinical drug candidates. *J. Med. Chem.* **2016**, *59*, 16–41.

(131) Roberts, C. D.; Peat, A. J. HCV Replication Inhibitors that Interact with NS4B. In *Successful Strategies for the Discovery of Antiviral Drugs*; Daesai, M. C., Meanwell, N. A., Eds.; RSC Publishing: Cambridge, 2013; pp 111–145.

(132) Chen, G.; Ren, H.; Zhang, N.; Lennox, W.; Turpoff, A.; Paget, S.; Li, C.; Almstead, N.; Njoroge, F. G.; Gu, Z.; Graci, J.; Jung, S. P.; Colacino, J.; Lahser, F.; Zhao, X.; Weetall, M.; Nomeir, A.; Karp, G. M. 6-(Azaindol-2-yl)pyridine-3-sulfonamides as potent and selective inhibitors targeting hepatitis C virus NS4B. *Bioorg. Med. Chem. Lett.* **2015**, *25*, 781–786.

(133) Zhang, N.; Zhang, X.; Zhu, J.; Turpoff, A.; Chen, G.; Morrill, C.; Huang, S.; Lennox, W.; Kakarla, R.; Liu, R.; Li, C.; Ren, H.; Almstead, N.; Venkatraman, S.; Njoroge, F. G.; Gu, Z.; Clausen, V.; Graci, J.; Jung, S. P.; Zheng, Y.; Colacino, J. M.; Lahser, F.; Sheedy, J.; Mollin, A.; Weetall, M.; Nomeir, A.; Karp, G. M. Structure-activity relationship (SAR) optimization of 6-(indol-2-yl)pyridine-3-sulfonamides: Identification of potent, selective, and orally bioavailable small molecules targeting Hepatitis C (HCV) NS4B. *J. Med. Chem.* **2014**, *57*, 2121–2135.

(134) Krammer, F.; Smith, G. J. D.; Fouchier, R. A. M.; Peiris, M.; Kedzierska, K.; Doherty, P. C.; Palese, P.; Shaw, M. L.; Treanor, J.; Webster, R. J.; García-Sastre, A. Influenza. *Nat. Rev. Dis. Primers* **2018**, *4*, 3.

(135) Carrat, F.; Flahault, A. Influenza vaccine: the challenge of antigenic drift. *Vaccine.* **2007**, *25*, 6852–6862.

(136) Moscona, A. Neuraminidase inhibitors for influenza. *N. Engl. J. Med.* **2005**, *353*, 1363–1373.

(137) Byrn, R. A.; Jones, S. M.; Bennett, H. B.; Bral, C.; Clark, M. P.; Jacobs, M. D.; Kwong, A. D.; Ledeboer, M. W.; Leeman, J. R.; McNeil, C. F.; Murcko, M. A.; Nezami, A.; Perola, E.; Rijnbrand, R.; Saxena, K.; Tsai, A. W.; Zhou, Y.; Charifson, P. S. Preclinical activity of VX-787, a first-in-class, orally bioavailable inhibitor of the influenza virus polymerase PB2 subunit. *Antimicrob. Agents Chemother.* **2015**, *59*, 1569–1582.

(138) Clark, M. P.; Ledeboer, M. W.; Davies, I.; Byrn, R. A.; Jones, S. M.; Perola, E.; Tsai, A.; Jacobs, M.; Nti-Addae, K.; Bandarage, U. K.; Boyd, M. J.; Bethiel, R. S.; Court, J. J.; Deng, H.; Duffy, J. P.; Dorsch, W. A.; Farmer, L. J.; Gao, H.; Gu, W.; Jackson, K.; Jacobs, D. H.; Kennedy, J. M.; Ledford, B.; Liang, J.; Maltais, F.; Murcko, M.; Wang, T.; Wannamaker, M. W.; Bennett, H. B.; Leeman, J. R.; McNeil, C.; Taylor, W. P.; Memmott, C.; Jiang, M.; Rijnbrand, R.; Bral, C.; Germann, U.; Nezami, A.; Zhang, Y.; Salituro, F. G.; Bennani, Y. L.; Charifson, P. S. Discovery of a novel, first-in-class, orally bioavailable azaindole inhibitor (VX-787) of influenza PB2. *J. Med. Chem.* **2014**, *57*, 6668–6678.

(139) Wagaman, P. C.; Leong, M. A.; Simmen, K. A. Development of a novel influenza A antiviral assay. *J. Virol. Methods* **2002**, *105*, 105–114.

(140) Boyd, M. J.; Bandarage, U. K.; Bennett, H.; Byrn, R. R.; Davies, I.; Gu, W.; Jacobs, M.; Ledeboer, M. W.; Ledford, B.; Leeman, J. R.; Perola, E.; Wang, T.; Bennani, Y.; Clark, M. P.; Charifson, P. S. Isosteric replacements of the carboxylic acid of drug candidate VX-787: Effect of charge on antiviral potency and kinase activity of azaindole-based influenza PB2 inhibitors. *Bioorg. Med. Chem. Lett.* **2015**, *25*, 1990–1994.

(141) Farmer, L. J.; Clark, M. P.; Boyd, M. J.; Perola, E.; Jones, S. M.; Tsai, A.; Jacobs, M. D.; Bandarage, U. K.; Ledeboer, M. W.; Wang, T.; Deng, H.; Ledford, B.; Gu, W.; Duffy, J. P.; Bethiel, R. S.; Shannon, D.; Byrn, R. A.; Leeman, J. R.; Rijnbrand, R.; Bennett, H. B.; O'Brien, C.; Memmott, C.; Nti-Addae, K.; Bennani, Y. L.; Charifson, P. S. Discovery of novel, orally bioavailable beta-amino acid azaindole inhibitors of influenza PB2. *ACS. Med. Chem. Lett.* **2017**, *8*, 256–260.

(142) Bandarage, U. K.; Clark, M. P.; Perola, E.; Gao, H.; Jacobs, M. D.; Tsai, A.; Gillespie, J.; Kennedy, J. M.; Maltais, F.; Ledeboer, M. W.; Davies, I.; Gu, W.; Byrn, R. A.; Nti Addae, K.; Bennett, H.; Leeman, J. R.; Jones, S. M.; O'Brien, C.; Memmott, C.; Bennani, Y.; Charifson, P. S. Novel 2-substituted 7-azaindole and 7-azaindazole analogues as potential antiviral agents for the treatment of influenza. *ACS Med. Chem. Lett.* **2017**, *8*, 261–265.

(143) McGowan, D. C.; Balemans, W.; Embrechts, W.; Motte, M.; Keown, J. R.; Buyck, C.; Corbera, J.; Funes, M.; Moreno, L.; Cooymans, L.; Tahri, A.; Eymard, J.; Stoops, B.; Strijbos, R.; Van den Berg, J.; Fodor, E.; Grimes, J. M.; Koul, A.; Jonckers, T. H. M.; Raboisson, P.; Guillemont, J. Design, synthesis, and biological evaluation of novel indoles targeting the influenza PB2 cap binding region. *J. Med. Chem.* **2019**, *62*, 9680–9690.

(144) Gillis, E. P.; Eastman, K. J.; Hill, M. D.; Donnelly, D. J.; Meanwell, N. A. Applications of fluorine in medicinal chemistry. *J. Med. Chem.* **2015**, *58*, 8315–8359.

(145) COVID-19 Treatment guidelines panel. *Coronavirus disease 2019 (COVID-19) treatment guidelines*; National Institutes of Health; https://www.covid19treatmentguidelines.nih.gov/ (accessed July 3, 2020).

(146) Ghosh, A. K.; Brindisi, M.; Shahabi, D.; Chapman, M. E.; Mesecar, A. D. Drug development and medicinal chemistry efforts toward SARS-coronavirus and COVID-19 therapeutics. *Chem. Med. Chem.* **2020**, *15*, 907–932.

(147) Gil, C.; Ginex, T.; Maestro, I.; Nozal, V.; Barrado-Gil, L.; Cuesta-Geijo, M. Á.; Urquiza, J.; Ramírez, D.; Alonso, C.; Campillo, N. E.; Martinez, A. COVID-19: Drug targets and potential treatments. *J. Med. Chem.* **2020**, *63*, 12359.

(148) https://www.excelra.com/covid-19-drug-repurposing-database (accessed May 20, 2020).

AO

(149) Spinelli, F. R.; Conti, F.; Gadina, M. HiJAKing SARS-CoV-2? The potential role of JAK inhibitors in the management of COVID-19. *Sci. Immunol.* **2020**, *5*, No. eabc5367.

(150) Stebbing, J.; Krishnan, V.; de Bono, S.; Ottaviani, S.; Casalini, G.; Richardson, P. J.; Monteil, V.; Lauschke, V. M.; Mirazimi, A.; Youhanna, S.; Tan, Y. J.; Baldanti, F.; Sarasini, A.; Terres, J.; Nickoloff, B. J.; Higgs, R. E.; Rocha, G.; Byers, N. L.; Schlichting, D. E.; Nirula, A.; Cardoso, A.; Corbellino, M. Sacco Baricitinib Study Group. Mechanism of baricitinib supports artificial intelligence-predicted testing in COVID-19 patients. *EMBO molecular medicine* **2020**, *12*, e12697.

(151) Glebov, O. O. Understanding SARS-CoV-2 endocytosis for COVID-19 drug repurposing. *FEBS. J.* **2020**, *287*, 3664−3671.

(152) Wrapp, D.; Wang, N.; Corbett, K. S.; Goldsmith, J. A.; Hsieh, C. L.; Abiona, O.; Graham, B. S.; McLellan, J. S. Cryo-EM structure of the 2019-nCoV spike in the prefusion conformation. *Science.* **2020**, *367*, 1260−1263.

(153) Huang, C.; Wang, Y.; Li, X.; Ren, L.; Zhao, J.; Hu, Y.; Zhang, L.; Fan, G.; Xu, J.; Gu, X.; Cheng, Z.; Yu, T.; Xia, J.; Wei, Y.; Wu, W.; Xie, X.; Yin, W.; Li, H.; Liu, M.; Xiao, Y.; Gao, H.; Guo, L.; Xie, J.; Wang, G.; Jiang, R.; Gao, Z.; Jin, Q.; Wang, J.; Cao, B. Cao, Clinical features of patients infected with 2019 novel coronavirus in Wuhan, China. *Lancet* **2020**, *395*, 497−506.

(154) Coperchini, F.; Chiovato, L.; Croce, L.; Magri, F.; Rotondi, M. The cytokine storm in COVID-19: An overview of the involvement of the chemokine/chemokine-receptor system. *Cytokine Growth Factor Rev.* **2020**, *53*, 25−32.

(155) Richardson, P.; Griffin, I.; Tucker, C.; Smith, D.; Oechsle, O.; Phelan, A.; Rawling, M.; Savory, E.; Stebbing, J. Baricitinib as potential treatment for 2019-nCoV acute respiratory disease. *Lancet* **2020**, *395*, e30−e31.

(156) Zhong, J.; Tang, J.; Ye, C.; Dong, L. The immunology of COVID-19: is immune modulation an option for treatment? *Lancet Rheumatol.* **2020**, *2*, e428−e436.

(157) Stebbing, J.; Phelan, A.; Griffin, I.; Tucker, C.; Oechsle, O.; Smith, D.; Richardson, P. COVID-19: combining antiviral and anti-inflammatory treatments. *Lancet Infect. Dis.* **2020**, *20*, 400−402.

(158) Viswanathan, T.; Arya, S.; Chan, S.-H.; Qi, S.; Dai, N.; Misra, A.; Park, J.-G.; Oladunni, F.; Kovalskyy, D.; Hromas, R. A.; Martinez-Sobrido, L.; Gupta, Y. K. Structural basis of RNA cap modification by SARS-CoV-2. *Nat. Commun.* **2020**, *11*, 3718.

(159) Sun, Y.; Wang, Z.; Tao, J.; Wang, Y.; Wu, A.; Yang, Z.; Wang, K.; Shi, L.; Chen, Y.; Guo, D. Yeast-based assays for the high-throughput screening of inhibitors of coronavirus RNA cap guanine-N7-methyltransferase. *Antivir. Res.* **2014**, *104*, 156−164.

(160) Krafcikova, P.; Silhan, J.; Nencka, R.; Boura, E. Structural analysis of the SARS-CoV-2 methyltransferase complex involved in RNA cap creation bound to sinefungin. *Nat. Commun.* **2020**, *11*, 3717.